

IMPROVING FRACTURE TOUGHNESS OF SILICON CARBIDE BASED CERAMICS BY  
MICROSTRUCTURE TAILORING

by

SHEIKH FAHAD FERDOUS

Presented to the Faculty of the Graduate School of  
The University of Texas at Arlington in Partial Fulfillment  
of the Requirements  
for the Degree of

DOCTOR OF PHILOSOPHY

THE UNIVERSITY OF TEXAS AT ARLINGTON

August 2015

Copyright © by Sheikh Fahad Ferdous 2015

All Rights Reserved



## Acknowledgements

Guidance of my advisor, supports from my family, and assist from friends made me stand at this position.

I would like to gently acknowledge my advisor, Dr. Ashfaq Adnan with the deepest gratitude for his instruction, excellent, guidance, patience, and deliver me a magnificent environment for doing research. He was supervising my research for the last five years and assisting me to create a background on atomistic level of mechanics. He always navigates the research in wide areas from soft to hard materials. He also suggested taking courses in such a way that I got a solid knowledge about the physics and mechanics of materials.

I would like to thank Dr. Chan, Dr. Luo, Dr. Pranesh and Dr. Huda for becoming a committee member of my dissertation defense.

I would like to thank MMPL lab members, my research fellows for giving their best suggestion in my research and respond at any time when help was requested.

I am always thankful to my parents, two elder brothers. They always encouraged me with their best wishes.

I would also mention the name of my better half, Priyanka who continuously supported and encouraged me during my research time

May 28, 2015

## Abstract

# IMPROVING FRACTURE TOUGHNESS OF SILICON CARBIDE BASED CERAMICS BY MICROSTRUCTURE TAILORING

Sheikh Fahad Ferdous, PhD

The University of Texas at Arlington, 2015

Supervising Professor: Ashfaq Adnan

Ceramic materials are one of the most promising materials for wide variety of technical applications such as automotive, aerospace, medical, and other applications. They have very high strengths and high melting points relative to metals. However, low fracture toughness is one of the main barriers of ceramics prohibiting their wide-spread applications. This is because ceramics are mainly bonded with directional bonds which don't allow dislocations based deformation. Several attempts have been made to increase the toughness of ceramic materials without sacrificing significantly the other mechanical properties. Here three different types of SiC based ceramics have been computationally (atomistic and up-scaled modeling) developed and studied to understand the deformation mechanism. They are: (1) Nanodiamond reinforced SiC nanocomposites, (2) "carbon" enriched SiC nanostructures and (3) Diamond-SiC nanoscale multilayered films where fraction of "Si" atoms is replaced by "C" atoms. Initial results from atomistic level and subsequent continuum level studies show enhancement in both strength and toughness. Conventional strong but brittle ceramics can't be applied in many future engineering applications where the high stiffness of ceramics is very favorable but unavoidable low toughness is the disappointing point. The outcome of research is shows a successful indication of proposing computationally made a new class of ceramic

materials with high hardness as well as desirable high toughness. It will increase the area of applications of ceramic materials and will meet the future demand of desired material properties.

## .Table of Contents

Acknowledgements .....	iii
Abstract .....	iv
List of Illustrations .....	xi
List of Tables .....	xv
Chapter 1 Introduction.....	1
1.1 Scientific Impact.....	3
Chapter 2 Background, Significance, and Motivation .....	4
2.1 Background and Significance .....	4
2.2 Several Processing Methods of Ceramic Materials.....	8
2.2.1 Traditional Way of Processing Ceramic Materials .....	9
2.2.1.1 Raw Material Preparation/ Milling .....	9
2.2.1.2 Batching and Mixing.....	10
2.2.1.3 Forming .....	10
2.2.1.4 Drying.....	10
2.2.1.5 Firing .....	10
2.2.2 Technical Ceramic Materials Manufacturing Techniques .....	11
2.2.2.1 Sintering .....	11
2.2.2.2 Hot Pressing.....	11
2.2.2.3 Tape Casting.....	12
2.2.2.4 Hot Isostatic Pressing (HIP).....	12
2.2.2.5 Chemical Vapor Deposition (CVD) .....	12
2.2.2.6 Reaction Bonding.....	12
2.2.2.7 Sol Gel .....	12
2.2.2.8 Some Other Processing Methods .....	13

2.2.3 Several Recent Processing Ceramic Materials by the Researchers .....	13
2.3 Main approach of this dissertation .....	15
2.4 Motivation .....	15
2.4.1 Polymer Nanocomposite .....	15
2.4.2 Surface Defect on Nickle Nanowire.....	18
2.5 Proposed Ideas to Enhance Fracture Toughness .....	21
2.5.1 Specific Research Goal .....	23
2.5.2 Outline of Dissertation .....	24
Chapter 3 Generated Models and Software .....	25
3.1 Overview of Molecular Dynamics (MD) simulation .....	25
3.1.1 Fundamental Concepts .....	26
3.1.2 Used Simulation Software .....	28
3.2 Overview of Finite Element Analysis .....	29
3.3 Deformation Analysis.....	29
3.4 Requirements of Others Facilities .....	30
Chapter 4 On the Mode-I Fracture Toughness Prediction of Brittle Nanocrystalline Material Using Atomistic Simulation: A Case Study with Nanoscale Diamond.....	31
4.1 Atomistic Computations of Elastic Properties of Single Crystal Diamond .....	33
4.2 Fracture Toughness Calculations.....	38
4.2.1 Relation between Stress Intensity Factor ( $K_{IC}$ ) and Energy Release Rate ( $G_{IC}$ ) for Single-crystals (with Three Independent Elastic Constants) .....	38

4.2.2 Mode I Fracture Toughness of Diamond using MD Simulation .....	39
4.2.2.1 Griffith's Energy Release Rate via MD Simulation .....	41
4.2.2.2 Crack Tip Opening Displacement (CTOD, $\delta_t$ ) Method via MD Simulation .....	42
4.2.3 $K_{IC}$ and $G_{IC}$ Calculation from Integrated MD-FEM Analysis. ....	45
4.2.3.1 $K_{IC}$ from Irwin's Method .....	48
4.2.3.2 Crack Closure Method via Finite Element Analysis .....	49
4.3 Summary and Conclusions.....	50
Chapter 5 Computational Design of Novel Carbon Enriched $Si_{1-x}C_x$ Ceramics.....	54
5.1 Introduction and Background.....	55
5.2 Molecular Simulations of "Carbon" Enriched SiC .....	58
5.3 Results and Discussions .....	60
5.3.1 Effect of "C" Enrichment on Free Energy Minimization .....	60
5.3.2 Effect of "C" Enrichment on Density .....	61
5.3.3 Effect of "C" Enrichment on Morphology .....	63
5.4 Summary .....	68
Chapter 6 Mechanical Properties of Computationally Designed Novel Carbon Enriched $Si_{1-x}C_x$ Ceramics .....	70
6.1 Introduction and Background.....	71
6.2 Molecular Models and Simulation Procedure .....	73
6.3 Results and Discussions .....	74
6.3.1 Effect of carbon enrichment on Tensile and Shear Response.....	75
6.3.2 Effect of Loading Direction. ....	79
6.3.3 Effect of Random Distribution.....	83
6.3.4 Effect of Free Surface .....	86

6.4 Summary and Conclusions.....	89
Chapter 7 Improving Fracture Toughness of Silicon Carbide Ceramics with Nanodiamond Reinforcements and via Nanoscale Multilayer Ceramics.....	91
7.1 Fracture Toughness Improvement via Reinforcement.....	91
7.1.1 Introduction and Background.....	91
7.1.2 Molecular Modeling of Structure.....	93
7.1.3 Molecular Simulation of Structure.....	95
7.1.3.1 Equilibrium State.....	95
7.1.3.2 Stress Strain Curve from Simulation.....	95
7.1.4 Results and Discussions.....	96
7.1.4.1 Mode-I Fracture.....	96
7.1.4.2 Mode-II Fracture.....	101
7.2 Fracture Toughness Improvement via Nanoscale Multilayer Ceramics.....	103
7.2.1 Introduction and Background.....	103
7.2.2 Molecular Modeling of Structure.....	104
7.2.3 Molecular Simulations of Structure.....	105
7.2.3.1 Equilibrium State.....	106
7.2.3.2 Stress Strain Curve from Simulation.....	106
7.2.4 Results and Discussions.....	106
7.2.4.1 Mode-I Fracture.....	106
7.2.4.2 Mode-II Fracture.....	108
7.2.5 Crack at Interface.....	110
7.2.5.1 Crack at Interface in Different Orientation.....	112
7.3 Conclusion.....	113
Chapter 8 Summary and Conclusion.....	114

8.1 Summary .....	114
8.2 Conclusion .....	114
8.3 Future Recommendations .....	115
References .....	116
Biographical Information .....	137

## List of Illustrations

Figure 1-1 Applications of Ceramic Based Materials.....	2
Figure 2-1 Material Selection [1].....	5
Figure 2-2 Schematic diagram of a) Metallic bond b) Covalent bond.....	6
Figure 2-3 General flow diagram for ceramic processing.....	9
Figure 2-4 MD snapshots of PB, PC and PE models taken at un-deformed states.....	16
Figure 2-5 Effect of nanoparticle dispersion on the bulk stress-strain response of polymer nanocomposites.....	17
Figure 2-6 Cross-sections of all nanowire models are shown at the top. The bottom two images show the nanowire surface of perfect and defect for smallest model.....	20
Figure 2-7 Failure modes of all models studied for the effect of cross-section. The top row and the bottom row represent for perfect and non-perfect systems respectively.....	20
Figure 2-8 Stress-Strain Curves for Cross-section Study.....	21
Figure 2-9 Crystal Structure of (a) Silicon Carbide and (b) Nanodiamond.....	23
Figure 2-10 Strategy to enhance the fracture toughness of SiC.....	24
Figure 3-1 Basic steps of molecular dynamics simulations.....	26
Figure 4-1 Atomistic Model of Diamond with Dimensions.....	34
Figure 4-2 $\sigma_{yy}$ vs $\epsilon_{yy}$ , $\sigma_{xx}$ vs $\epsilon_{yy}$ and $\tau_{xz}$ vs $\gamma_{xz}$ curves generated from molecular simulation of diamonds.....	36
Figure 4-3 Initial atomistic models of diamond with three different crack lengths.....	40
Figure 4-4 a) Atomistic snapshot of deformed “7a0” model, b) a magnified view of right crack tip with illustration to show how CTOD is measured.....	44
Figure 4-5 a) Atomistic snapshots and stress-strain plot of crack-free diamond model simulated for obtaining yield strength (a) snapshots taken at $\epsilon_{yy}=0$ and at $\epsilon_{yy} > 0.2$ (post yield/post failure) and (b) stress strain curve until failure.....	44

Figure 4-6 Schematics to show how equivalent quarter model for finite element analysis has been developed based on original MD model. The sketch of quarter model (bottom right) shows the imposed boundary condition. Note that B.C. #4 has been obtained from the strain at failure  $\epsilon_{yy}$  data obtained from MD simulation of models with different crack lengths (bottom left). ..... 47

Figure 4-7 The  $\sigma_{yy} \sqrt{2\pi x}$  ( $K_{\text{apparent}}$ ) vs.  $x$  plots for the three cracked models and the corresponding projections at  $x=0$  line ..... 48

Figure 4-8 Virtual crack extension simulated by finite elements: (a) before crack extension and (b) after crack extension ..... 50

Figure 4-9 Summary of predicted fracture toughness of diamond using four different methods, (a)  $G_{IC}$  (b)  $K_{IC}$  ..... 52

Figure 5-1 Unit Cell of SiC ..... 59

Figure 5-2 Potential Energy Profile of the “C” enriched models with time. Here  $Si_{0.5}C_{0.5}$  stands for pure SiC and  $Si_{0.0}C_{1.0}$  is for pure Diamond. The energy shown here is normalized per atom. .... 61

Figure 5-3 Change in density of  $Si_{1-x}C_x$  systems as a function of “C” enrichments..... 62

Figure 5-4 Effect of “C” enrichments on the morphology of  $Si_{1-x}C_x$  systems. It is obvious that pure SiC and pure Diamond have predominantly  $sp^3$  bonded atoms. However, the other “C” enriched systems have some bonding other than  $sp^3$  type. .... 63

Figure 5-5 Equilibrated Crystal Structure of different “C” enriched models projected on 2D plane..... 65

Figure 5-6 “Ideal” radial distribution plot based on initial SiC model that shows different atom-atom neighbor distances..... 67

Figure 5-7 Radial distribution plot of different “C” enriched systems. Note the sharp peaks in the SiC and Diamond systems. Also note that Si-C to C-C bond transition in other “C”

enriched systems. Presence of “disturbed” microstructure is evident from wider “width” of different peaks.....	69
Figure 6-1 Equilibrated Crystal Structure of different “C” enriched models projected on 2D plane.....	77
Figure 6-2 Stress-Strain curves for different carbon enriched models (a) Tensile response, (b) Shear response .....	78
Figure 6-3 Tensile failure snapshots for different “C” enriched models.....	79
Figure 6-4 Shear failure snapshots for different “C” enriched models. To clearly identify shear failure locations, atoms are colored by coordination number and von-mises shear strain at the top and bottom figures .....	79
Figure 6-5 Tensile response of “small” models (total 2744 atoms) along (a) x, (b) y and (c) z directions.....	81
Figure 6-6 Tensile response of “large” models (total 57600 atoms) along (a) x, (b) y and (c) z directions.....	83
Figure 6-7 Equilibrium MD snapshots of three independently created Si <sub>0.2</sub> C <sub>0.8</sub> samples (each system contains 57600 atoms). The circles with light blue color and grey color represent Si and C atoms respectively. ....	84
Figure 6-8 Effect of random distributions on the tensile response of carbon enriched models. Figures (a) to (c) represent responses of three different set of models .....	86
Figure 6-9 Tensile failure snapshots for different “C” enriched models simulated without any periodic boundary conditions in the lateral directions .....	88
Figure 6-10 comparative Tensile Stress-Strain curves for different carbon enriched models simulated with and without periodic boundary conditions in the lateral directions .....	88
Figure 7-1 a) Pure SiC structure (Blue = Si, Red = Carbon), b) Pure ND structure .....	93

Figure 7-2 a) Pure SiC with crack b) A sliced view of ND reinforced SiC with crack. c) A sliced view of hollow ND reinforced SiC with crack, d) A sliced view of uniformly dispersed ND reinforced SiC with crack .....	94
Figure 7-3 Stress-strain curve when pure ND is inserted as nanoparticle .....	96
Figure 7-4 Failure snapshots of a) Pure SiC with crack. b) ND reinforced SiC with crack .....	97
Figure 7-5 Stress-strain curve when pure ND as frozen is inserted as nanoparticle .....	98
Figure 7-6 Failure snapshots of rigid ND reinforced SiC with crack .....	98
Figure 7-7 Stress-strain curve when pure ND as frozen is inserted as nanoparticle .....	99
Figure 7-8 Failure snapshots of hollow ND reinforced SiC with crack.....	99
Figure 7-9 Stress-strain curve when frozen hollow ND is inserted as nanoparticle .....	100
Figure 7-10 Failure snapshots of rigid ND reinforced SiC with crack .....	100
Figure 7-11 Stress-strain curve when pure Si is inserted as nanoparticle .....	101
Figure 7-12 Stress-strain curve for shear load in all cases.....	102
Figure 7-13 Failure snapshots of shear failed (a) ND-SiC composites, (b) Pure SiC ....	102
Figure 7-14 SiC in the middle containing crack and ND are on the both side of SiC. Upper and lower layers are created for applying load a) SiC:ND=1:1, b) SiC:ND=2:1, c) SiC:ND=3:1 .....	105
Figure 7-15 Stress-strain curve for tensile loading .....	107
Figure 7-16 Failure snapshots of tensile failure .....	108
Figure 7-17 Stress-strain curve for mode II fracture .....	109
Figure 7-18 Failure snapshots of mode II fracture .....	109
Figure 7-19 Snapshots for Models a) ND, b) SiC, c) Interphase .....	110
Figure 7-20 Failure Snapshots for ND, SiC, Interphase .....	111
Figure 7-21 Curves for different crystal orientation of Silicon Carbide .....	112

## List of Tables

Table 4-1 Predicted elastic properties of diamond in comparison with reported data .....	37
Table 4-2 Predicted fracture toughness of diamond via Griffith's energy release rate criterion.....	42
Table 4-3 Predicted critical strain energy release rate of diamond using CTOD method	45
Table 4-4 Predicted critical stress intensity factor of diamond using CTOD method .....	45
Table 4-5 Boundary conditions used in finite element analysis for predicting fracture toughness using Irwin's stress intensity factor method and crack closure method .....	46
Table 4-6 Predicted fracture toughness of diamond using Irwin's stress intensity factor method .....	49
Table 4-7 Predicted fracture toughness of diamond using crack closure method.....	50
Table 4-8 Comparison of Predicted Fracture Toughness of Diamond with existing literature .....	51
Table 6-1 Measured Properties of different "C" enriched systems from atomistic simulations .....	75

## Chapter 1

### Introduction

The objective of my research was to understand the toughening mechanism of ceramic materials without sacrificing significantly other mechanical properties. In order to reach my goal, I have been investigating computational design of novel ceramic materials by nano-scale micro structure engineering and proposed several potential models to achieve target.

Ceramic materials are generally classified as nitrides, oxides, carbides, etc. They are nonmetallic, inert, crystalline or non-crystalline materials composed of metals and non-metals. It has been utilized from thousand years back in pottery industries and many other industries, and recently it has been considered for structural applications (as shown below) due to their strong, stiff, brittle, withstanding capability in high temperature, wear, corrosion and abrasive resistance, and other properties. Ceramics materials are also light weight structure compare to other structural materials such as steel and it also carries lower cost than steel. Ceramic materials have lot of applications shown in figure 1-1 for their incomparable properties and a chart is shown below the wide variety of applications. It is highly expected in most engineering applications that a material should be tough as well as stiff but unfortunately low toughness property of ceramics limits their applications in many areas. This low toughness property cause difficulties to control dimensional tolerance while processing, propagate crack easy and fail the material very quickly, make crack when heavy items hit on it. Researchers are trying to overcome this problem by enhancing the fracture toughness property of ceramic materials in several ways.

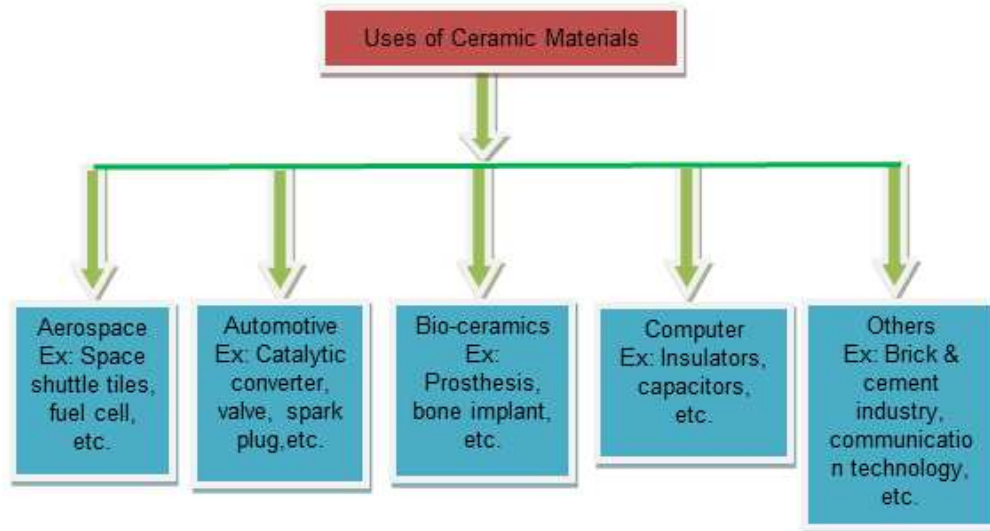


Figure 1-1 Applications of Ceramic Based Materials

Fracture toughness is the resistance to crack growth implying it quantifies how a material responds to resist ultimate failure. Cracks are always generated when a part experiences loading, especially fatigue loading. These cracks are accumulated and cause a catastrophic failure in brittle material such as in ceramics. Fracture toughness is also directly related with ductility as more ductile material has higher fracture toughness. Ductility of a material is the ability to deform under loading which is important to dissipate energy.

Strength and toughness are mutually exclusive in majority of materials though it is desired in most of the engineering applications [1]. Natural bio-materials offer an excellent opportunity to accommodate a wide range of desired properties due to their multi-scale hierarchical structure (e.g. bone). Ceramic materials can survive in harsh environment such as very high temperature compared to metals but their low toughness property is the major barrier. Several techniques have been employed by researchers

and experts, both experimentally and computationally, to avail the required mechanical properties such as co-existing high strength and high toughness in ceramic materials.

### 1.1 Scientific Impact

Ceramic materials have wide variety of potential applications because of their high strength, inertness, wear resistance, etc. But the brittleness of ceramic restricts its applications where a lot of energy required to be absorbed. This brittleness of ceramic materials comes from their bonding character. Atomic bonding in ceramic materials can be both ionic and covalent in character. Covalent bonding character prevails in the carbides of ceramic materials. The degree of covalent bonding character increases if the difference between electro-negativity of atoms is decreased. Covalent bond is a directional bond which doesn't easily allow dislocation motion of atoms. These factors are responsible for low toughness property in ceramic materials as dislocation is directly related with toughness.

Toughness property increases the durability of a material and prevent from catastrophic failure. It will ensure a long life where the ceramic materials are being used for their unique property of high strength, resistance to high temperature and corrosion, etc. Ceramic materials can be a best candidate in applying more sectors if the fracture toughness property can be enhanced.

## Chapter 2

### Background, Significance, and Motivation

#### 2.1 Background and Significance

Ceramics are very strong material compared to metal as they are bonded with covalent or ionic bonds. These bonds are stronger than metallic bond which exhibit a high hardness. Ceramic materials have high melting point compared to metals or other materials which is a reason for choosing ceramic materials for high temperature applications. Mechanical properties of different classes of materials are shown in figure 2-1 which exhibits that ceramic materials have low fracture toughness property. This low fracture toughness of ceramic materials is the main obstruction for using harsh environment such as high temperature. The directional covalent bond impedes the deformation as well as dislocation of the material which results a low toughness property of entire material. Several researchers are extensively trying to increase the toughness (no crack is present) and fracture toughness property (when a crack is present) of ceramic materials without losing significantly other mechanical properties of ceramic materials. We can see from the figure 2-1 [1] that polymer types of material has low fracture toughness and yield strength. Metallic alloys are not as strong as ceramic materials. We can see another candidate like metallic glasses which are amorphous and cannot be used in high temperature as these materials become weakened and soft. So the only candidate remains which are ceramic based materials and they are the strongest but fracture toughness is the lowest. Now we will discuss about the reason why metal shows the ductility but ceramic materials not. Valence electrons which remain at outermost shell play an important role to explain the ductility of a material.

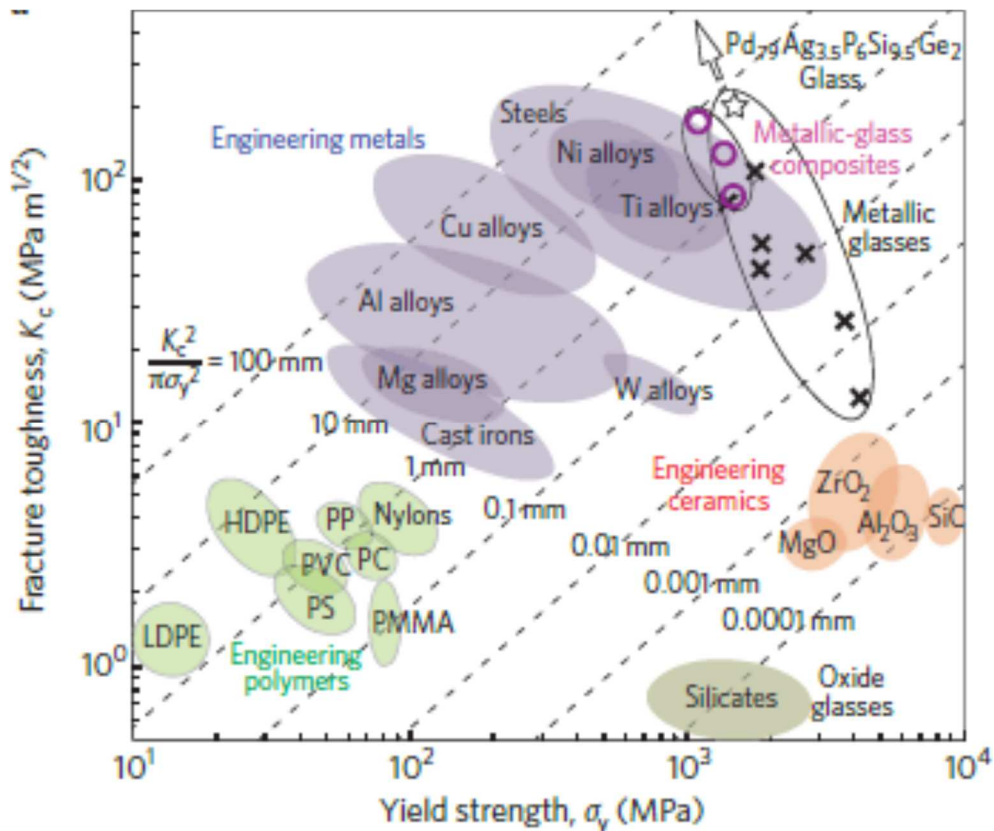


Figure 2-1 Material Selection [1]

Valence electrons are loosely bonded in metallic materials with positive charge which is shown in figure 2-2 (a). These electrons allow deforming the whole materials. Moreover, metals especially for face centered cubic crystal structured ones, allow dislocations along the maximum planar atomic density planes. Dislocations are directly related to plastic deformation, which in turn, can enhance the toughness of materials. Ceramic materials don't allow dislocation as it has covalent bond which is directional shown in figure 2-2 (b). So tailoring of mechanical properties especially toughness is no longer an easy task though the experts are trying to come up with a desirable material which will have high stiffness as well as demanded toughness.

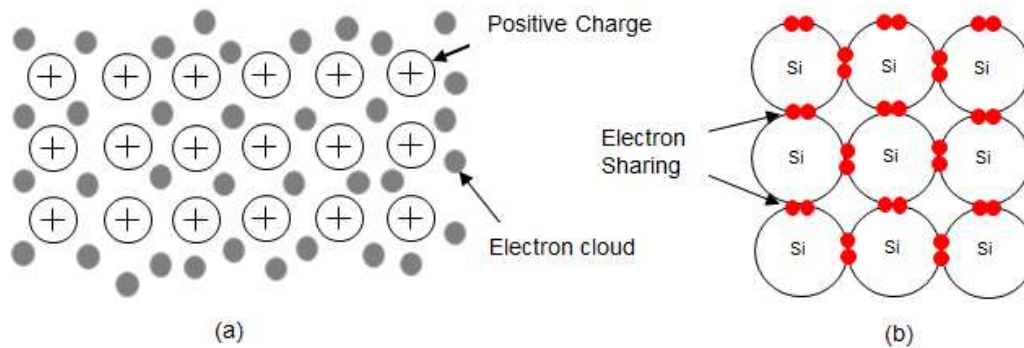


Figure 2-2 Schematic diagram of a) Metallic bond b) Covalent bond

Materials which have higher toughness generally experience a ductile fracture. Dislocation always plays an important role in ductile fracture by intensifying plastic deformation. It is important to emphasize on atomistic level to understand the behavior of material. Investigation of atomistic level of ceramic structure is more focused to comprehend the mechanical behavior.

Crack is nucleated under loading conditions in every materials and propagation of crack causes disaster for entire structure. Brittleness of ceramic material cannot resist the crack when it propagates which represent the lower toughness property. So it is generally expected higher fracture toughness property in a material. Researchers are in venture to come up with a new ceramic based material with higher fracture toughness. Zhang et al. described [2] several experimental techniques to enhance the fracture toughness property of materials including crack blunting, crack bridging or strain field relaxation around the crack tip. They also described the layer by layer arrangement of ductile and brittle materials which ultimately shows greater toughness and strength by combining their properties. Kueck et al. exhibit that [3] doping of rare earth series additive such as Yttrium (Y) can increase the toughness of a material. They doped 0.5% and

0.7% of Yttrium in two different samples in SiC which contains 3% of Aluminum, 0.6% Boron and 6% carbon. The fracture toughness and stiffness has been increased for 0.7% of Yttrium compare to 0.5% in amount of 40% and 61% respectively. They also investigated that only amount of doping is not playing the key role whether the location has something to do. They have shown that doping in grain boundary phase can enhance fracture toughness. Jumpei et al. have shown [4] experimentally that vapor grown carbon nanofiber can play an important role to enhance fracture toughness property of silicon carbide ceramic. With addition of 6 mass% VGCF, the fracture toughness property can be increased to 5.2 MPa.m<sup>1/2</sup>. 8 mass% Al<sub>4</sub>C<sub>3</sub> and 2 mass% B<sub>4</sub>C are also used as sintering aid. Edwin H Craft and Richard H. Smoak have experimentally shown that [5] fracture toughness of alpha silicon carbide depends technique of measurement such as single edge notched beam (SENB), double torsion (DT), etc. V. Hatty et al. interpreted that [6] fracture toughness is structure insensitive material property. They did the experiment with SiC on Si wafer and SiC on SiO<sub>2</sub> got almost the same value of fracture toughness. Fracture toughness is possible to enhance at higher pressure and temperature which is explained by Zhao et al [7]. They used 90:10 of diamond to silicon carbide mixture and did an indentation test. Moreover, SiC can exhibit better fracture toughness property in cryogenic temperature which is around 77 K. It is shown by Yi et al [8] by an indentation process and the samples were made through spark plasma sintering (SPS). A small amount of carbon incorporation can enhance the fracture toughness property of Al<sub>2</sub>O<sub>3</sub>/TiC ceramic composite. Increasing the content of 4% can increase the fracture toughness property of 22% which is reported by Xu et al [9]. Fracture toughness can be enhanced [10] by enriching Aluminum (Al) in Silicon Carbide (SiC). Boron (0.6%) and Carbon (2%) are also added in certain amount in SiC. Al is varied from 3-7% (3ABC-7ABC) in total material system of SiC where boron and carbon

are already incorporated. Here SiC is containing Aluminum (Al), Boron (B) and Carbon(C) so it is called Silicon Carbide Ceramics (ABC-SiC).

Researchers are becoming interested in computer simulation due to the availability of immense power of computational facility. Complex models can be built and it is easy to make a prediction what might happen in experiment through computational technique. Now-a-days millions of atoms can be simulated to understand the atomistic level of science. Many Software of molecular dynamics simulation are available to model and analyze numerous atoms. Kalia et al [11] used molecular dynamics simulation and explained that the interfacial area of nanoparticles is amorphous which actually act like a closed loop for nucleated crack. They revealed that nanostructured  $\text{Si}_3\text{N}_4$  has fracture toughness property of six times than crystalline  $\alpha$ -  $\text{Si}_3\text{N}_4$ .

J. Yi et al [8] have shown that quartz glass could show an enhanced fracture toughness property at very low temperature as 77 K. Mo et al. [12] reported a non-diffusional mechanism of reducing grain size which will eventually hinder the crack growth by plastic flow along grain boundary.

Experts are still continuing their endeavor to discover a new idea to increase the fracture toughness. More works of researchers will be discussed in different chapter.

## 2.2 Several Processing Methods of Ceramic Materials

Ceramic materials processing is important to get the desired size, shape, properties and ability to refine the materials. Second World War is the turning point for actual revolution in material processing industry to meet the requirements of high performance materials. In line of the research, numerous advanced ceramic materials have been invented which actually contribute to strengthen in nuclear industry, military,

communications, aerospace, automotive and other fields. Ceramic materials also have a contribution in electronic industry after having many advanced ceramics. Ceramic materials are producing for couple of hundreds decade to meet the requirements of pottery and others in a conventional way and now-a-days it is producing in different ways based on the applications with desired properties.

### 2.2.1 Traditional Way of Processing Ceramic Materials

Pottery is the oldest use of ceramic materials about four thousand years ago. Clay was used to make the pottery. A traditional way of making ceramic materials is furnished here in figure 2-3..

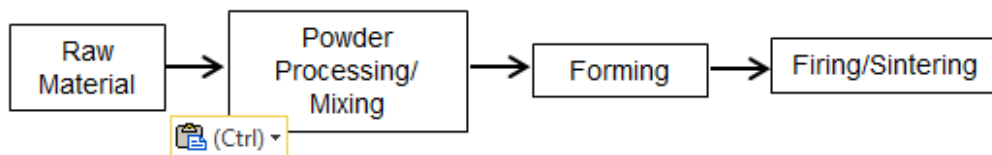


Figure 2-3 General flow diagram for ceramic processing

#### 2.2.1.1 Raw Material Preparation/ Milling

In past days, the potters had to dig the soil to get the desired clay as raw material but now-a-days it is commercially available in market. Large pieces are broken into small pieces in milling process by applying mechanical means such as compression or impact. Jaw, roller and cone crusher are the example of compression mill and ball milling is the example of impact mill.

#### 2.2.1.2 Batching and Mixing

Batching is the system of weighing for specific recipes and then it is mixed with the help of machine. It is trying to mix in such a way that there should be no bubble inside.

#### 2.2.1.3 Forming

It is the procedure of making shape for the applications such as toilet bowl, basin or pottery. A numerous process is involved in this stage such as casting, molding, pressing and other methods. It is very important step as the materials are shaped for specific use. It is the step of before drying called green body which is very soft and malleable. It is handled carefully as extra load can change the shape.

#### 2.2.1.4 Drying

The main purpose of this step is to remove the waters from the green body. Heat is applied on the green body to remove the water. It is done carefully as excessive heat can cause the thermal cracking and surface defects. The material becomes smaller and brittle after drying process.

#### 2.2.1.5 Firing

The main chemical change is occurred in this stage after passing through a controllable heating process. Sintering and bonding take place to get the desired properties.

### *2.2.2 Technical Ceramic Materials Manufacturing Techniques*

The uses of ceramic materials are increasing as technical ceramics. The processing techniques are modified to obtain the specific desired properties. One of the disadvantages is to control the dimensional tolerances during processing. Ceramics are classified based on their applications are:

- ✓ Glasses (Households, containers, etc)
- ✓ Clay products (White ware, toilet bowl, etc)
- ✓ Refractories (Bricks, etc)
- ✓ Abrasives (Cutting, sand papers, etc)
- ✓ Cements (Structural material)
- ✓ Advanced ceramics (Automotive, military, mining, etc)

Almost all ceramics start with powder form of raw materials and binders. Some of the better known ceramic manufacturing processes combine sintering with forming.

#### 2.2.2.1 Sintering

Ceramic components are mixed and placed in a high temperature. The densification is occurred by eliminating porosity and growing grain in ceramic. The part is shrunk and ready when the temperature reduced to ambient temperature.

#### 2.2.2.2 Hot Pressing

This method is for making simple geometry but dense product. The powder is placed in mold and uniaxial pressure and temperature is applied. Mold is formed based on the required shape.

#### 2.2.2.3 Tape Casting

A chamber is required to place the ceramic slurry and a doctor blade is appointed to control a small gap of the chamber. Slurry is then passed through the gap of chamber and doctor blade.

#### 2.2.2.4 Hot Isostatic Pressing (HIP)

A capsule is required to pack the powder form of raw materials. The capsule should withstand in uniform high pressure and temperature. It can create simple as well as complex shape.

#### 2.2.2.5 Chemical Vapor Deposition (CVD)

This is the process where gases is continuously deposited on a substrate and make a monolayer. Controlling temperature and pressure is the critical point. The material is pure but it involves high cost. The product is sometimes susceptible to corrosion.

#### 2.2.2.6 Reaction Bonding

It is a chemical reaction based process where the ceramic powders are bonded in a solid form. The binder creates porous platform after heating and the reactants are infiltrated in porosity. It is done above the melting temperature. One of the main problems in this process is high porosity.

#### 2.2.2.7 Sol Gel

Metal salt is the starting material which is converted to metal oxides. Dilute acid or water is added to make a gel. After removing the water, it becomes stiff gel. Mainly

oxides are produced by this method and the required temperature is lower than other processes.

#### 2.2.2.8 Some Other Processing Methods

- ✓ Polymer pyrolysis
- ✓ Hydrothermal synthesis
- ✓ Gas phase synthesis
- ✓ Microwave processing
- ✓ Extrusion
- ✓ Die processing
- ✓ Injection molding

#### 2.2.3 Several Recent Processing Ceramic Materials by the Researchers

Technical ceramics are dominating in numerous areas of applications which require a specific processing path. S.R. Wylie et al. [13] describe a ceramic fibers processing method from ceramic rod which is used in fiber reinforced polymer composite. Microwave plasma jet is a source of intense, chemically inert, localized heat. Generation of microwave plasma jet can be used in processing of fibers. Tailoring the properties of plasma jet can be suitable for processing different tasks. A method of carbon film production on  $\beta$ -SiC is described by Y.G. Gogotsi et.al [14]. They exhibit that by reacting with  $\text{Cl}_2$  and SiC can produce carbon film and observed by using TEM, SEM, XRD, etc.

Solid state tunable laser is a necessary technology for remote sensing and Narasimha S. Parad et al. [15] explained a solid state laser of Neodymium doped Yttria. A mixture of Yttrium oxide and Neodymium oxide are primarily used as raw material and only synthesis and characterization are described in this paper. Moreover, factors such

as firing temperature, soaking time, etc. of the processing method play an important role on technical properties. D. Njoya [16] explained these by investigating with X-ray diffraction and scanning electron microscopy. Fracture toughness property can be increased by producing a nanostructured diamond-SiC composites. Y. Zhao et al. [7] describes about this composite which can be generated in ball milling as well as a rapid reactive sintering process. Stephen T. Rasmussen et al. [17] have shown a particle size dependency on sintering shrinkage for dental porcelain. They have shown that mixing of smaller particle size lead to a lower shrinkage. Dry pressing method can be used for high production. The easy procedure make very popular of two methods such as die pressing and cold isostatic pressing [18, 19, 20] in industrial production of ceramic materials. Novel processing methods [21] are also using for past decade such as direct casting method. The main concept is to contain homogeneous state of dense slurry before sintering to ensure high reproducibility and reliability. Cellular ceramics are a new class of material with high porosity (at least 60%). Paolo Colombo [22] describes several methods to process cellular ceramics such as foams, honeycomb, etc. Foams are manufactured by so called replica technique and honeycomb is produced by paste extrusion technique. J. Binner et al. [23] describe gravity fed infiltration method of processing ceramic metal composites. The processing parameters are studied such as temperature, atmosphere, gas flow to understand the infiltration kinematics. The composites are characterized by SEM. F.F. Lange et al. reviewed [24, 25, 26, 27] several papers based on processing in infiltration and pyrolysis method. They have also shown that porous matrix can be stronger than partially dense material. D. Hotza and P.Greil reviewed [28, 29, 30, 31] several works base on various casting processing methods such as tape casting, doctor blade processes. Mostly alumina powders are used as primary material and additives such as binders, cellulose ethers, and plasticizers are used. Process variable have

significant effect when slurries are employed. R. Chaim et al. reviewed [32, 33, 34] several papers based on sintering process including pressure less sintering, microwave sintering, hot pressing, etc.

### 2.3 Main approach of this dissertation

Researchers are trying to develop new ceramic materials as composite in different ways as it is becoming a challenge to enhance the fracture toughness property of ceramic materials. In my research, Silicon carbide (SiC) has been chosen because of their high hardness and it's a goal to increase the fracture property so that it becomes a good candidate material in several applications that described before. Silicon (Si) and Carbon (C) has electro-negativity respectively 1.8 and 2.5. It shows that SiC has 88.47% ( $e^{-((2.5-1.8)^2)/4}$ ) of covalent bond in character. It is really a vigorous job to infuse toughness property in SiC because of their directional bond. Dislocation movement is quite unfavorable considering inherently rigid bond network and directional properties. Movement of crack craves bonds to be broken and remade at the same time distortion of bond angles to be happened. Several attempts have been taken computationally to enhance the mechanical properties of Silicon Carbide (SiC) by intrinsic and extrinsic process. More details will be discussed in different chapters.

### 2.4 Motivation

#### 2.4.1 *Polymer Nanocomposite*

This work has been published in journal Polymer [35] which is available online. The work is reused here under the license agreement between Sheikh F Ferdous (author) and Elsevier of license number 3622581034120 which is provided by Copyright Clearance Center.

Nano-particle infusion in matrix material is becoming a common practice to enhance the mechanical properties as well as other properties of that material after having a numerous study. Size and shape of nano-particle [36] also play a key role to tailor the mechanical properties. For example, we have investigated the effects of nanoparticle in polyethylene matrix to comprehend the essence of atomic level mechanics.

Dispersion and intensity of filler and matrix interface interactions were center of interest to observe the mechanical properties of bucky ball ( $C_{60}$ ) as nanoparticle reinforced polyethylene nanocomposites. We have compared the mechanical properties of neat polymer (PE) and twenty seven bucky balls reinforced in neat polymer matrix. Bucky balls were either clustered (PC) or homogeneously distributed (PB) which is shown in figure 2-4. We have also investigated the interaction between polymer and bucky balls by altering the van der waals interaction energy potential. Hydrostatic tensile test is done for all three conditions. We have generated stress-strain curves to perceive how the nanoparticle can modify matrix morphology which eventually control the total polymer matrix nanocomposite.

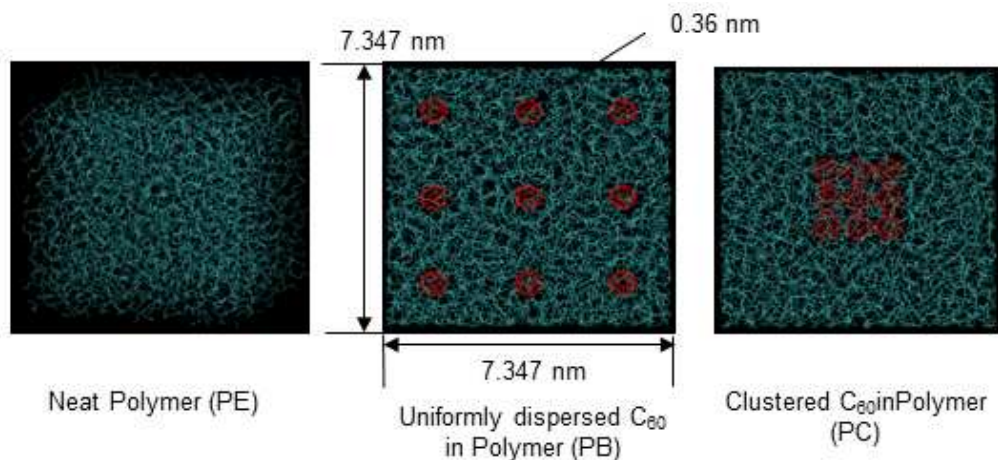


Figure 2-4 MD snapshots of PB, PC and PE models taken at un-deformed states

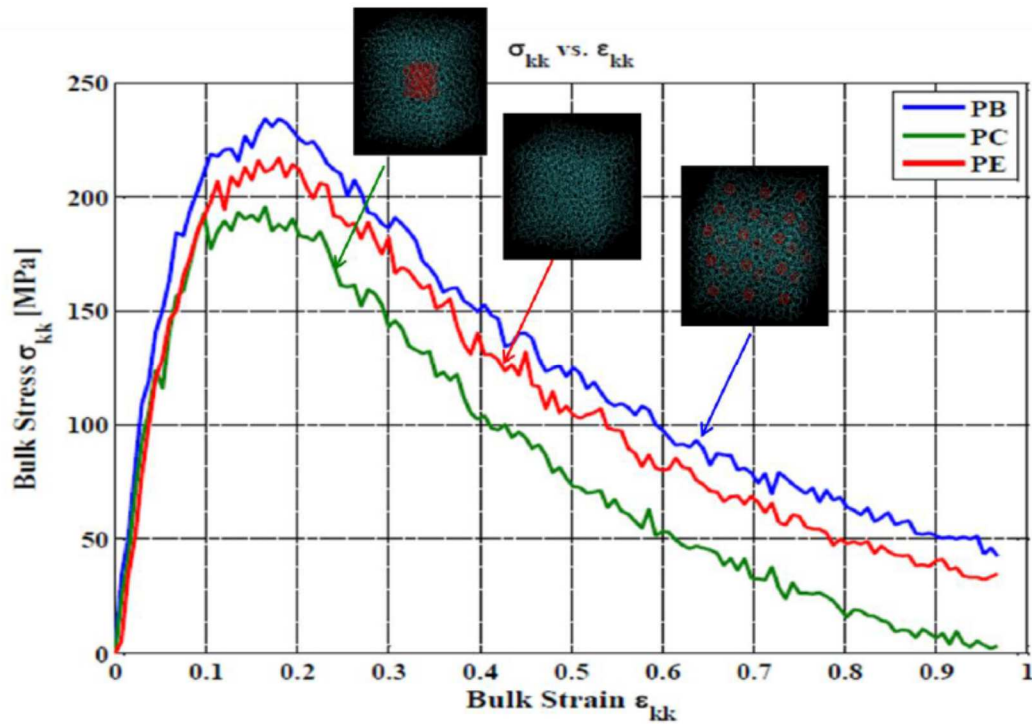


Figure 2-5 Effect of nanoparticle dispersion on the bulk stress-strain response of polymer nanocomposites

We have already introduced that  $C_{60}$  nanoparticles are uniformly distributed in the PB system but remain in clustered form in the PC system. We have furnished the result of bulk response in figure 2-5. The PB system shows ~7.8% improvement in bulk failure strength and 16% improvement in bulk stiffness in compare to PE system. PC system is showing the poorest performance among the three systems. It is clearly showing that inclusion of nanoparticle can alter the mechanical properties in a matrix system.

#### *2.4.2 Surface Defect on Nickel Nanowire*

This work has been published in journal Computational Material Science [37] which is available online. The work is reused here under the license agreement between Sheikh F Ferdous (author) and Elsevier of license number 3622581262207 which is provided by Copyright Clearance Center.

Using molecular dynamics (MD) simulation method, we have studied the stress-strain response of the single-crystalline nickel nanowire containing a single surface defect. To gain quantitative understanding on the deformation process, we have systematically studied the effect of nanowire cross-section, nanowire length, test temperature, randomness in defect location and location of defect from nanowire edge on the tensile mechanical properties of defective Ni nanowires and contrasted with perfect systems. In each case study, we investigated the comparative deformation processes and the associated stress-strain laws to reveal the role of single defect on the mechanical behavior of Ni nanowires. Our study reveals that even a single defect can cause significant degradation in the failure strength and toughness of a perfect nanowire as long as the cross section of nanowires is in the nanometer range. Our study also reveals that the effect of point defect becomes less critical when nanowires become thicker.

It can be inferred from these studies that presence of surface defects influences the nanowire thermodynamics and microstructures. It is however, not very clear how does a single surface defect influence overall mechanical performance of nanowires. The effect of cross-section is only furnished here where the cross-section of Nickel nanostructure has been increased by keeping the height constant. For each case, we developed model pairs comprised of a perfect (P) and defective (non-perfect) (NP) (single atom missed on surface) models. Molecular models of single crystal Nickel (Ni) are developed by expanding the F.C.C unit cell of Ni in three directions. Six models of

Nickel with identical length (3.52 nm) but varying cross sections are created as shown in Fig.2-6. Only square cross section models are developed. The cross sections are varied by using different expansion factor (EF) along the respective direction (X and Y) when models were built from the Ni unit cells. The smallest model has EF = 5 which yield a total of 1000 atoms in the system. Bigger models are built by incrementing EF by one and the largest model has EF = 10. Defect is created only on a surface parallel to nanowire length axis (XZ or YZ plane).

Six models have been simulated to study the effect of cross-section on the mechanical properties of Ni nanowire with a single surface defect effect. The length of all models is 3.52 nm and the smallest model has a cross-section of  $1.76 \times 1.76 \text{ nm}^2$ . In the larger models, the cross-sections were increased and the largest model has a cross-section of  $3.52 \times 3.52 \text{ nm}^2$ . All models have single atom missing on their surface. All models are compared corresponding to its non-perfect counterpart. Failure snapshots are shown in Fig. 2-7.

It is evident from Fig. 2-7 that the failure always initiates from the defective position of all non-perfect models. All models appear to be failed in shear. Figure 2-8 shows the corresponding stress-strain curves. It can be inferred from Fig. 2-8 that all non-perfect models exhibit lower failure strength than perfect models when cross sections eight or smaller layers thick. For thicker models, the strengths of perfect and non-perfect systems coincide implying the role of one single defect becomes insignificant. The difference in failure strength between perfect and non-perfect becoming closer as the cross-section is increased.

Failure started from the defect position in all type of study. Only effect of cross-section has been discussed here which motivated towards the next step of research and detailed has been described in manuscript.

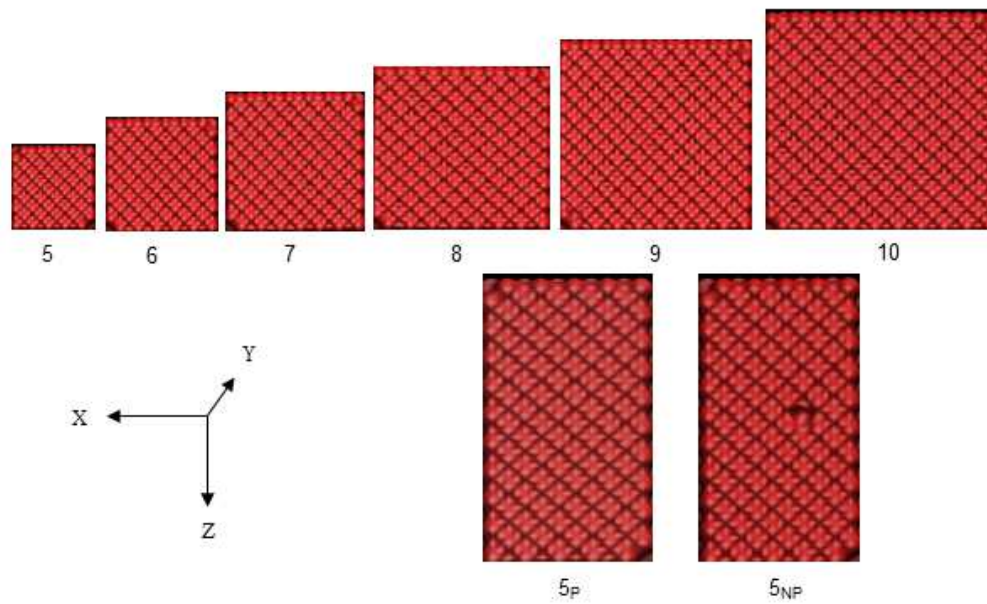


Figure 2-6 Cross-sections of all nanowire models are shown at the top. The bottom two images show the nanowire surface of perfect and defect for smallest model

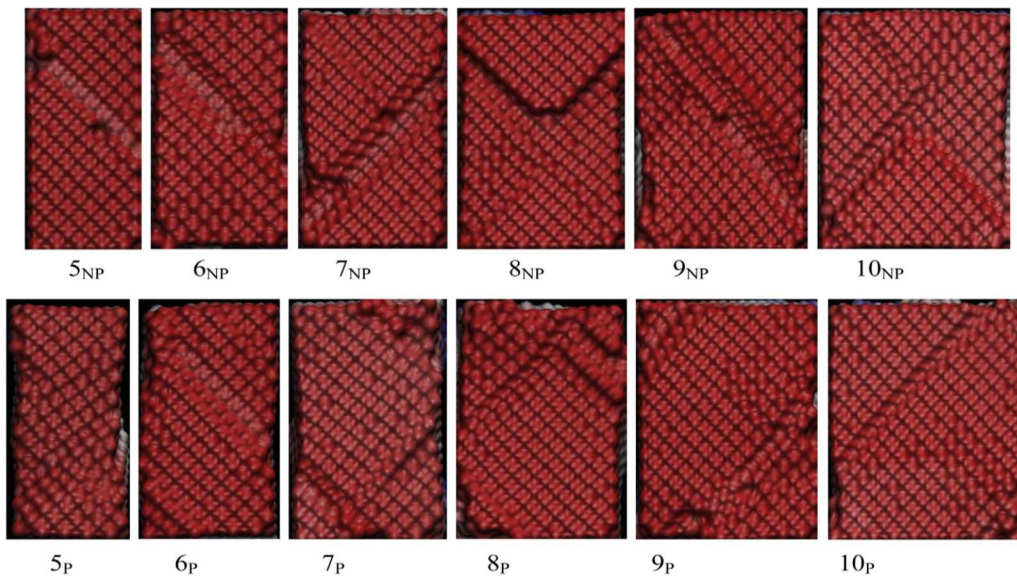


Figure 2-7 Failure modes of all models studied for the effect of cross-section. The top row and the bottom row represent for perfect and non-perfect systems respectively

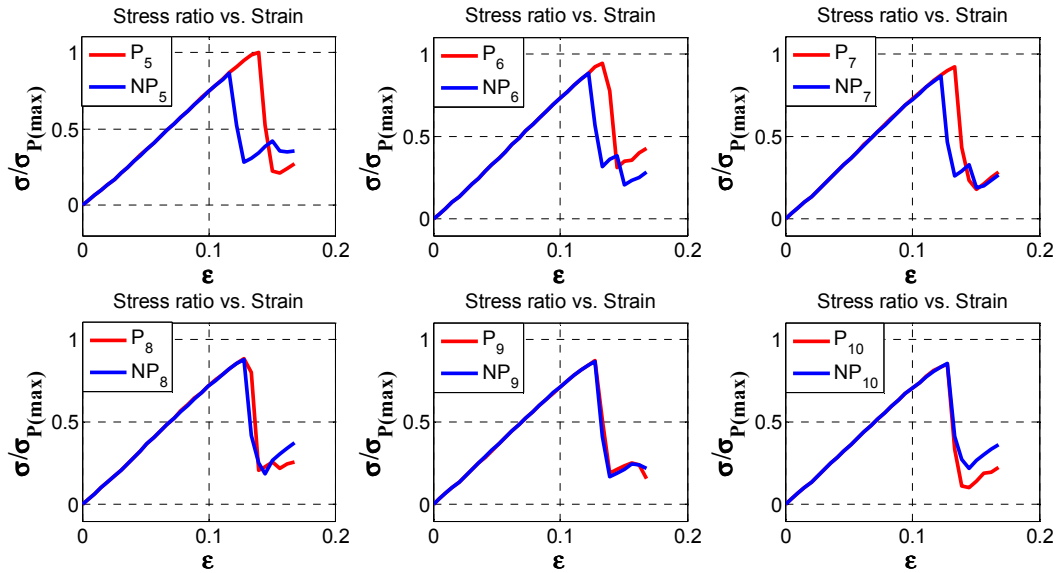


Figure 2-8 Stress-Strain Curves for Cross-section Study

These investigations carry lot of interest about surface damage [38, 39, 40] and crack propagation which direct the research towards enhancement of fracture toughness of ceramic materials. Surface damage and impact failure are also concern for any material now a day [41, 42, 43, 44, 45, 46]. The reason to select the ceramic materials has already been discussed.

Investigations of the mechanics of biomaterials [47, 48] also motivate to find the research direction at the earlier stage of my degree.

## 2.5 Proposed Ideas to Enhance Fracture Toughness

Ceramic materials are really promising material as advanced structural material but low toughness is one of the main barrier. Toughness can be enhanced either by using “Extrinsic” or “Intrinsic” mechanisms. The intrinsic mechanism results essentially

from plasticity and enhances a material's inherent damage resistance and the extrinsic toughening mechanisms act primarily behind the tip to impede crack advance. Ceramic material experts are trying extensively to come up with a new class of material which will have high toughness as well as high hardness. Some approaches are as follows:

- ✓ Bio-inspired ceramics [49] is a new class of material with combination of 98.5 vol.% alumina (mainly platelets and nanoparticles), 1.3 vol.% silica and 0.2 vol.% calcia. It is like a nacre structure.
- ✓ Transformation toughening [50, 51, 52, 53, 54] that involves transformation from one phase to another phase due to stress. Zirconia toughened alumina is one of the example.
- ✓ Micro-crack toughening [55, 56, 57, 58] where one constituent (e.g  $\text{Si}_3\text{N}_4$  in SiC) assists to create microscale cracks in the microstructure to enhance toughness via additional energy dissipation.
- ✓ Ductile phasing [59, 60] where strain relaxation is happened due to a ductile phase deformation around crack tip. Crack blunting also increase the fracture toughness in ceramic materials.
- ✓ Multi-layering [61, 62, 63, 64, 65, 66, 67, 68] to enhance adhesion between film and substrate (e.g TiN/ZrN multilayers).
- ✓ Fiber bridging [69, 70, 71, 72, 73, 74, 75, 76] where cracks are deflected at the fiber/matrix interface (e.g. alumina/SiC).

Researchers are also trying by inclusion of other materials and by reducing the grain boundaries but most of them are extrinsic techniques.

### 2.5.1 Specific Research Goal

Three methods have been approached to enhance the fracture toughness property both extrinsic and intrinsic techniques without losing significantly other properties especially strength. We selected here silicon carbide (SiC) as main ceramic material and nanodiamond (ND) (shown in figure 2-9) as a supportive material to enhance the fracture toughness of SiC. Both SiC and ND have the similar zinc blend structure.

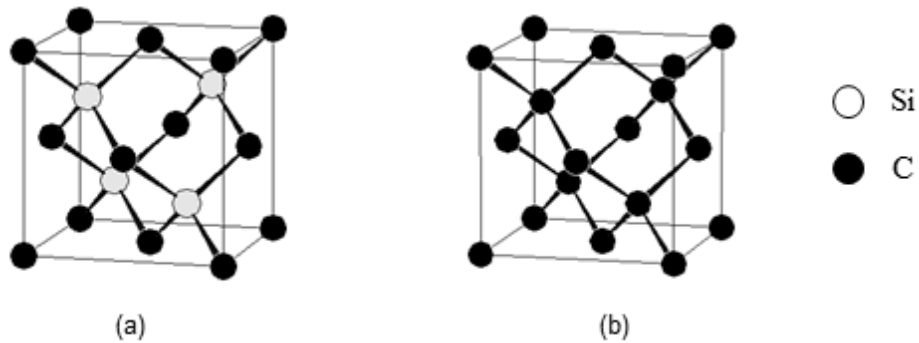


Figure 2-9 Crystal Structure of (a) Silicon Carbide and (b) Nanodiamond

We are proposing to develop three types (figure 2-10) of ceramic materials:

- ✓ Type 1: "Carbon" enriched SiC nanostructures where a fraction of "Silicon" atoms is replaced by "Carbon" atoms,
- ✓ Type 2: Nanodiamond (Np) reinforced SiC nanocomposites, and
- ✓ Type 3: Diamond-SiC nanoscale multilayered nanofilms.

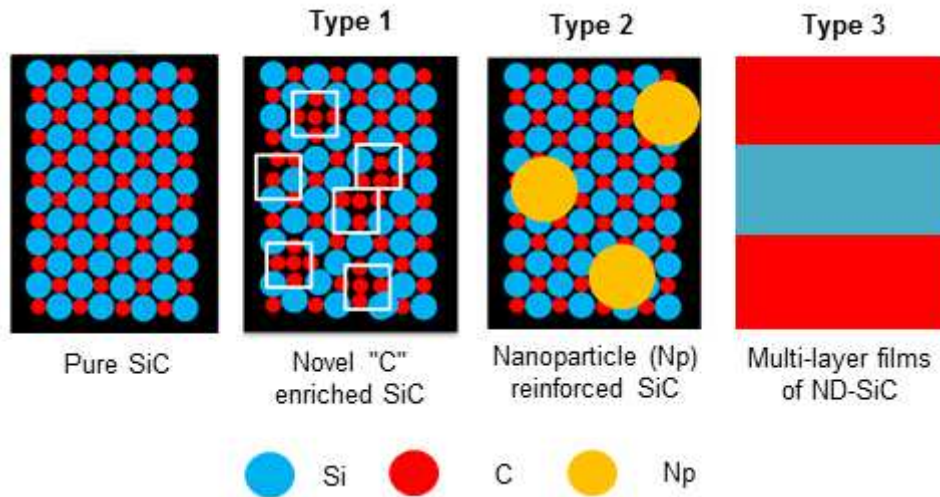


Figure 2-10 Strategy to enhance the fracture toughness of SiC

### 2.5.2 Outline of Dissertation

The remainder of this dissertation is organized as follows: In chapter 3, availed research facilities are discussed. Molecular dynamics simulation software, FEA simulation software, molecular graphics software and numerical computing software are contributing to get the models and post-process results. In chapter 4, possible way of estimating fracture toughness in nanoscale has been discussed. In chapter 5, carbon enrichment process is proposed to enhance the mechanical properties of silicon carbide. In chapter 6, effect of carbon enrichment process on mechanical properties of SiC has been analyzed. In chapter 7, tuning of properties of SiC ceramic by layering nano diamond and SiC is discussed as well as a method to make tougher of SiC ceramic by reinforcing similar structured material such as nanodiamond is also furnished. Finally, summary and possible more works has been described in chapter 8.

## Chapter 3

### Generated Models and Software

The primary objective of research is to comprehend the fundamental physics and mechanics of crack propagation and material failure of ceramic based nanostructure. It is well known from the physics that every material regardless of their behavior is made from atoms (which are made from mainly electron, proton, and neutron). So if something breaks then it has to break from atomistic level. However, atomistic level is completely ignored if the order of material is macroscale and analyzed as bulk material. Now-a-days the modern technology requires new materials to meet demand and involve in research in atomistic level. Hence, molecular level modeling and simulation becomes inevitable to comprehend the mechanics of nanomaterials. A set of computational software along with supercomputing facilities are required to conduct the research. A brief description is given below.

#### 3.1 Overview of Molecular Dynamics (MD) simulation

Classical MD simulation is a numerical investigation technique where physical and dynamical properties of substance are allowed to study at the atomistic level [77, 78, 79]. Atoms are treated as single point of mass individually and time integration of Newton's 2<sup>nd</sup> law computes the velocities and forces of all atoms. It is important to know how the molecular dynamics simulations happen to comprehend how the desired physical properties are evaluated. The schematic simulation framework is shown in figure 3-1. Mainly three files play the important role to run the simulations which contain three types of information. First file (Model) contains the information about the atom co-ordinate position. Second file contains (Driver) the information about the atomic potential which represents how the atoms will interact with each other such as for energy relation

between particles in terms of spatial coordinates. The third file (Controller) keeps the information about the thermodynamic atmosphere such as temperature, pressure, etc. Propagator is the core part which conducts molecular dynamics simulation by integrating the Equation of Motion (EOM) using LF algorithm. In the proposed research, MD simulation technique will be used in various occasions.

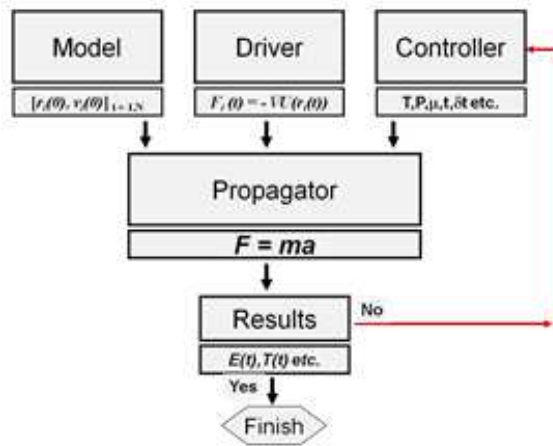


Figure 3-1 Basic steps of molecular dynamics simulations

### 3.1.1 Fundamental Concepts

Newton's equation of motion is the core part of molecular dynamics (MD) which is used in step-by-step process to solve and for a group of molecules or atoms can be furnished as.

$$m_i \ddot{r}_i^\alpha = F_i^\alpha \quad 3.1$$

Here,  $\alpha$  is the direction towards force,  $F_i$  acting on each atom,  $i$  corresponding to mass  $m_i$ . Again,  $r_i^\alpha$  is  $\alpha^{\text{th}}$  component of the  $i$  atomic position. Hamiltonian dynamics is generally used for computational convenience to obtain the equation of motion. Particle position and momenta are applied to express total energy. Hamiltonian  $H$  can be expressed as follows which is constant in a closed system.

$$H = \sum_{i=1}^N \frac{p_k^i p_k^i}{2m^i} + U(r_i^N) \quad 3.2$$

Here, momenta of particle is expressed for particle  $i$  in the  $k$ th direction as  $p_k^i$ , potential energy is expressed as  $U(r^N)$ , and total number of particles is  $N$ . Eqn. 3.1 is used to obtain the force  $F$ .

But the closed form solution of EOM is not easy to avail when a large number of particle interact, therefore finite difference method is used to solve EOM numerically. Verlet Leapfrog (LF) integration scheme is used which is very well know and it requires positions ( $r$ ), force ( $f$ ), and velocity ( $v$ ) remain half a time step behind of each particle at The velocities are proceeded to  $t + (1/2)\Delta t$  by integration of the force at any instant of time.

$$\vec{v}\left(t + \frac{1}{2}\Delta t\right) = \vec{v}\left(t - \frac{1}{2}\Delta t\right) + \Delta t \quad 3.3$$

Here,  $\Delta t$  is the timestep and  $m$  is the mass of a particle

Then the new positions are:

$$\vec{r}\left(t + \frac{1}{2}\Delta t\right) = \vec{r}(t) + \Delta t \vec{v}\left(t + \frac{1}{2}\Delta t\right) \quad 3.4$$

Velocities at time  $t$  are measured as the average of velocities of half time step advance and behind. It is done due to simulation requires positions and velocities at same time.

$$\vec{v}(t) = \frac{1}{2} \left[ \vec{v}\left(t + \frac{1}{2}\Delta t\right) + \vec{v}\left(t - \frac{1}{2}\Delta t\right) \right] \quad 3.5$$

LF algorithm predicts the new positions, along with velocities and net force in the next step by using previous and current position. This is how the simulation propagates.

### 3.1.2 Used Simulation Software

We will use DLPOLY [80, 81] software to conduct our MD simulations and the classical Tersoff Potential [82] will be used as force field. From MD simulation, it is possible to generate stress-strain curve of a material, checking of energy equilibrium and the morphology of structure.

The stress component ( $\sigma_{ij}$ ) at the atomic level is taken from *virial stress* [83] as,

$$\sigma_{ij} = -\frac{1}{V} \sum_{\alpha} \left( M^{\alpha} v_i^{\alpha} v_j^{\alpha} + \frac{1}{2} \sum_{\beta \neq \alpha} F_i^{\alpha\beta} r_j^{\alpha\beta} \right) \quad 3.6$$

Where  $V = \sum_{\alpha} V^{\alpha}$  is the characteristic volume of MD unit cell. Here atomic volume of  $\alpha$  is  $V^{\alpha}$  and  $v_i^{\alpha}$  is the velocity of i-component of atom  $\alpha$ . The i-component of the force between atom  $\alpha$  and  $\beta$ , and i-component of the separation distance between atoms  $\alpha$  and  $\beta$  is respectively  $F_i^{\alpha\beta}$  and  $r_i^{\alpha\beta}$  is the. Eqn. 3.6 represents the average atomic stress for the entire volume of the unit cell. It is the combination of two terms where the first term is related with the kinetic energy and second part is related with the potential energy. Kinetic energy comes from the thermal vibrations of atoms and potential energy initiates due to applied deformation. The sign convention is opposite in MD simulation compare continuum level which is negative for tensile and positive for compressive. In our simulation we estimated the total volume  $V$  as,

$$V = L_x L_y L_z \quad 3.7$$

Here,  $L_x$ ,  $L_y$  and  $L_z$  are the lengths of the unit cell along x, y, and z directions, respectively. Usually height,  $h$  of the models is  $L_y$ . It has been revealed in a recent study that [68] atomic scale *virial* stresses are equivalent to continuum Cauchy stresses.

### 3.2 Overview of Finite Element Analysis

In our study, fracture toughness properties (normal) of different models will be assessed from the following relation [84]:

$$K_I = \lim_{x \rightarrow 0} \sqrt{2\pi x} \sigma_{yy} \quad 3.8$$

Where  $x$  is the distance measured from the crack tip and  $\sigma_{yy}$  is the opening stress normal to the initial crack surface. In our study, using Finite Element Analysis (FEA) (ANSYS [85]),  $\sigma_{yy}$  will be recorded ahead of the crack tip for a prescribed displacement obtained from MD simulations. Equation 3.8 will then be used to estimate  $K_I$ . Since,  $\delta_{\text{failure}}$  from MD will be used as the FEA boundary conditions, the calculated  $K_I$  values essentially will imply critical stress intensity factor  $K_{Ic}$ . Crack closure method was also used by using FEA which will be described in next chapter.

### 3.3 Deformation Analysis

The raw data produced from MD simulations will be post-processed to understand deformation mechanisms of the advanced ceramics. To trace any evidence of plasticity, both direct and indirect methods will be followed. All atoms in the studied materials are bonded by  $sp^3$  hybridization implying the coordination number of each atom is equal to 4. If micro structural changes occur due to lattice mismatch, the coordination number may be reduced or increased. Such change will be an indirect indication of dislocation type defect formation in the material. We will employ coordination number analysis to assess trace of plastic deformation in our “proof-of-concept” studies. For more detailed studies, we will use the direct method called “centro-symmetry parameter” analysis [86].

The centro-symmetry property of some lattices can be used to differentiate them from other structures. It distinguishes of those structures where crystal defects present means the local bond symmetry is broken. Kelchner et al. [87] have developed a metric, and well known as centro-symmetry parameter (CSP). It estimates the local loss of centro-symmetry at an atomic site, which is characteristic for most crystal defects. The visualization program is AtomEye and VMD [88, 89].

### 3.4 Requirements of Others Facilities

Modeling and post process in molecular dynamics simulation is assisted with programming language. A few software are required to assist the work such as Graphics user interface (GUI), Cygwin, Programming language such as FORTRAN and MATLAB. Supercomputing facilities were also important to run the simulations. UT Arlington supercomputing facilities were used to run the molecular dynamics simulation.

## Chapter 4

### On the Mode-I Fracture Toughness Prediction of Brittle Nanocrystalline Material Using Atomistic Simulation: A Case Study with Nanoscale Diamond

Over the past several years, nanoscale structures and devices have been increasingly applied in electronics, biomedical, structural and many other novel applications. Obviously, maintaining structural integrity of these tiny devices during their service life is very important. Like any materials, nanomaterials contain some level of process-induced or damage-induced flaws and defects. A quantitative understanding of the response of such flaws or defects under mechanical loading is important for accurate predictions of failure properties of nanomaterials. In mechanics, tiny flaws or interconnected defects are defined as cracks, and “fracture toughness” is used as measures of material resistance to extension of a crack. For conventional large scale materials, there are number of standardized experimental, numerical as well as finite element based computational techniques available to determine fracture toughness properties of materials. The stress intensity factor  $K$ , the elastic energy release rate  $G$ , the  $J$ -integral, the crack-tip-opening displacement (CTOD) and the crack-tip opening angle (CTOA) are some of the parameters used in fracture mechanics more frequently [90, 84, 91] Due to extremely small size, applying experimental fracture mechanics techniques on nanoscale materials is not quite viable. As such, in the recent years, significant efforts have been made to understand fracture mechanism of material at the nanoscale using simulations or alternative methods [92, 93, 94, 95, 96, 97, 98]. Gao and Ji [92] studied fracture of nanoscale crystals using virtual internal bond method (VIB) and showed that tensile (opening mode) fracture toughness of nanomaterials deviates significantly from the Griffith's prediction. Karimi et al [93] studied the effect of defects in

Nickel crystal via molecular dynamics simulations and observed that the critical strain necessary for tensile crack propagation in defective Ni depends on the defect configuration and can either increase or decrease relative to the defect-free system. Dynamic fracture process of silicon crystals was investigated by Swadener et al. [94] using molecular dynamics simulation. They have found that the crack propagation speeds vary over a large range of fracture energy and can be well-predicted by MD simulation. Kikuchi et al. [95] demonstrated that for some crystal orientation, fracture toughness of SiC can be predicted by Griffiths Law. Zhang et al. [96] studied the applicability of the Griffith criterion in predicting the onset of crack extension in crystal lattices using atomistic and multiscale simulations. They showed that for a monolithic crystal lattice, a characteristic crack length (about ten lattice spacing) exists below which the Griffith fracture stress markedly overestimates the theoretical Griffith load. Pugno and Ruoff [97] developed a quantized fracture mechanics (QFM) theory, where the classical stress intensity factor is redefined by considering an infinitesimal crack extension at the crack tip. Mattoni et al. [98] proposed a modified Griffith condition, where Young's modulus and surface energy density are shown to be strain dependent. Some recent studies also suggest that materials may become insensitive to flaws at the nanoscale [99, 100].

It can be noted that many of these studies were carried out based on the assumption that linear elastic fracture mechanics works at the nanoscale. In an effort to find the limit beyond which continuum fracture theories could be employed, recently, few researchers [101, 102, 103, 104, 105] have performed series of MD simulations for a range of crack lengths and compared atomistic simulation results with the classical Griffith theory. It can be inferred from these above mentioned studies that there exists a

characteristic crack length (about four lattice spacing) below which the Griffith fracture stress markedly overestimates the theoretical Griffith load.

In this paper, we report atomistic simulation-based analysis to compute fracture toughness properties of nanoscale diamonds. Four different continuum fracture mechanics theories have been employed on nano-size diamond block to predict fracture toughness. Three different crack sizes have been considered. The remainder of the chapter is organized as follows. First, we evaluate essential constitutive properties of diamonds using atomistic simulations. Next, we describe different fracture toughness calculation methods using molecular dynamics simulations. Finally, we provide a discussion on our findings and conclude.

#### 4.1 Atomistic Computations of Elastic Properties of Single Crystal Diamond

Diamonds are known for their high hardness and surface smoothness. Structurally, diamonds are built on zinc-blend crystal structure where each carbon atom is tetrahedrally connected with four carbon atoms via  $sp^3$  hybridization. The equilibrium lattice constant of diamond is 3.57 Å. To evaluate elastic properties of nanodiamond via atomistic computations, first we have built a 17.493 nm × 8.925 nm × 2.142 nm rectangular diamond nanoblock. The model contains a total of 58,800 atoms (figure 4-1). The interaction between C-C is described by Tersoff potential [82]. Periodic boundary conditions are employed in all there x, y, z directions. All simulations are done at 300K with a simulation time step set at 0.5 fs. The model is then equilibrated for 10,000 steps in NPT ensemble to attain stress free state. The time constants for the heat and pressure baths have been set at 1ps. In the next step, uniform tensile and shear strain fields (0.25%) have been separately applied “in increment” to the identical clones of the

equilibrated model by appropriately scaling the MD cell along the required directions. In this step, the NVT ensemble has been used. We have used DL-POLY (version 4.0) simulation package developed by Daresbury Laboratory (Daresbury, Warrington, Cheshire, UK) to generate all data in our study. It is a freely available (as academic license) open source molecular simulation code.

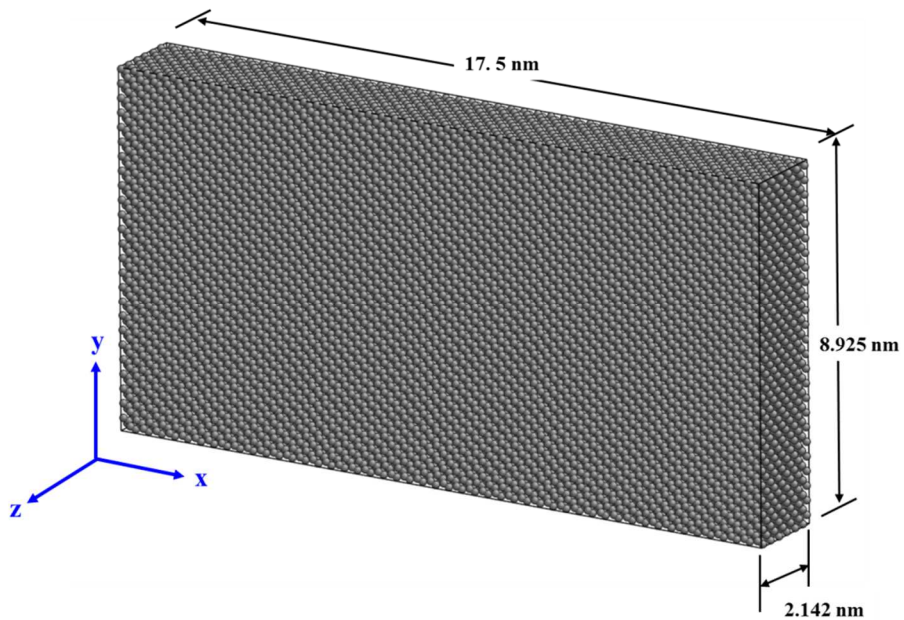


Figure 4-1 Atomistic Model of Diamond with Dimensions

To generate stress-strain data, the MD cell is rescaled in every 2000 steps between each strain increment (0.25%). Of this, the first 1000 steps store equilibration data and the second 1000 steps store useful thermodynamic data. Engineering virial stresses are calculated by averaging the stress data collected from the second 1000 steps of simulations. In principle, the computed “time-averaged” virial stresses represent engineering stress states corresponding to the applied incremental strain fields [103, 104,

105]. We continue to apply the incremental strain until failure is observed. To calculate elastic constants  $C_{11}$  and  $C_{12}$ , incremental tensile strain is applied along y-direction. For evaluating the constant  $C_{44}$ , incremental shear strain is applied along zx plane. Note that single crystal material like diamond has three independent elastic constants. As such, our tensile and shear simulation is sufficient to obtain complete stiffness matrix  $[C_{ij}]$  ( $i, j = 1-3$ ) of diamond. Using the recorded stress-strain data, three different stress-strain curves, namely,  $\sigma_{yy}$  vs  $\epsilon_{yy}$ ,  $\sigma_{xx}$  vs  $\epsilon_{yy}$  and  $\tau_{xz}$  vs  $\gamma_{xz}$  have been generated as shown in figure 4-2, and the initial slopes of each curve are equal to  $C_{11}$ ,  $C_{12}$  and  $C_{44}$ , respectively. The generated stiffness matrix of diamond is shown in equation 4.1 below. The unit is in GPa.

$$[C] = \begin{bmatrix} C_{11} & C_{12} & C_{12} & 0 & 0 & 0 \\ C_{12} & C_{11} & C_{12} & 0 & 0 & 0 \\ C_{12} & C_{12} & C_{11} & 0 & 0 & 0 \\ 0 & 0 & 0 & C_{44} & 0 & 0 \\ 0 & 0 & 0 & 0 & C_{44} & 0 \\ 0 & 0 & 0 & 0 & 0 & C_{44} \end{bmatrix} = \begin{bmatrix} 1026.2 & 90.558 & 90.558 & 0 & 0 & 0 \\ 90.558 & 1026.2 & 90.558 & 0 & 0 & 0 \\ 90.558 & 90.558 & 1026.2 & 0 & 0 & 0 \\ 0 & 0 & 0 & 314.3 & 0 & 0 \\ 0 & 0 & 0 & 0 & 314.3 & 0 \\ 0 & 0 & 0 & 0 & 0 & 314.3 \end{bmatrix} \quad [4.1]$$

Next, we calculated the Young's modulus  $E$  and the Poisson's ratio  $\nu$  of diamond using the following relations [106]:

$$E = \frac{(C_{11} + 2C_{12})(C_{11} - C_{12})}{(C_{11} + C_{12})} = 1011.514 \text{ GPa} \quad [4.2]$$

and,

$$\nu = \frac{C_{12}}{(C_{11} + C_{12})} = 0.0811 \quad [4.3]$$

In principle, the shear modulus  $G$  and already computed  $C_{44}$  represents the same quantity. Therefore, the shear modulus  $G$  of diamond is equal to 314.3 GPa.

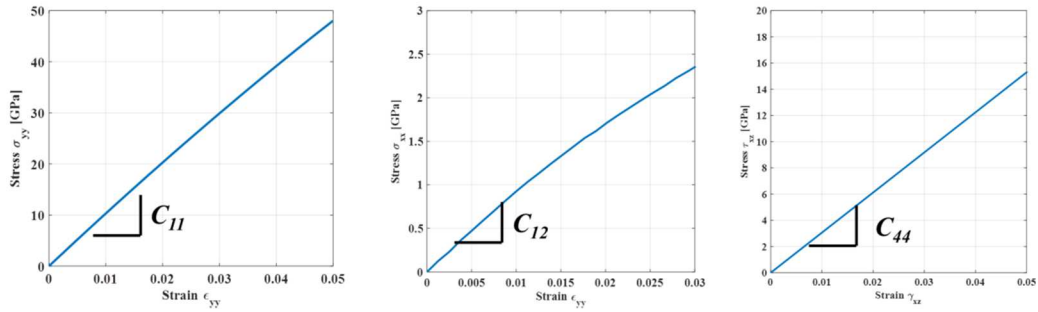


Figure 4-2  $\sigma_{yy}$  vs  $\epsilon_{yy}$ ,  $\sigma_{xx}$  vs  $\epsilon_{yy}$  and  $\tau_{xz}$  vs  $\gamma_{xz}$  curves generated from molecular simulation of diamonds

Reports on material properties ( $E$  and  $\nu$ ) of single crystal diamonds are rare. Naturally or artificially made diamonds are polycrystalline and the size of grains depends on manufacturing conditions [107, 108, 109]. Both  $E$  and  $\nu$  appears to be dependent on grain sizes and manufacturing induced impurity contents. For example, Murkus mohr et al. [110] studied nanocrystalline (NCD) and ultra-nanocrystalline (UNCD) diamonds to measure their properties using ultrasonic resonance method. In their study, the sample size was few hundred micrometers with average grain size of  $\sim 6$  nm for UNCD and  $\sim 20$  nm for NCD. Considering isotropic material properties, they estimated Young's modulus of NCDs and UNCDs as  $873 \pm 164$  GPa and  $501 \pm 49$  GPa, respectively. The Poisson's ratio for NCDs and UNCDs were measured as  $0.034 \pm 0.017$  and  $0.201 \pm 0.041$ , respectively. They also measured the shear modulus  $G$  of NCD diamond as  $\sim 367$  GPa. Anirudha V. Sumant et al. [109] estimated that the Young's modulus of single crystal nanodiamond could vary between 980 GPa and 1220 GPa. Butler and Sumant [108] estimates that single crystal diamonds (all  $sp^3$  bonding character) have Young's modulus of 1100 GPa. They also found that diamond's stiffness can vary between 500 and 1120 GPa due to different gas chemistry and bonding character. The Young's modulus of

nanodiamond containing < 0.1% sp<sup>2</sup> carbon atoms (impurities) can be as high as 1120 GPa. Klein and Cardinale [111] argued that the  $\nu$  of single crystal nanodiamond should be less than 0.2. They have shown that the diamond's  $E$  can be 1106-1164 GPa and  $\nu$  from 0.056 to 0.0791. Peter Hess [112] explained that the  $E$  and  $\nu$  depend on the crystal orientations. According to them, the Young's modulus can be ranging from 1050-1210 GPa and Poisson's ratio from 0.00786 to 0.115. In Table 4-1, we have summarized openly available  $E$ ,  $G$  and  $\nu$  values of diamond [107, 108, 109, 111, 110, 112] and compared them with our findings. It should be noted that the cited properties have been obtained from diamond samples with varying grain sizes and chemical contents. These factors play vital part on the mechanical properties of diamond and lead to a wide variation in the properties. In our study, we have considered 100% pure defect-free single crystal nanoscale diamond. As such, our predicted properties should be compared with the upper bound values of the reported properties. In this regard, our findings are in good agreement with the published literatures.

Table 4-1 Predicted elastic properties of diamond in comparison with reported data.

Young's Modulus ( $E$ ) [GPa]	Shear Modulus ( $G$ ) [GPa]	Poisson's ratio ( $\nu$ )	Reference
1011.5 (NCD)	314.3	0.0811	Current study
1050-1210	-	0.00786 - 0.115	[97]
501 ± 49 (UNCD)	367	0.201 ± 0.041 (UNCD)	[95]
873 ± 164 (NCD)		0.034 ± 0.017 (NCD)	
980 - 1220	-	-	[94]
500-1120	-	-	[93]
1106-1164	-	0.056 - 0.0791	[96]

## 4.2 Fracture Toughness Calculations

We have calculated Mode I fracture toughness of nanoscale diamond by using molecular dynamics simulation. In certain cases, MD simulation results are incorporated into finite element analysis (FEA). In this study, we have considered (i) the crack tip opening displacement (CTOD) method (MD only), (ii) Griffith's energy release rate (MD only), (iii) Irwin's K-based method (MD + FEA) and (iv) the crack closure method (MD + FEA) to compute fracture toughness properties of diamonds. For FEA, the mechanical properties ( $E, G, \nu$ ) evaluated in section 4.1 were used. The boundary conditions for FEA (input) were also obtained from the stress-strain data generated from MD simulation (MD output).

There are two popular parameters are frequently used to express Mode I fracture toughness of a material – (i) critical energy release rate  $G_{IC}$  and (ii) critical stress intensity factor  $K_{IC}$  [90, 84, 91]. Other parameters such as  $CTOD$ ,  $CTOA$ ,  $J$ -integral etc. are also used. For most engineering materials (isotropic and orthotropic), using established mathematical relations, it is possible to convert one fracture toughness parameter to another [90, 84]. Such conversion requires material's constitutive and failure properties. In our study, we expressed all our findings in terms of critical energy release rate  $G_{IC}$  and critical stress intensity factor  $K_{IC}$ .

### *4.2.1 Relation between Stress Intensity Factor ( $K_{IC}$ ) and Energy Release Rate ( $G_{IC}$ ) for Single-crystals (with Three Independent Elastic Constants)*

The relation between  $K_{IC}$  and  $G_{IC}$  can be obtained from the  $G$ - $K$  relations developed by G. Sih [113] for orthotropic materials as shown in equation. (4.4)

$$G_I = K_I^2 \left( \frac{b_{11}b_{22}}{2} \right)^{1/2} \left[ \left( \frac{b_{22}}{b_{11}} \right)^{1/2} + \frac{2b_{12} + b_{66}}{2b_{11}} \right]^{1/2} \quad 4.4$$

Here  $b_{ij}$  are the reduced elastic compliances in plane strain conditions, which is related to plane stress compliance  $a_{ij}$ 's by the following relations(here (  $i,j= 1,2,6$ ):

$$b_{ij} = a_{ij} - \frac{a_{i2}a_{j3}}{a_{33}} \quad 4.5$$

in which  $a_{ij}$  are related to the elastic constants shown in Eqn. (1) as:

$$a_{ij} = [C_{ij}]^{-1} \quad 4.6$$

For single crystal material such as diamond, there are three independent constants,  $b_{11}$ ,  $b_{12}$  and  $b_{16}$ , and  $b_{11} = b_{22}$ . We obtain  $b_{11}$ ,  $b_{12}$  and  $b_{16}$  of diamond by converting  $C_{11}$ ,  $C_{22}$  and  $C_{44}$  of diamond (Using equation. 4.1, 4.4, 4.5, and 4.6).

#### 4.2.2 Mode I Fracture Toughness of Diamond using MD Simulation

In section 4.1, we described atomistic simulation method to generate stress-strain curves and evaluate elastic properties of “crack-free” homogenous diamond models. For fracture toughness studies, we have introduced center cracks in those models and applied tensile loading. To allow “crack-induced non-homogenous” deformation in the vicinity of cracks as the models are elongated along y direction, we added rigid atomic layers (parallel to the planes normal to y-direction) in the opposite ends of the model. Periodic boundary conditions were applied in x and z direction only but not along the loading direction (y-direction). We applied equal and opposite incremental displacement fields to these rigid planes only. The remaining deformable part of the model (containing the crack) follows the rigid planes as the atoms in the deformable part interact with the atoms in the rigid part via interatomic potential. This approach is different from atomic “rescaling” done in section 4.1 to apply mechanical

force. The “rescaling” type displacement is good for imposing uniform displacement throughout the whole material/structure mainly to obtain elastic properties of material.

Center cracks with three different sizes have been considered to calculate fracture toughness properties of diamond. In particular, the crack-lengths considered in this study are:  $5a_0$ ,  $7a_0$  and  $9a_0$ , where  $a_0 = 0.357$  nm is diamond's lattice constant. We will refer these three different models as  $5a_0$ ,  $7a_0$  and  $9a_0$ , respectively in the remainder of the paper. Figure 4-3 shows the MD snapshots of the initial cracked models that are made from the crack-free models considered in section 4.1 (see Fig. 4-1). Like before, incremental tensile displacements are applied until complete fracture of the material occurred. Stress-strain data is recorded and archived for further analysis.

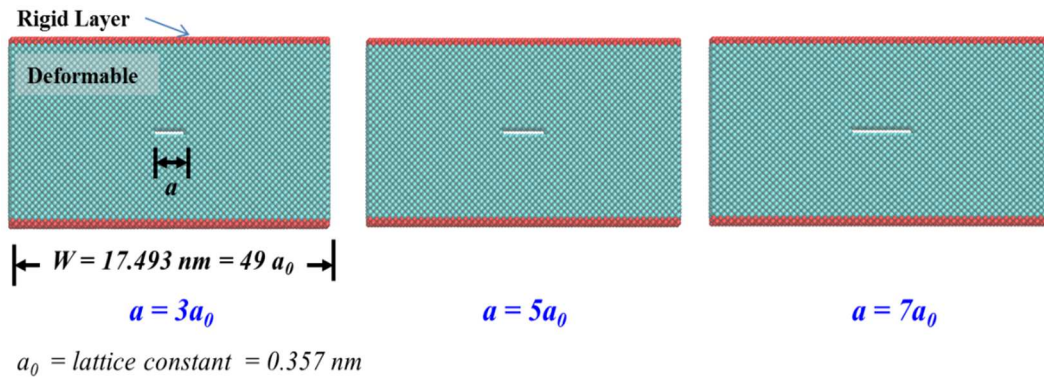


Figure 4-3 Initial atomistic models of diamond with three different crack lengths

#### 4.2.2.1 Griffith's Energy Release Rate via MD Simulation

By definition, the Griffith's energy release rate [91, 114] is equal to the work done on an elastic body to create per unit fracture area. It is the potential energy released due to crack propagation. It is also equal to J-integral,  $J$ . Mathematically, this energy is expressed as

$$G = J = \frac{dU}{dA} = \frac{dU}{Bda} \quad 4.7$$

Here,  $U$  is the strain energy stored in the material body,  $a$  is the crack length and  $B$  is the specimen thickness.

In our study, the critical energy release rate ( $G$ ) of diamond has been estimated from eqn. 4.7. The quantity  $dU$  (difference in strain energy) is obtained from the difference of MD generated equilibrium potential energy value of two models (e.g. “ $5a_0$ ” and “ $7a_0$ ” models). In principle, the energy difference should reflect the energy required to extending a crack from, say, “ $5a_0$ ” to “ $7a_0$ ”. Then  $da$  would be the crack length difference of those models (i.e.  $2a_0$ ), and thickness  $B$  is as measured before (2.142 nm). Table 4-2 shows the result. It is evident that the estimated  $G_{IC}$  for diamond is  $\sim 85-87 \text{ J/m}^2$ . Using Eqns. (4.4-4.6), the corresponding  $K_{IC}$ 's for diamond have been estimated and found to be  $\sim 8.8 \text{ MPa}\cdot\text{m}^{0.5}$ . It is evident that the measured critical energy release rate and the corresponding fracture toughness values remain nearly constant over the range of cracked sizes considered.

Table 4-2 Predicted fracture toughness of diamond via Griffith's energy release rate criterion

Mode-I	Energy (J)	Crack length (m)	Thickness (m)	G <sub>IC</sub> (J/m <sup>2</sup> )	K <sub>IC</sub> (MPa.m <sup>0.5</sup> )
5a <sub>0</sub>	7.3357e-14	17.85e-10	21.42e-10	85.89	8.8166
7a <sub>0</sub>	7.3226e-14	24.99e-10	21.42e-10	87.43	8.8953
9a <sub>0</sub>	7.3092e-14	32.13e-10	21.42e-10	-	-

#### 4.2.2.2 Crack Tip Opening Displacement (CTOD, δ<sub>t</sub>) Method via MD Simulation

Crack tip opening displacement (δ<sub>t</sub>) is another method to find fracture toughness of material. By definition, it is the displacement measured at the original crack tip and the 90° intercept [91, 105]. Irwin [90, 84] showed the CTOD (δ<sub>t</sub>) is related to strain energy release rate *G* by the equation:

$$\delta_t = m \frac{G}{\sigma_{ys}} \quad 4.8$$

Where, σ<sub>ys</sub> is the yield strength of diamond and *m* represents a geometric factor. In the original Irwin's formulation, *m* = 4/π. Later, Dugdale proposed a model [115] with *m* close to unity. Separately, Rice and Rosengren [116] proposed similar formulation with *m* ranging between 1 and 2 and argued that value of *m* would depend on the stress state.

Figure 4-4 shows how we calculated CTOD from the snapshots of atomistic models. The illustration is shown using the "7a<sub>0</sub>" model. Identical procedure was followed to calculate CTOD for the "7a<sub>0</sub>" and "9a<sub>0</sub>" models. As shown in Fig. 4-4, δ<sub>t</sub> is the distance between points *A* and *B* that are located at the top and bottom crack surfaces, respectively. Both these points are the intercept points of the lines *AO* and *BO* at the crack surface. The lines *AO* and *BO* have common origin *O* at the crack tip and they are drawn at ± 45° angle with respect to the horizontal line intersecting the crack tip at *O*. To

measure the yield strength  $\sigma_{ys}$  of diamond, first, we have developed a crack-free diamond model confined between two rigid layers of diamond. Then, we applied incremental tensile displacement field to the rigid layers until failure. The stress-strain data is generated and the failure stress is recorded as  $\sigma_{ys}$ . The MD snapshots taken at  $\varepsilon_{yy} = 0$  and at  $\varepsilon_{yy} > 0.2$  (post yield/post failure) and stress-strain curve until failure are shown in Fig. 4-5. As shown in Fig. 4-5, our estimated  $\sigma_{ys}$  is  $\sim 240$  GPa. The corresponding  $G_{IC}$  and  $K_{IC}$  values are shown in Table 4-3 and 4-4 respectively. Note the range of  $G_{IC}$  and  $K_{IC}$  values for the same crack length (i.e. same CTOD value) due to various chosen “ $m$ ” values. It is evident that the  $G_{IC}$  and  $K_{IC}$  values obtained from these calculations are different from our previous calculations. We believe that the variation in  $G_{IC}$  and  $K_{IC}$  estimates are influenced by our measured yield strength values of diamond as well as our choice of factor “ $m$ ”. Note that our calculation is based on a defect-free 100% perfect diamond crystal structure. Hence, the reported  $\sigma_{ys}$  should be interpreted as the highest possible strength, or theoretical strength of diamond. In reality, all diamonds contain some level of defects and impurities, and all these factors typically reduce diamond’s yield strength. Since we calculated  $G_{IC}$  or  $K_{IC}$  using Eqn. 4.8 where the “theoretical”  $\sigma_{ys}$  of diamond was inserted as yield strength, the fracture toughness values are significantly higher than usual. Reports on strengths of single crystal diamond are rare. Based on the existing literatures, we found that strengths of single crystal diamond can vary between 60 GPa and 225 GPa [117, 118]. Considering the CTOD data obtained from our calculations and using the reported range of yield strengths of diamonds, we recalculated the  $G_{IC}$  or  $K_{IC}$  values as shown in Table 4-3 and 4-4. The range of  $G_{IC}$  or  $K_{IC}$  values includes the  $G_{IC}$  or  $K_{IC}$  values we obtained earlier. Despite the fact that we do not have “exact” diamond strengths, the obtained  $G_{IC}$  or  $K_{IC}$  values for samples with different crack lengths are very consistent.

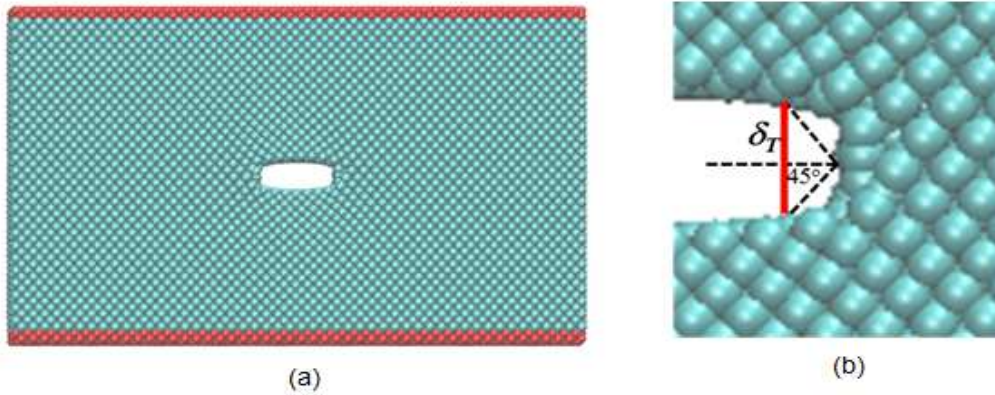


Figure 4-4 a) Atomistic snapshot of deformed “7a0” model, b) a magnified view of right crack tip with illustration to show how CTOD is measured.

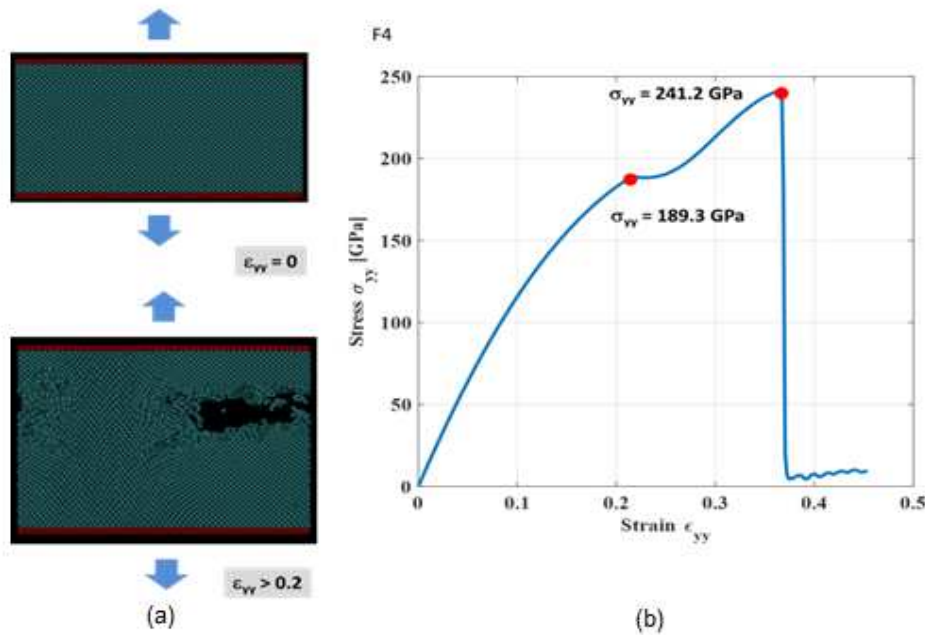


Figure 4-5 a) Atomistic snapshots and stress-strain plot of crack-free diamond model simulated for obtaining yield strength (a) snapshots taken at  $\epsilon_{yy}=0$  and at  $\epsilon_{yy} > 0.2$  (post yield/post failure) and (b) stress strain curve until failure.

Table 4-3 Predicted critical strain energy release rate of diamond using CTOD method

Model	Critical Strain Energy Release Rate $G_{IC}$ (J/m <sup>2</sup> )						
	CTOD value (nm)	Yield Strength = 189.3 GPa			Yield Strength = 241.2 GPa		
		m = 1	m = 2	m = 4/π	m = 1	m = 2	m = 4/π
5a <sub>0</sub>	0.607	114.72	57.36	90.06	146.29	73.14	114.84
7a <sub>0</sub>	0.624	117.94	58.97	92.58	150.38	75.19	118.05
9a <sub>0</sub>	0.624	117.94	58.97	92.58	150.38	75.19	118.05

Table 4-4 Predicted critical stress intensity factor of diamond using CTOD method

Model	Critical Stress Intensity Factor $K_{IC}$ (MPa.m <sup>0.5</sup> )						
	CTOD value (nm)	Yield Strength = 189.3 GPa			Yield Strength = 241.2 GPa		
		m = 1	m = 2	m = 4/π	m = 1	m = 2	m = 4/π
5a <sub>0</sub>	0.607	10.18955	7.205101	9.027966	11.50622	8.136127	10.19454
7a <sub>0</sub>	0.624	10.33127	7.305308	9.153525	11.66625	8.249283	10.33632
9a <sub>0</sub>	0.624	10.33127	7.30531	9.153527	11.66625	8.249284	10.33632

#### 4.2.3 $K_{IC}$ and $G_{IC}$ Calculation from Integrated MD-FEM Analysis.

Irwin's stress intensity factor method [90, 84] and modified crack closure method [119] are widely used continuum methods for estimating  $K_{IC}$  and  $G_{IC}$ , respectively. Calculations of  $K_{IC}$  and  $G_{IC}$  using the two methods from MD only calculations are not typically possible. As discussed in the subsequent sections, the Irwin's method requires local stress distribution ahead of the crack tip, and from MD point of view, the definition of "local stress" and its connection to continuum level stress is very ill-defined. The crack closure method requires local nodal force value at the crack tip. The definition is "node" or "local nodal force" is also ill-defined from MD perspective. As discussed in the subsequent sections, we overcame the MD challenges by integrating MD simulation results with FEM analysis.

The finite element method is employed to calculate the energy release rates and stress intensity factors of the three cracked models. In FEM analysis, the constitutive properties of diamonds have been inserted based on our MD analysis (Eqn. 4.1). As shown in Fig. 4-6, an equivalent FE model (quarter model) has been developed using identical MD model geometry. From symmetry, boundary conditions 1-3 have been set. The loading boundary condition (B.C. # 4) has been obtained from molecular dynamics simulations results. As shown in Fig. 4-6, we first extracted the strain-to-fracture for each model. Then using the relation,  $\epsilon_{yy} = \frac{\delta_{MD}}{L_y}$ , where  $L_y$  = undeformed model height = 8.925 nm, we obtained the corresponding displacement-at-failure for each model as shown in Table 4-5.

Table 4-5 Boundary conditions used in finite element analysis for predicting fracture toughness using Irwin's stress intensity factor method and crack closure method

Model	$\delta_{MD}$ (nm) (B.C. # 4)	(B.C. # 3) $X=0$ $0 < Y < H$	(B.C. # 2)		(B.C. # 1) $X=W$ $0 < Y < H$
			$Y=0$ $0 < X < a$	$Y=0$ $a < X < W$	
$5a_0$	0.720	$u_x = 0$	Free surface	$\underline{u}_y = 0$ $u_x = 0$	$u_x = 0$
$7a_0$	0.650	$u_x = 0$	Free surface	$\underline{u}_y = 0$ $u_x = 0$	$u_x = 0$
$9a_0$	0.605	$u_x = 0$	Free surface	$\underline{u}_y = 0$ $u_x = 0$	$u_x = 0$

All FEM results are obtained using the finite element code ANSYS APDL v15.0. The eight-noded solid element (SOLID 183) with the full integration scheme is used in all cases. To ensure accuracy in results, a fine mesh is used near the crack tip. The resolution of the fine mesh is such that the spacing between nodes along the crack axis

is small enough (~1% of crack length) with respect to crack length. Using the FEM simulation data, the  $K_{IC}$  and  $G_{IC}$  values for each cracked model has been obtained.

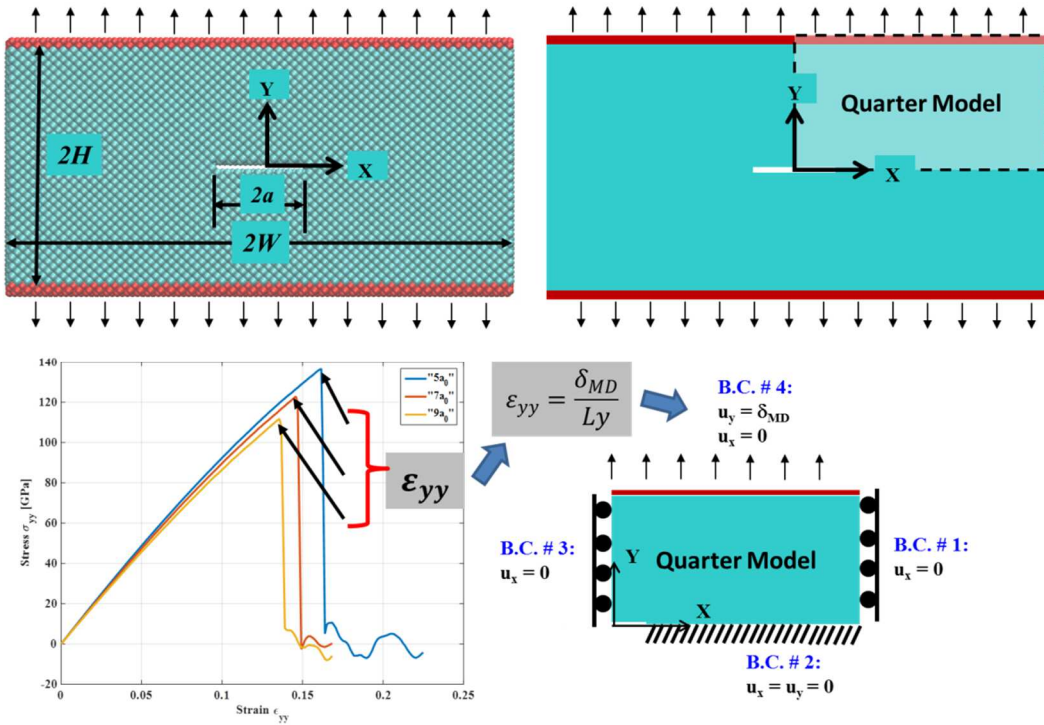


Figure 4-6 Schematics to show how equivalent quarter model for finite element analysis has been developed based on original MD model. The sketch of quarter model (bottom right) shows the imposed boundary condition. Note that B.C. #4 has been obtained from the strain at failure  $\epsilon_{yy}$  data obtained from MD simulation of models with different crack lengths (bottom left).

#### 4.2.3.1 $K_{IC}$ from Irwin's Method

For a 2D solid, the stress intensity factor  $K_I$  can be calculated from the relation [90, 84]:

$$K_I = \lim_{x \rightarrow 0} \sqrt{2\pi x} \sigma_{yy} \quad 4.9$$

where  $x$  is the distance measured from the crack tip and  $\sigma_{yy}$  is the opening stress normal to the initial crack surface. Because  $\sigma_{yy}$  is singular at the crack tip ( $x = 0$ ), the FEA generated near-tip stress field is not accurate and  $K_I$  is usually determined by the projected values of  $\sigma_{yy} \sqrt{2\pi x}$  at  $x = 0$ . Figure 4-7 shows the  $\sigma_{yy} \sqrt{2\pi x}$  vs.  $x$  plots for the three models and the corresponding projections at  $x = 0$  line. The corresponding  $K_{IC}$  values are listed in Table 4-6. Using equations 4.4-4.6, the associated  $G_{IC}$  values are also reported in Table 4-6.

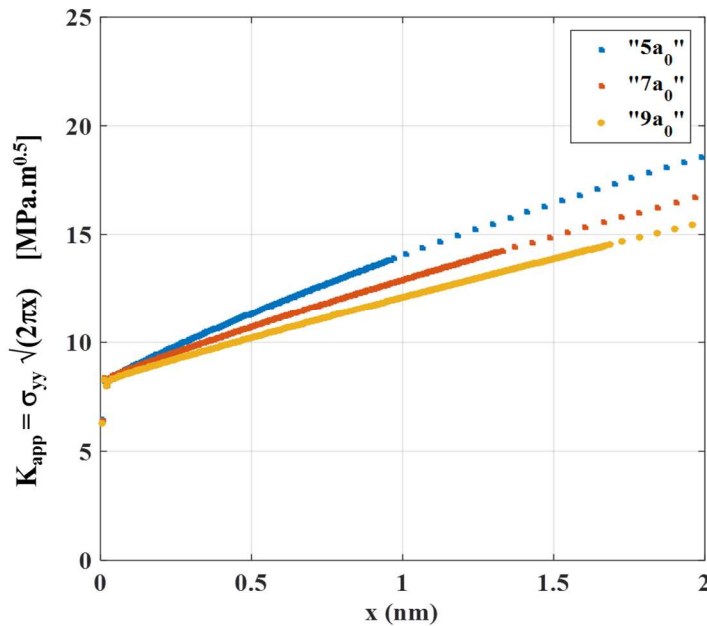


Figure 4-7 The  $\sigma_{yy} \sqrt{2\pi x}$  ( $K_{\text{apparent}}$ ) vs.  $x$  plots for the three cracked models and the corresponding projections at  $x=0$  line

Table 4-6 Predicted fracture toughness of diamond using Irwin's stress intensity factor method

Model	$K_{IC}$ (MPa.m <sup>0.5</sup> )	$G_{IC}$ (J/m <sup>2</sup> )
5a <sub>0</sub>	8.3607	77.237
7a <sub>0</sub>	8.4632	79.1425
9a <sub>0</sub>	8.405	78.0577

#### 4.2.3.2 Crack Closure Method via Finite Element Analysis

According to the modified crack closure method [119], the critical energy release rate  $G_{IC}$  can be calculated using the following equation:

$$G_I = \frac{1}{2\Delta a} (F_y^c [u_y^a - u_y^b] + F_y^g [u_y^e - u_y^f]) \quad 4.10$$

where  $F_y^c$  and  $F_y^g$  represent the vertical component of nodal force at node "c" and node "g",  $u_y^a$ ,  $u_y^b$ ,  $u_y^e$ , and  $u_y^f$  correspond to the vertical component of displacements at node "a", "b", "e", and "f", respectively. The locations of these points are schematically shown in Fig. 4-8. It is noted that in the modified crack closure method – based on the assumption of small  $\Delta a$  the nodal displacements at nodes *c* and *d* after virtual crack extension are approximated by the nodal displacements at nodes *a* and *b*, respectively before the virtual crack extension. Similarly, the nodal displacements at nodes *m* and *n* after virtual crack extension are approximated by the nodal displacements at nodes *k* and *l*, respectively. Using this procedure, the critical energy release rates are obtained and shown in Table 4-7. Like before, using equations 4.4-4.6, the associated  $K_{IC}$  values for each model have been computed and shown in Table 4-7.

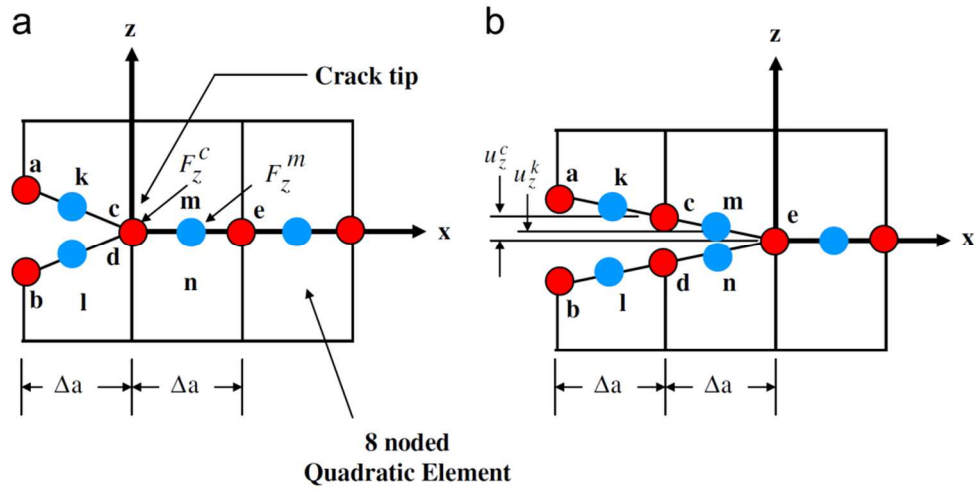


Figure 4-8 Virtual crack extension simulated by finite elements: (a) before crack extension and (b) after crack extension

Table 4-7 Predicted fracture toughness of diamond using crack closure method

Model	$G_{IC}$ (J/m <sup>2</sup> )	$K_{IC}$ (MPa.m <sup>0.5</sup> )
$5a_0$	84.11	8.7248
$7a_0$	87.52	8.89
$9a_0$	86.27	8.8361

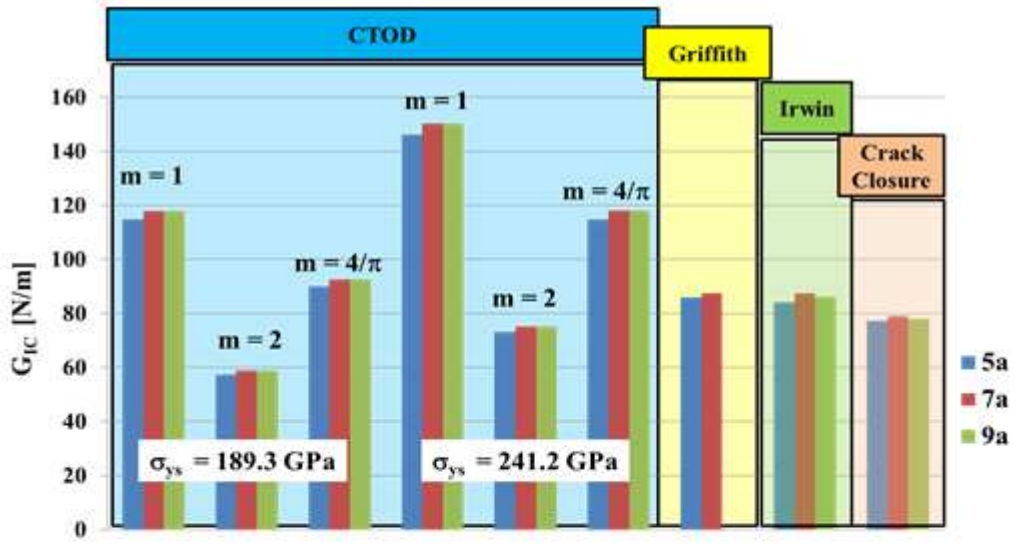
### 4.3 Summary and Conclusions

A summary of our findings are shown in Fig. 4-9. Note the wide variation in the stress intensity factors obtained using CTOD method. The reason is obvious. We used three different “ $m$ ” values and two different yield strength values (referring Eqn. 4.8) in obtaining  $G_{IC}$  and  $K_{IC}$  values from CTOD data. Of these, the combination  $m = 4/\pi$  and  $\sigma_{ys} = 189.3$  GPa is more reasonable. This is because the values  $m = 1$  [115] or  $m = 2$  [116] can be chosen in “specific” situations and may not be applicable to our case. The choice

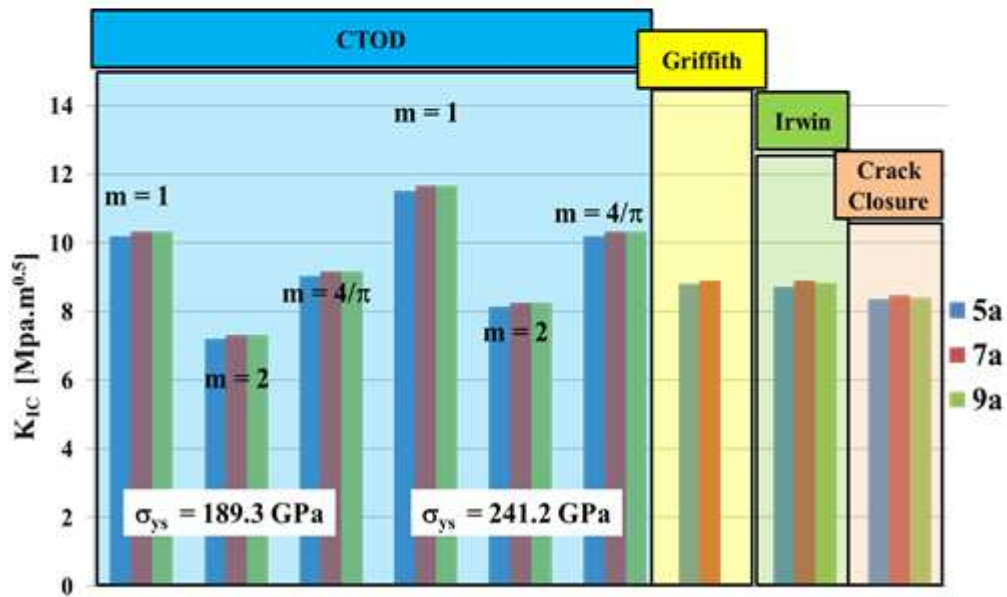
of  $m = 4/\pi$  is originally proposed by Irwin [90, 84]. According to Fig. 4-4, the choice of  $\sigma_{ys} = 189.3$  GPa is more realistic. In addition, MD simulations mostly predict “theoretical strengths” and naturally overestimate strength values. Despite these issues, predicted fracture toughness values appear to be crack length dependent. Fracture toughness values predicted by the three other methods are very promising. The Griffith’s, Irwin’s and Crack closure method exhibit almost identical fracture toughness values for any crack length considered. We estimate  $G_{IC}$  and  $K_{IC}$  of diamond should be  $\sim 84$  J/m<sup>2</sup> and  $\sim 8.7$  MPa.m<sup>0.5</sup>, respectively.

Table 4-8 Comparison of Predicted Fracture Toughness of Diamond with existing literature

<b>K<sub>IC</sub> (MPa.m<sup>0.5</sup>)</b>	<b>Reference</b>
8.85	Current study (Griffith)
8.46	Current study (Irwin)
8.84	Current study (Crack – Closure)
10.33	Current study (CTOD)
7.8 ± 1.3	[120]
6.5	(LPHT)
13	(HPHT) [121]
4.7-7.2	[112]
7-14	[112]
7-8	[122]
8.5	[123]
8.7	[124]



(a)



(b)

Figure 4-9 Summary of predicted fracture toughness of diamond using four different methods, (a)  $G_{IC}$  (b)  $K_{IC}$

Reports on pure diamond's fracture toughness are rare. In Table 4-8, we listed available fracture toughness values of ultra-nanocrystalline or single crystal diamonds along with our current values. It is evident that reported fracture toughness of diamonds varies between 4.7 to 14 MPa.m<sup>0.5</sup>. Several factors such as crystal structure variation, impurities content, experimental methods used are responsible for such disparities in diamond's toughness. Nevertheless, our current predictions are well within the reported values.

We are convinced from this study that continuum fracture mechanics theories are quite applicable at the nanoscale. The current study used diamond as a reference material. We believe that our study will be applicable to any other nanoscale material that exhibit brittle mechanical behavior.

## Chapter 5

### Computational Design of Novel Carbon Enriched $\text{Si}_{1-x}\text{C}_x$ Ceramics

This work has been published in journal Computational Material Science [125] which is available online. The work is reused here under the license agreement between Sheikh F Ferdous (author) and Elsevier of license number 3622581371404 which is provided by Copyright Clearance Center.

Silicon Carbide (SiC) exhibits excellent mechanical, thermal, and electrical properties. Low fracture toughness is one of the limiting properties of SiC that hinders its widespread applications. Recent studies suggest that preferable alteration of local microstructure may lead to dislocation nucleation in certain SiC polytypes. Here we report classical molecular dynamics simulations results that demonstrate thermodynamic viability of a new type SiC-based “C-enriched” ceramics where certain Si atoms are substituted by C atoms. We studied five different systems with different fraction of “C” enrichments, namely 10%, 20%, 30%, 40%, and 50%. We hypothesize that if “Si” atoms from SiC are randomly substituted by “C” atoms, then the bond lengths in the vicinities of the newly formed “C-C” bonds (in place of “Si-C” bonds) will be shortened but the overall crystal structure may not change significantly because both “C-C” and “Si-C” bonds are  $\text{sp}^3$  type. After equilibrating all types of enriched systems as well as the control SiC system, We studied their equilibrium densities, free energy profiles and internal morphologies as a function of “C” enrichment amount. The energy profiles suggest that all “C” systems should be thermodynamically viable because total configuration energies for all systems were minimized and remained stable over a long period of time. The densities of different “C” enriched system drop from  $3.25 \text{ gm/cm}^3$  to  $3.05 \text{ gm/cm}^3$  for “C” enrichment upto 20%. For higher than 20% “C” enrichments, densities then increase

monotonically. Since C-C bond distance is shorter than Si-C bonds, ideally densities of “C” enriched systems should have been increased with the increase of “C” enrichments. The opposite trend in densities upto 20% enrichment suggests additional microstructural change due to C enrichment. We explore the microstructures by measuring the average coordination number and radial distribution functions of different systems. Both these studies confirm that the newly designed materials have local microstructure change. Two dimensionally projected planner atomistic snapshots of all systems suggest that overall crystal structures of the new systems remain fairly unchanged.

## 5.1 Introduction and Background

Silicon Carbide (SiC) exhibits excellent wear resistance [126], high hardness and strengths [127], high temperature stability [128], high electrical stability [129], corrosion resistance [130] and many other useful properties for which it is widely considered for many structural and electromechanical system applications [131]. One limiting factor of SiC is that like most ceramic materials, it exhibits low toughness ( $\sim 4.6 \text{ MPa}\cdot\text{m}^{0.5}$ ) properties [132]. The strong covalent and ionic bonds that form the microstructure of SiC are responsible for such mechanical responses of SiC.

To enhance the toughness properties as well as to achieve novel properties in SiC compared to other conventional ceramic materials, many research groups investigated microstructure tailoring of SiC over the past couple of years [133, 134, 135, 136]. For example, Park et al. [133] and others [134, 135] developed microstructure-tailored  $\text{Si}_3\text{N}_4$ -SiC nanocomposites by hot pressing a blend of  $\text{Si}_3\text{N}_4$  and 3C-SiC at high temperatures ( $\sim 1800^\circ\text{C}$ ) for 1-2 hours. The process produces distinct  $\text{Si}_3\text{N}_4$ -SiC interface which leads to enhanced flexural strength and fracture toughness, both at room and elevated temperatures ( $\sim 1500^\circ\text{C}$ ). Using Spark Plasma Sintering (SPS), SiC-based

nanocomposites are processed by some groups [136, 137, 138]. Gao et al [136] developed mullite-SiC nanocomposite using SPS at 1500°C. The process yields improvement in flexural strength but reduction in fracture toughness compared to the properties of the constituents. Other nanocomposite systems such as YAG (Yttrium Aluminum Garnet)-SiC [137] and SiC-TiC [138] nanocomposites are also developed by SPS at high temperature (between 1550°C and 1800°C). Both strength and fracture toughness are enhanced in these new systems. It can be inferred from these studies that altered microstructure may play pivotal roles in improving the mechanical properties of these systems.

Formation of altered microstructure is also observed in monolithic SiCs. Most of these structures are formed during manufacturing stage [139, 140, 141] and often remain metastable. Nevertheless, such “process-induced” microstructures often yield enhanced properties. A recent work by Demenet et al [139] suggests that toughness enhancement via dislocation is possible in certain SiC polytypes along the basal (111) plane where each basal layer contains only one atom type (Si or C). Such dislocations are realized in both cubic (3C type) and hexagonal type (4H and 6H) SiC crystals. Studies by Hamada [140] and Ma [141] reveal that a metastable super-screw type dislocation in hexagonal SiC is possible during bulk growth of this material. Gogotsi et al [142] and Wittorf [143] attempted to develop diamond from SiC by depleting Si from SiC during CVD process. When long enough time is spent, this process yields pure C structure (diamond). At the intermediate stage, a distinct “C-rich” SiC interface microstructure often produced. It is, however, not clearly known how stable such intermediate microstructure would be or how would be their mechanical properties. There are some studies have been performed on developing “C” enriched SiC systems [144, 145]. Shen et al [144] employed finite temperature Quantum Molecular Dynamics (QMD) to study the effect of excess carbon

(up to 20%) in SiC on carrier mobility. They argue that additional carbon in SiC would enhance the carrier mobility because carbon is highly conductive. Their study suggests that stable carbon rich SiC structure is kinetically favorable when excess carbon amount is small. For higher fraction of excess carbon, the structure is metastable. Battistig et al [145] used low energy ion bombardment to produce carbon-enriched 6H-SiC system. Their study suggests that the amount of carbon-enrichment is ion polarity dependent. It can be inferred that it might be possible to develop carbon enriched SiC ceramics if favorable processing condition is provided. In essence, such processing conditions need to be related with “C” solubility in SiC systems. Recent works by Morgan and Szlufarska’s group show that atomic diffusion in SiC, such as Cs or Ag [146, 147, 148] in SiC, is possible. While it was not clearly known in the earlier days whether “C” can be dissolved in SiC or Si systems, Space and Slack [149] suggested that “C” can be diffused and dissolved in Si or SiC. Independent works by Wernera [150], Newman [151], Ivanovskii [152] and Chiang [153] later prove that “C” can be dissolved in Si [150, 151] or SiC [151, 152]. Our current study is somewhat motivated by such phenomena.

Here, we have investigated the feasibility of a new type of “C-enriched” SiC or  $\text{Si}_{1-x}\text{C}_x$  system where some Si atoms of SiC are substituted by C atoms using classical molecular dynamics simulation. We hypothesize that if “Si” atoms from SiC are randomly substituted by “C” atoms, then the bond lengths in the vicinities of the newly formed “C-C” bonds (in place of “Si-C” bonds) will be reduced but the overall crystal structure will not be changed significantly because both “C-C” and “Si-C” bonds are  $\text{sp}^3$  type (bonding type responsible for forming diamond/Zinc-blend lattice) [131, 132]. The simulation study will allow us to determine the equilibrium density, free energy and morphology of the newly designed ceramic materials as a function of “C” enrichment amount. As detailed in the next section, the energy profile will allow us to assess whether the “C-enriched” SiC is

thermodynamically acceptable or not. The studies on equilibrium bulk density and morphology of the structures will allow us to assess the nature of microstructure. The remaining part of the paper is outlined as follows. The next section describes detailed simulation procedure for modeling the novel “C” enriched SiC systems. The subsequent section covers the simulation results and pertinent discussions. A brief summary of our study is also provided.

## 5.2 Molecular Simulations of “Carbon” Enriched SiC

The proposed “C” enriched models have been built from a base 3C-SiC model. The base SiC model has been developed by folding the cubic SiC unit cell (with nominal lattice constant = 4.35 Å) seven times along the x, y and z directions. The unit cell of 3C-SiC, as shown in Fig 5-1, conforms to cubic zinc-blende crystal structure [132]. The crystal coordinates and nominal lattice constant of SiC unit cell was obtained from Ref. [154]. Once the base SiC model is developed, subsequently five “C” enriched models are built by randomly substituting selected fraction of “Si” atoms with “C” atoms. In this study, 10%, 20%, 30%, 40% and 50% Si atom substitution has been considered. These new “C” enriched structures will be referred as “Si<sub>1-x</sub>C<sub>x</sub>” systems where x represents the fraction of “C” atoms (0.5 < x < 1) by composition. Since SiC has 50% Si and 50% C atoms, according to our designation, SiC would be referred as Si<sub>0.5</sub>C<sub>0.5</sub>. The other five models will be referred as Si<sub>0.4</sub>C<sub>0.6</sub>, Si<sub>0.3</sub>C<sub>0.7</sub>, Si<sub>0.2</sub>C<sub>0.8</sub>, Si<sub>0.1</sub>C<sub>0.9</sub> and diamond (Si<sub>0.0</sub>C<sub>1.0</sub>) system. Once folding is complete, each “simulation-ready” cube-sized model contains a total of 2744 atoms with length of the side equals to 3.038 nm.

The interactions between Si and C have been described by the classical Tersoff Potential [82]. Periodic boundary conditions have been employed along all directions. Unless otherwise specified, all simulations have been carried out at 300 K. The equilibrium configurations of these models are obtained by performing simulations for 20 ps with isobaric-isothermal ensemble (constant number of atoms, pressure and temperature or NPT) [155]. The time constants for the thermostats [heat bath] and the barostats [pressure bath] are set to 1ps. The integration time step is set to 0.5 fs. Once simulation is complete, the final atomistic configurations and simulated data are post-processed and analyzed to assess the thermodynamic viability of “carbon” enriched SiC systems by determining the effect of “C” enrichment on (1) free energy minimization, (2) density, and (3) morphology. We argue that the energy profile will help us assess the thermodynamic stability of the “C” enriched structures. The density profile as a function of “C” enrichment will show the trend of density change. Since we know the nominal density of SiC and Diamond, the densities of the other “C” enriched structure should, at least in principle, fall between the two extremes. The morphologies of the structure will be assessed by determining the coordination numbers and radial distribution functions of the different models.

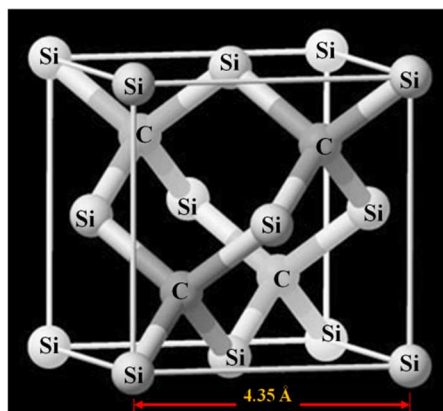


Figure 5-1 Unit Cell of SiC

### 5.3 Results and Discussions

As indicated before, our goal in this study is to investigate the thermodynamic viability of  $\text{Si}_{1-x}\text{C}_x$  systems as novel ceramic materials. We traced the energy profile, final equilibrium density and microstructure to assess the stability of the new ceramic system.

#### 5.3.1 Effect of “C” Enrichment on Free Energy Minimization

We argue that the “C” enriched  $\text{Si}_{1-x}\text{C}_x$  structures are thermodynamically stable if the following two conditions are satisfied: (1) overall free energy of the new systems must minimize after equilibration and (2) the minimum energy state must remain stable with time. Fig. 5-2 shows the potential energy profile of these six models (normalized with number of atoms) with time. It is evident from Fig. 5-2 that the “C” enrichment minimizes overall potential energy and the energy profile remains unchanged approximately after 1 ps during equilibration. It can also be observed that the equilibrium potential energies-per-atom for systems up to 20% carbon enrichment are very similar ( $\sim 6.2$  eV/atom). The equilibrium energies dramatically start to alter for carbon enrichment more than 20%. At this stage, we do not quite understand why there is a sudden change in energy (per atom) for the models with higher “C” enrichments. It is possible that the internal microstructure might have reorganized when excess carbons are more than 20%. We like to advise our readers to read further to gather further understanding of these phenomena. Nevertheless, this study demonstrates that the proposed “C” enriched SiC-based ceramics are thermodynamically feasible.

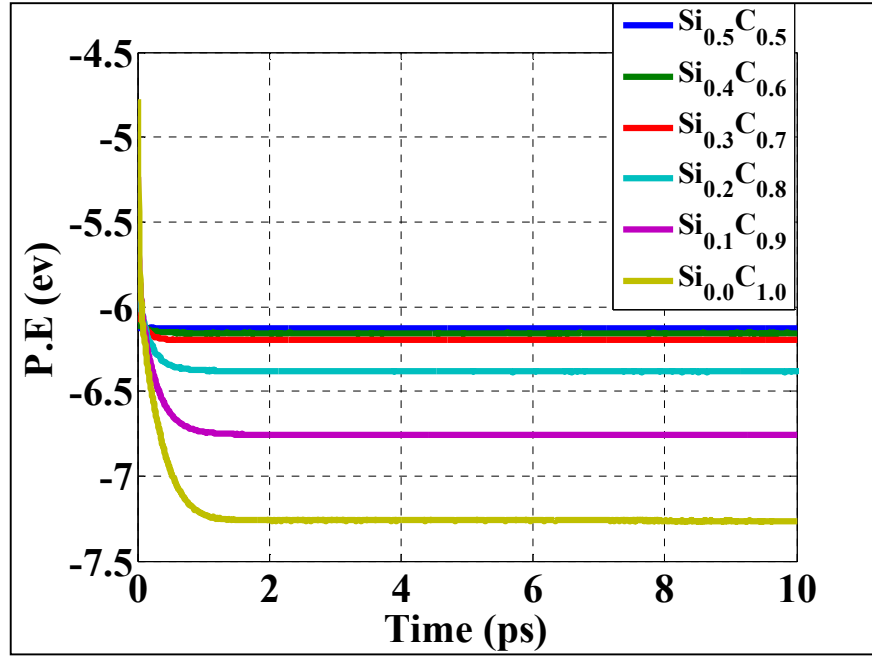


Figure 5-2 Potential Energy Profile of the “C” enriched models with time. Here  $\text{Si}_{0.5}\text{C}_{0.5}$  stands for pure SiC and  $\text{Si}_{0.0}\text{C}_{1.0}$  is for pure Diamond. The energy shown here is normalized per atom.

### 5.3.2 Effect of “C” Enrichment on Density

For each  $\text{Si}_{1-x}\text{C}_x$  system, we have computed densities using the following equation:

$$\rho_{avg} = \frac{N_{total}[M_{Si}(1-x) + M_C x]F}{V_{equilibrium}} \quad 5.1$$

Here,  $\rho_{avg}$  is the average density of  $\text{Si}_{1-x}\text{C}_x$  system in gm/cc unit,  $N_{total}$  is the total number of atoms present in the simulation supercell,  $M_{Si}$  is the molecular weight of Si = 28.0855 a.m.u,  $M_C$  is the molecular weight of C = 12.022 a.m.u,  $x$  is the fraction of enriched C atoms,  $F$  is the unit conversion factor = 1.6605402 and  $V_{equilibrium}$  is the volume of the super cell in  $\text{\AA}^3$ . The results are shown in Fig 5-3. It can be observed from

Fig. 5-3 that the relation between density and "C" enrichment up to 20% is different from the relation between density and "C" enrichment with more than 20% enriched carbon. In particular, it is observed that densities of  $\text{Si}_{1-x}\text{C}_x$  first decreases monotonically as fraction of "C" enrichment increases until 20% "C" enrichment, and then densities start to monotonically increase when "C" enrichment is beyond 20%. It is known that the densities of SiC and diamond are  $3.21 \text{ gm/cm}^3$  and  $3.51 \text{ gm/cm}^3$ , respectively [146]. It is evident from Fig. 5-3 that the densities of SiC (0% enriched system) and diamond (50% enriched system) from our studies are  $3.257 \text{ gm/cm}^3$  and  $3.459 \text{ gm/cm}^3$  respectively. Both these densities are less than 1.5% different from the reported values. What we do not understand at this point why the density decreases with "C" enrichment when "C" enrichment is less than 20%. We believe that the internal microstructure of different enriched systems might provide better insight on this matter.

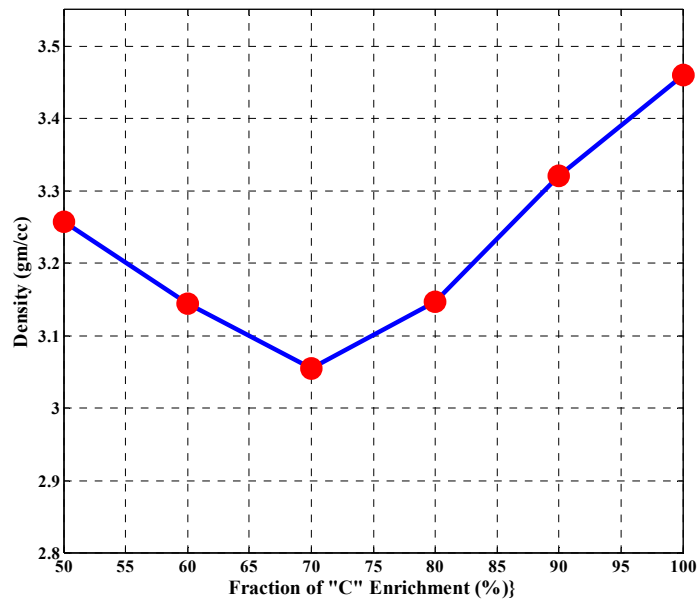


Figure 5-3 Change in density of  $\text{Si}_{1-x}\text{C}_x$  systems as a function of "C" enrichments

### 5.3.3 Effect of “C” Enrichment on Morphology

Our key argument about the  $\text{Si}_{1-x}\text{C}_x$  systems is that the local microstructure of “C” enriched system should alter the local microstructure of SiC because the “C” enrichment process locally replaces many Si-C bonds with C-C bonds, and Si-C bond is larger than C-C bond. However, such “sudden” bond length reduction should not destabilize the whole system because both C-C and Si-C bonding are  $\text{sp}^3$  type. In order to verify this hypothesis, we revisited the equilibrated  $\text{Si}_{1-x}\text{C}_x$  structures to check (1) whether there is any changes in their coordination numbers (C.N.) compared to their pristine counterpart (SiC) and (2) how the Si and C atoms reposition themselves when excess carbon atoms are added to the systems.

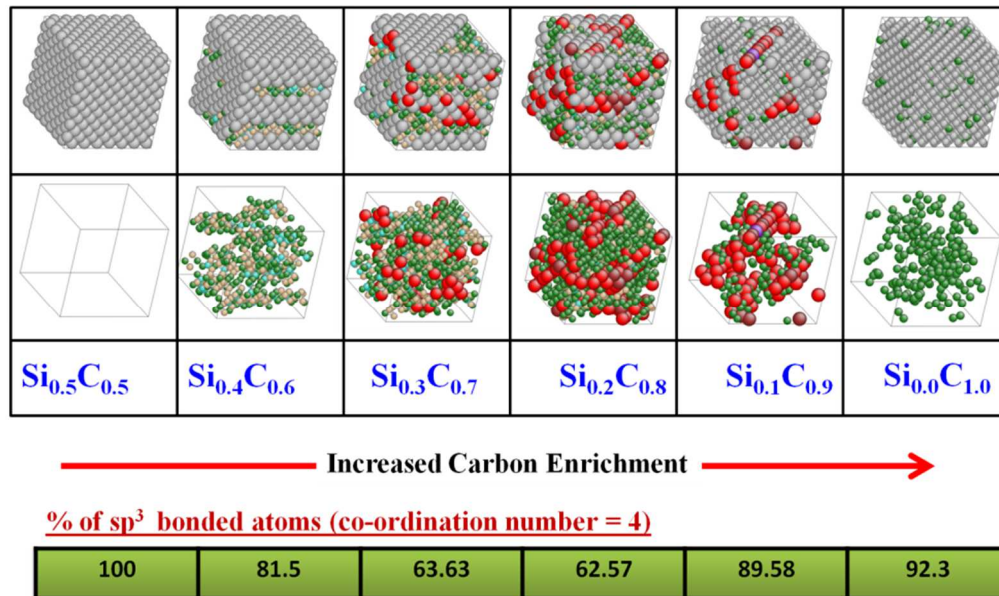


Figure 5-4 Effect of “C” enrichments on the morphology of  $\text{Si}_{1-x}\text{C}_x$  systems. It is obvious that pure SiC and pure Diamond have predominantly  $\text{sp}^3$  bonded atoms. However, the other “C” enriched systems have some bonding other than  $\text{sp}^3$  type.

Since pure SiC is built on Zinc-blend structure, the coordination number (C.N.) for any atom in SiC is equal to 4. In light of this, we argue that C.N.s can be used as the critical parameter to assess the microstructure morphology of the newly formed systems. The top row in Figure 5-4 shows the equilibrium structure of SiC (far left) and five other C enriched systems. Here the grey colored atoms are atoms with C.N = 4. Any deviation (increase or decrease) of any atom from C.N = 4 is represented by other than grey color [88]. The second row in Fig. 5-4 shows atoms with C.N  $\neq$  4 only. The percentages of the four coordinated atoms are also shown at the bottom of Fig.5-5. It is obvious from this result that “C” enrichment process alters the SiC microstructure significantly. To have a clearer view of overall crystal structure, same structures are projected on a 2D plan in Fig. 5-5. It can be seen that both SiC and Diamond show highly crystalline order. As expected, the other “C” enriched models exhibit some deviation from pure Zinc-blende structure (SiC). However, overall crystal structure is predominantly Zinc-blende type. This is because at least 60% of the atoms of any  $\text{Si}_{1-x}\text{C}_x$  system have C.N = 4. What we do not know at this point is why C.N. first reduces with increase in “C” percentage, and then start to increase with the increase in “C” percentage. We suspect that the sudden bond length changes, occurs due to random replacement of “Si” atoms by “C” atoms, may force other neighboring atoms to reconfigure so that overall stability is maintained. Different amount of “C” enrichment contributed differently to the overall structure. To gain further insight, we have measured the radial distribution function (RDF) [156] for all systems and plotted the result in Fig. 5-7. Figure 5-6 shows the “nominal” nearest neighbor distances of pre-simulated SiC crystal. This plot is constructed by identifying equidistant neighbors in a  $2 \times 2 \times 2$  SiC unit cell (contains a total 64 atoms). The population in the vertical axis represents the number of neighbors with same distance. For example, the 1<sup>st</sup> nearest neighbor in SiC is located at distance equals to 1.88 Å and there are 85 of such neighbor

present in that unit cell. It is also shown in Fig. 5-6 that Si-C atom pair is present at the first nearest neighbor. The second nearest neighbor is located at a distance equals to 3.08 Å and both C-C and Si-Si atom pairs are presence. The subsequent nearest neighbors (up to 5<sup>th</sup>) are also identified in Fig 5-6. This figure will guide us in identifying the type of atom pairs present in the radial distribution functions shown in Fig. 5-7.

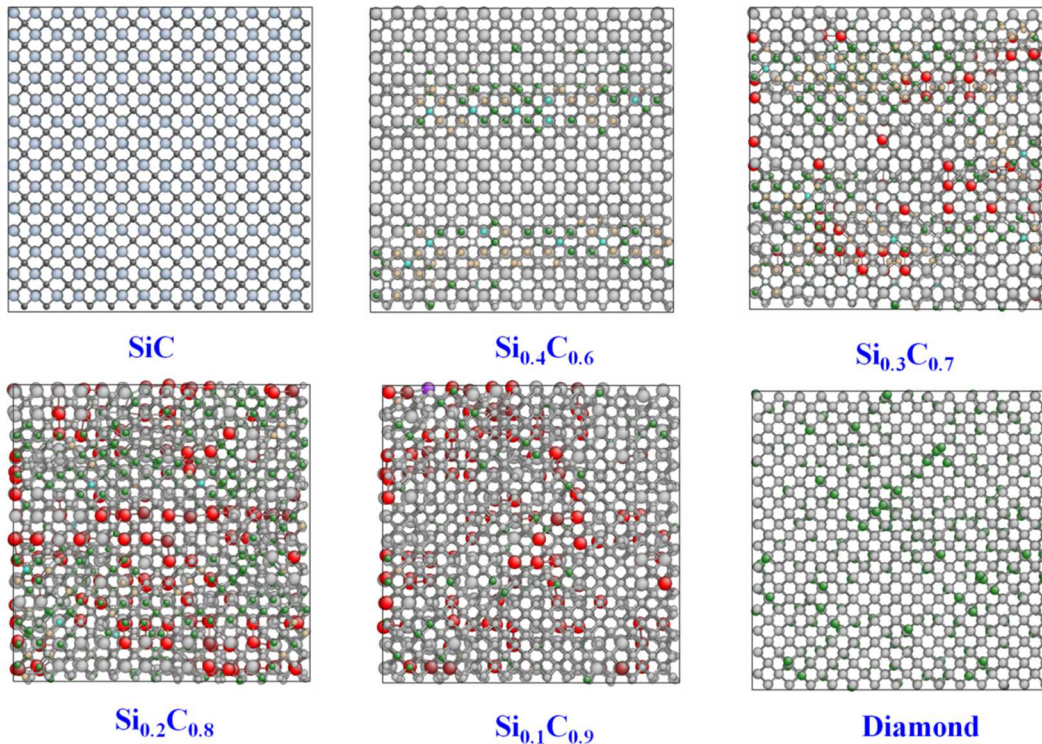


Figure 5-5 Equilibrated Crystal Structure of different “C” enriched models projected on 2D plane

It can be observed from Fig. 5-7 that SiC remain highly crystalline as evident from the presence of five distinct peaks. When the peaks are compared with the “nominal” peaks shown in Fig. 5-7, it is obvious that 1<sup>st</sup>, 2<sup>nd</sup> and 3<sup>rd</sup> neighbors in SiC system is Si-C, C-C/Si-Si and Si-C. With the increase of “C” enrichment, it appears that

new peaks start to form correspond newly created C-C bonds [157] in place of Si-C bond. For example, two small peaks (1.69 Å and 2.83 Å) are visible ahead of the first and second nearest neighbors (1.85 Å and 3.01 Å) of the  $\text{Si}_{0.4}\text{C}_{0.6}$  (10% enriched system). The first small peak essentially implies few C-C atom pairs attempting to form  $\text{sp}^3$  C-C bond (nominal distance = 1.54 Å) but could not do so because of dominant presence of Si-C bonds. The first Si-C neighbor at 1.85 Å also implies distance reduction as we compare this value with the nominal distance shown in Fig. 5-6. The reduction of Si-C bond distance (and other nearest neighbor distances) also implies reduction in system volume compared to SiC. The density of this system, however, is less than SiC. This is happened because the amount of volume reduction is not enough compared to the amount of mass reduction (by replacing heavier Si atoms with lighter C atoms). Hypothetically, if the C-C bond distances would have further reduced to its expected value (1.54 Å), the overall density might have been increased. The 20% and 30% enriched systems show a competition between newly formed C-C bonds and existing Si-C bonds in the short range (up to 3Å). The presence of wider “width” of the longer-distant peaks (more than 3 Å) implies disruption of long-range crystal ordering. The C.N. in Fig. 5-5 also confirms this fact. As we further enrich the system with more carbon atoms, the C-C bond starts to overtake the existing Si-C bond and eventually become highly crystalline diamond structure. The plots shown in Fig. 5-6 imply that the 10% “C” enrichment system is predominantly SiC type but the 40% “C” enrichment system is predominantly diamond type. The other two systems are somewhat a blend of SiC and diamond structure. We argue that there are two perfectly coordinated systems are involved – one being SiC ( $\text{Si}_{0.5}\text{C}_{0.5}$ ) and the other is Diamond ( $\text{Si}_{0.0}\text{C}_{1.0}$ ). As a result, systems with “C” enrichments less than 20% want to achieve more like SiC configurations (implying Si-C bonding is more desirable than C-C bonding) whereas the

systems with “C” enrichments higher than 30% want to achieve more like Diamond configurations (implying Si-C bonding is less desirable than C-C bonding). The overall structure is still crystalline. We are currently investigating the mechanical responses of these newly formed systems and understanding the role of “C” enrichment. These results will be presented in later publications.

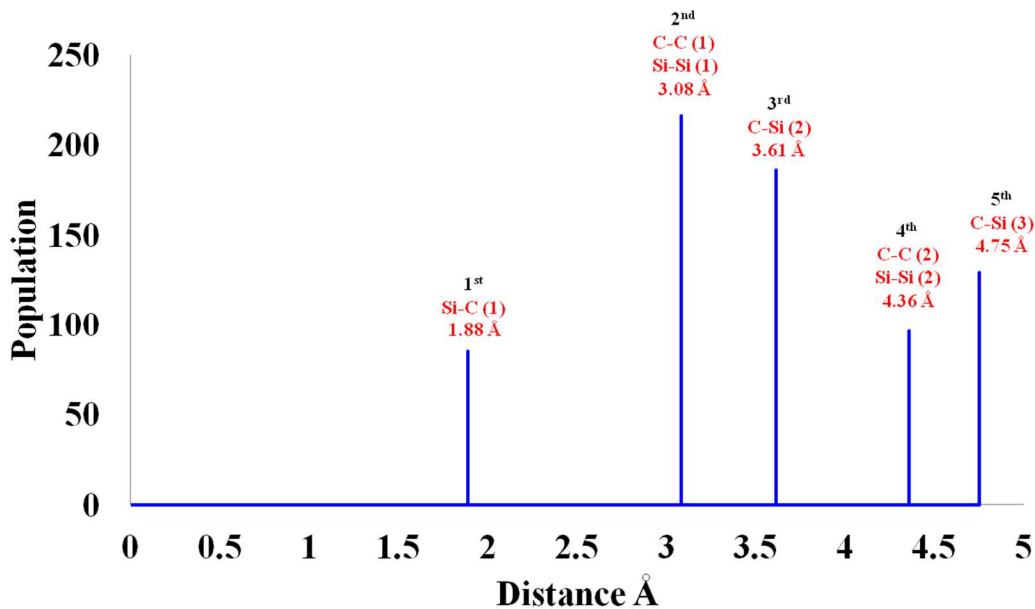


Figure 5-6 “Ideal” radial distribution plot based on initial SiC model that shows different atom-atom neighbor distances

## 5.4 Summary

A brief summary of our study is presented below:

- In this study, we have investigated thermodynamic viability of a new type of “C” enriched SiC ceramics using classical molecular dynamics simulations. We studied five different systems with different of “C” enrichments, namely 10%, 20%, 30%, 40%, and 50%.
- Our study was based on the hypothesis that if “Si” atoms from SiC are randomly substituted by “C” atoms, then the bond lengths in the vicinities of the newly formed “C-C” bonds (in place of “Si-C” bonds) will be shortened but the overall crystal structure may not change significantly because both “C-C” and “Si-C” bonds are  $sp^3$  type.
- We have studied the equilibrium densities, free energy profiles and internal morphologies of the “C” enrichment systems after equilibrating our models for 10 ps.
- The configurational energies for all “C” systems minimized and remain stable over a long period of time suggesting thermodynamic viability.
- The densities of different “C” enriched system drop from 3.25 gm/cm<sup>3</sup> to 3.05 gm/cm<sup>3</sup> for “C” enrichment upto 20%. For higher than 20% “C” enrichments, densities then increase monotonically. Since C-C bond distance is shorter than Si-C bonds, ideally densities of “C” enriched systems should have been increased with the increase of “C” enrichments. The opposite trend in densities upto 20% enrichment confirms additional microstructural change due to C enrichment.
- We explore the microstructures by measuring the average coordination number and radial distribution functions of different systems. These studies

confirm that the newly designed materials have remain crystalline but exhibit local microstructure change.

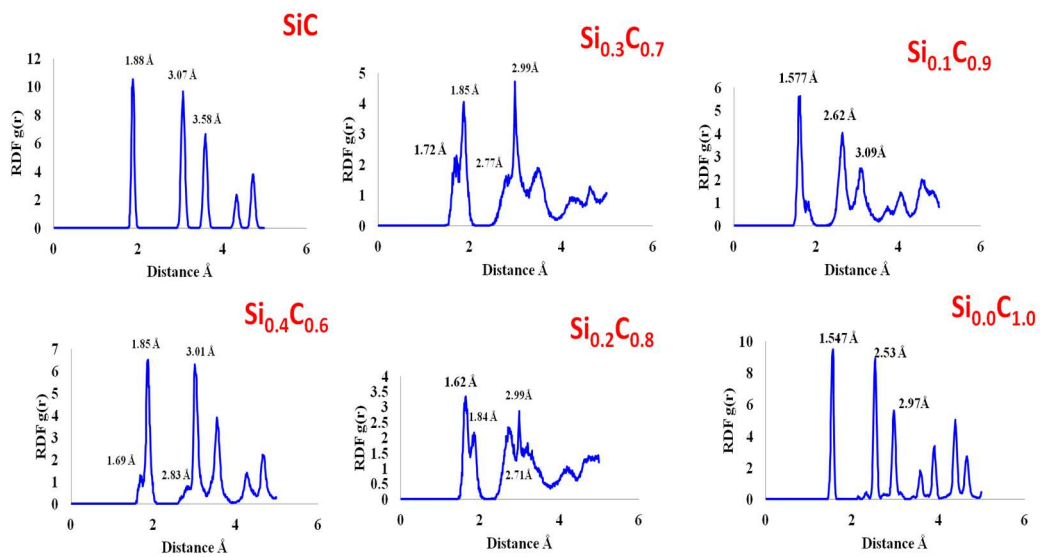


Figure 5-7 Radial distribution plot of different “C” enriched systems. Note the sharp peaks in the SiC and Diamond systems. Also note that Si-C to C-C bond transition in other “C” enriched systems. Presence of “disturbed” microstructure is evident from wider “width” of different peaks

## Chapter 6

### Mechanical Properties of Computationally Designed Novel Carbon Enriched $\text{Si}_{1-x}\text{C}_x$

#### Ceramics

Silicon Carbide (SiC) exhibits excellent mechanical, thermal and electrical properties. Low fracture toughness is one of the limiting properties of SiC that hinders its widespread applications. Recent studies suggest that controlled alteration of local microstructure may lead to dislocation nucleation in certain SiC polytypes. Here, we report classical molecular dynamics simulation results to demonstrate mechanical behavior of a new type SiC-based “C enriched” ceramics where certain Si atoms are substituted by C atoms. We studied five different systems with different fraction of “C” enrichments, namely 10%, 20%, 30%, 40% and 50%. Thermodynamic stabilities of such novel microstructures have been studied recently [125]. Significant effect of “C” enrichment on the tensile and shear properties of the new ceramic materials have been observed. Compared to pure SiC, the tensile strengths of enriched systems always increase but to a different extent depending on the amount of enrichment. Shear strengths, however, tend to decrease with increase in carbon enrichment until enrichment is 40%. The elastic constants  $C_{11}$  and  $C_{44}$  were measured and both increase significantly with carbon enrichment. The area under the stress-strain tensile and shear curves have been estimated to assess the tensile and shear toughness properties and it has been found that both types of toughnesses increase significantly with carbon enrichment.

## 6.1 Introduction and Background

Silicon Carbide (SiC) is an important structural material with excellent wear and corrosion resistance [158, 126, 130], high hardness and strengths [127], high temperature and electrical stability [128, 129] and many other useful properties. However, poor fracture toughness properties [132] of SiC often limits the scope of its applications [131]. Knowing that enhancing fracture toughness would require additional strain energy dissipation during deformation, several research groups attempted to incorporate such mechanisms in SiCs via microstructure tailoring [133, 134, 135, 136, 137, 138]. For example, Park et al. [133] and others [134, 135] developed microstructure-tailored Si<sub>3</sub>N<sub>4</sub>-SiC nanocomposites by hot pressing a blend of Si<sub>3</sub>N<sub>4</sub> and 3C-SiC at high temperatures (~1800°C) for 1-2 hours. The process produces distinct Si<sub>3</sub>N<sub>4</sub>-SiC interfaces which lead to enhanced flexural strength and fracture toughness, both at room and elevated temperatures (~1500°C). Using Spark Plasma Sintering (SPS), SiC-based nanocomposites are processed by some groups [136, 137, 138]. For example, the YAG (Yttrium Aluminum Garnet) - SiC [137] and the SiC-TiC [138] nanocomposites developed by SPS method (between 1550°C and 1800°C) exhibit both high strength and high fracture toughness compared to their constituents.

Forming altered microstructure to induce dislocation is also observed in monolithic SiCs. Most of these structures are formed during manufacturing stage [139, 140, 141] but often remain metastable. Nevertheless, such “process-induced” microstructures often yield enhanced properties. A recent work by Demenet et al [139] suggests that toughness enhancement via dislocation is possible in certain SiC polytypes along the basal (111) planes where each basal layer contains only one atom type (Si or C). Such dislocations are realized in both cubic (3C type) and hexagonal type (4H and

6H) SiC crystals. Studies by Hamada [140] and Ma [141] reveal that a metastable super-screw type dislocation in hexagonal SiC is possible during bulk growth of this material. Some other studies suggest that microstructure of SiC can also be tuned by infusing extra “C” atoms in SiC systems [144, 145], either as “Si” substitution or as interstitials. For example, Battistig et al [145] used low energy ion bombardment to produce carbon-enriched 6H-SiC system. Their study suggests that the amount of carbon-enrichment is ion polarity dependent. Gogotsi et al [142] and Wittorf et al [143] independently observed that a distinct “excess carbon SiC” interface layer is formed between SiC and Diamond during diamond formation from SiC using CVD method.

While these studies did not focus on the mechanical behaviors, we believe that the enriched systems may exhibit improved toughness properties because of favorable microstructural change. We argue that if “Si” atoms from SiC are randomly substituted by “C” atoms, then the bond lengths in the vicinities of the newly formed “C-C” bonds (in place of “Si-C” bonds) will be reduced but the overall crystal structure will not be changed significantly because both “C-C” and “Si-C” bonds are  $sp^3$  type (bonding type responsible for forming diamond/Zinc-blend lattice) [132, 131]. As such, there will be a significant number of distorted crystals within the bulk system, which, during deformation, will assist dissipating additional strain energy.

Thermodynamically, developing carbon enriched SiC ceramics depends on “C” solubility in the SiC systems, and it is obvious from SiC phase diagram [159] that C and Si are not soluble in room temperature. Yet, works of Scace and Slack [149], Kobayashi et al [160] and Mykhaylyk and Gadriza [161] independently suggested that under certain conditions “C” can be diffused and dissolved in Si or SiC. Independent works by Wernera [150], Newman [151], Ivanovskii [152] and Chiang [153] later prove that “C” can be dissolved in Si [150, 151] or SiC [151, 152]. Recently, using classical molecular dynamics

simulation, we [125] investigated the thermodynamic feasibility of a five different “C-enriched” SiC or  $\text{Si}_{1-x}\text{C}_x$  ( $0.5 < x < 1$ ) systems where some Si atoms of SiC are substituted by C atoms. Here, we report the mechanical behavior of such systems using molecular dynamics simulation.

## 6.2 Molecular Models and Simulation Procedure

Details on the development of the molecular models are described in Ref. [125]. Here we provide a brief description. To develop various “C” enriched models, we started with a base 3C-SiC single crystal [132, 154] containing 2744 atoms in total. Five different “C” enriched models are then built (figure 6-1) by randomly substituting selected fraction of “Si” atoms with “C” atoms. In particular, 10%, 20%, 30%, 40% and 50% Si atom substitutions have been considered. The interactions between Si and C have been described by the classical Tersoff Potential [82]. Periodic boundary conditions have been employed along all directions. Unless otherwise specified, all simulations have been carried out at 300 K. To develop tensile and shear stress-strain curves, atomistic models were equilibrated first to attain stress-free state; then models were subjected to incremental tensile and shear loading, respectively. During equilibration, simulation was run up to 20,000 time-steps in NPT ensemble [155]. During each incremental mechanical loading, a uniform strain was prescribed on the entire MD model. This is done by uniformly scaling (expanding) the dimensions of the MD cell in the direction of the deformation and re-scaling the new coordinates of the atoms to fit within the new dimensions. After this initial deformation, the MD simulation was continued and the atoms were allowed to equilibrate within the new MD cell dimensions. This process is repeated for the subsequent increments of deformation. The applied-strain increment for the axial

tension (y-direction) and shear (zx plane) was 0.25%. After that, all systems were relaxed for 0.25 ps (equilibration run), and then the developed components of “engineering virial” stresses [83] were averaged over an interval of 0.25 ps (production run). Stress–strain curves were then generated by pairing each average stress value with the corresponding strain increment value. Unless otherwise specified, the integration time step was set to 0.5 fs. The MD simulations were performed using DL-POLY (version 2.20) simulation package developed by Daresbury Laboratory (Daresbury, Warrington, and Cheshire, UK) [80], which is a freely available (for academic and similar institution) open source molecular simulation code.

### 6.3 Results and Discussions

The main scope of this study is to determine the effect of excess carbon fraction on the overall mechanical properties of the materials. We suspect that there are other parameters that might influence the mechanical properties as well. For example, we have randomly substituted silicon atoms with carbon atoms to develop the carbon enriched models. To confirm that mechanical properties of a particular carbon enrich models demonstrate statistically acceptable results, we independently developed three models for each carbon enrichment type. We also varied model size by 20 times (one type having 2744 atoms and other having 57600 atoms) to understand the role of model size on material properties. To study the role of free surface, we studied the effect of boundary conditions on the mechanical properties.

### 6.3.1 Effect of carbon enrichment on Tensile and Shear Response

Tensile and shear response of different carbon enriched models are shown in Fig. 6-2. It is evident from Fig. 6-2(a) that both tensile strengths and stiffness of  $\text{Si}_{1-x}\text{C}_x$  systems increase with carbon enrichments. Table 6-1 lists the failure strengths, strains and elastic constants  $C_{11}$  and  $C_{44}$  in tension and shear of the simulated models. It is evident from Table 6-1 that tensile strengths first increase by 23 GPa when “C” is 10%.

Table 6-1 Measured Properties of different “C” enriched systems from atomistic simulations

Property	“C” Enriched Systems				
	SiC	$\text{Si}_{0.4}\text{C}_{0.6}$	$\text{Si}_{0.3}\text{C}_{0.7}$	$\text{Si}_{0.2}\text{C}_{0.8}$	$\text{Si}_{0.1}\text{C}_{0.9}$
$\sigma_{\text{fail}}$ [GPa]	57	80	70	71	86
$\tau_{\text{fail}}$ [GPa]	72	53	48	56	78
$\varepsilon_{\text{fail}}$ [%]	0.33	0.41	0.35	0.26	0.2
$\gamma_{\text{fail}}$ [%]	0.12	0.4	0.34	0.31	0.36
$C_{11}$ [GPa]	342	465	740	760	780
$C_{44}$ [GPa]	205	400	270	280	272
Tensile Toughness [GPa]	112.86	190.65	259	197.6	156
Shear Toughness [GPa]	24.6	160	91.8	86.8	97.92

For additional 10% increase “C” enrichment, strength then reduce by 10 GPa and remain same even when “C” enrichment is 30%. For 40% enrichment, strengths then increase to 86 GPa. The shear strength, however, shows a different trend in that it decreases for “C” enrichment up to 30% and starts to increase when “C” enrichment is higher than 30%. The failure strains are also affected by “C” enrichments. Except for 10% “C” enrichments, any increase in “C” enrichment reduces tensile failure strains significantly. The scenario is completely different when models are loaded in shear. It is apparent from Table 6-1 that “C” enrichments enhance shear failure strains significantly. The Table 6-1 also suggests that elastic constant  $C_{11}$  increases monotonically with the

increase of “C” fractions in SiC. The shear modulus  $C_{44}$  also increases with “C” enrichment but not to the extent of  $C_{11}$  increase with “C” enrichment. The last two rows of Table 6-1 list tensile and shear toughness properties that are obtained from the area under the individual stress-strain curves. It is obvious that 10% “C” enrichment yields the toughest system. These results suggest that both the “C” enrichment fraction and loading direction play substantial role in controlling the strength, stiffness and toughness of SiC.

Figure 6-3 shows post-failure MD snapshots of SiC and each carbon enriched systems studied for tensile response. The smaller grey circles represent carbon atoms and larger light blue circles represent Si atoms. By closely inspecting the snapshots, we can clearly observe that failure of each model is caused by void formations (cavitation) near silicon-rich area. This is because the bond energies of “Si” rich zones are less compared to any other zones within the entire volume. Therefore, these locations represent the weakest link for the whole system. For shear deformation, we observe that mode of failures vary with different extent of carbon enrichment. For clarity, we have color coded the atoms according to coordination number and von Mises shear strains [88] as shown in the top and bottom rows of Fig. 6-4 respectively. Since atoms in all ceramics are bonded via  $sp^3$  bonding, the equilibrium coordination number of pure SiC is 4 and represented by grey color in Fig. 6-4 (also in Fig. 6-1). The coordination numbers of enriched system vary in equilibrium condition as shown in Fig. 6-1. Any abrupt change in coordination number during shear deformation would be an indication of failure path. Based on this argument, we can observe that all enriched system fail roughly along (100) direction. The color coded atoms based on von Mises shear strains also show abrupt change in local shear strains deviation along the predicted failure paths based on coordination number analysis. This is probably the reason why we observed dramatic

increase in shear failure strain as well as toughness for the enriched systems as compared to pure SiC.

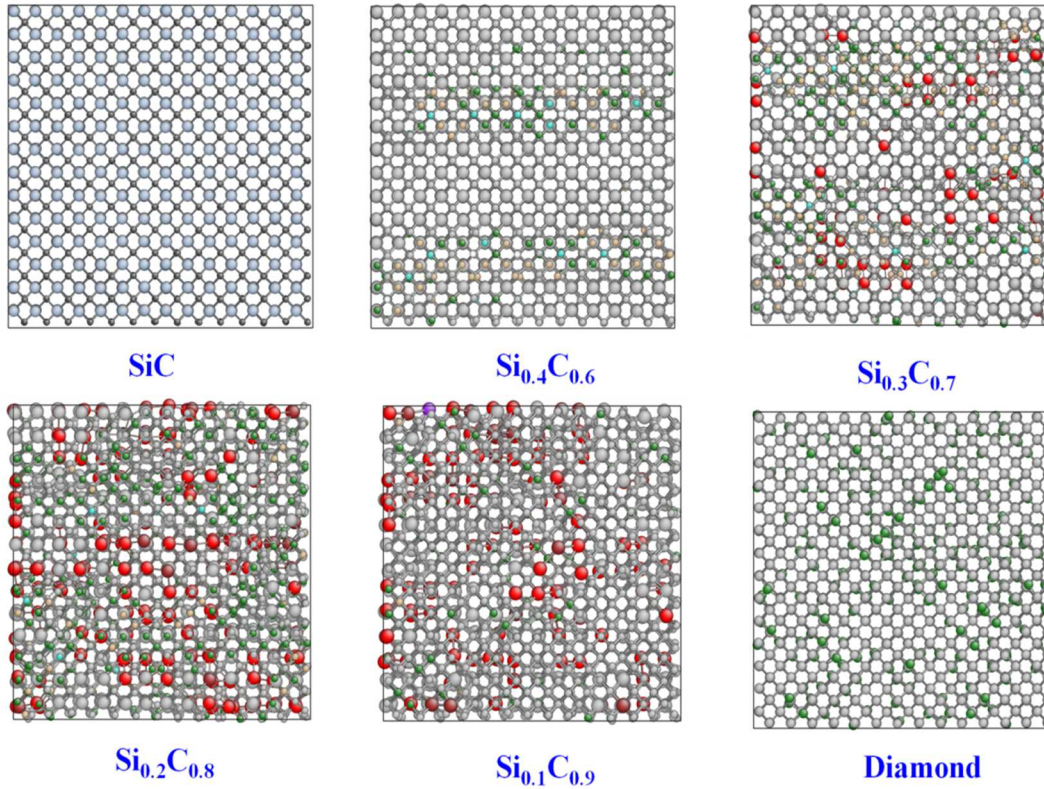
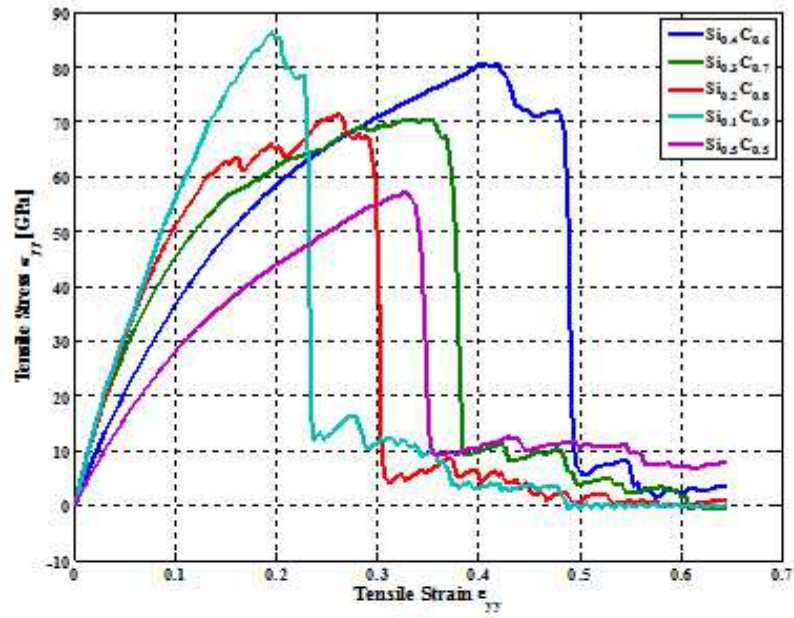
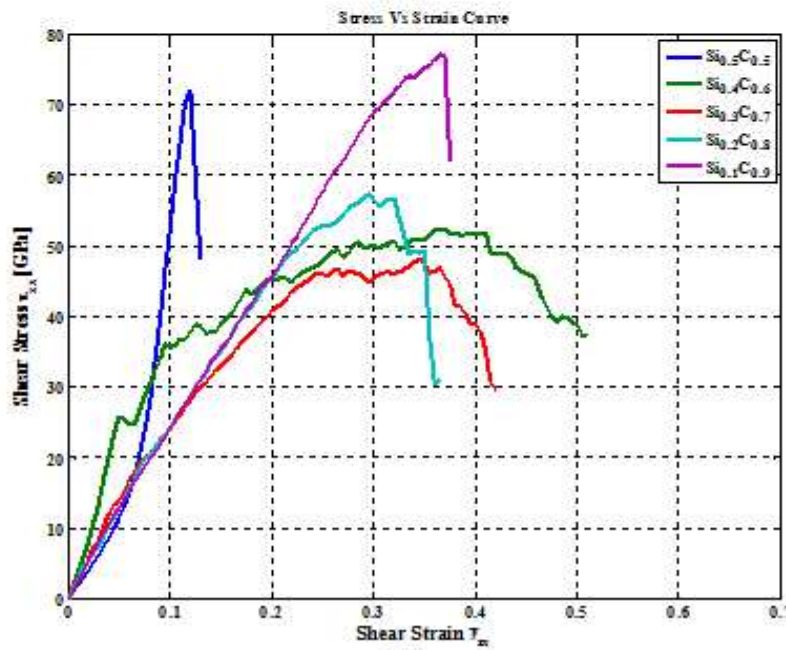


Figure 6-1 Equilibrated Crystal Structure of different “C” enriched models projected on 2D plane



(a)



(b)

Figure 6-2 Stress-Strain curves for different carbon enriched models (a) Tensile response, (b) Shear response

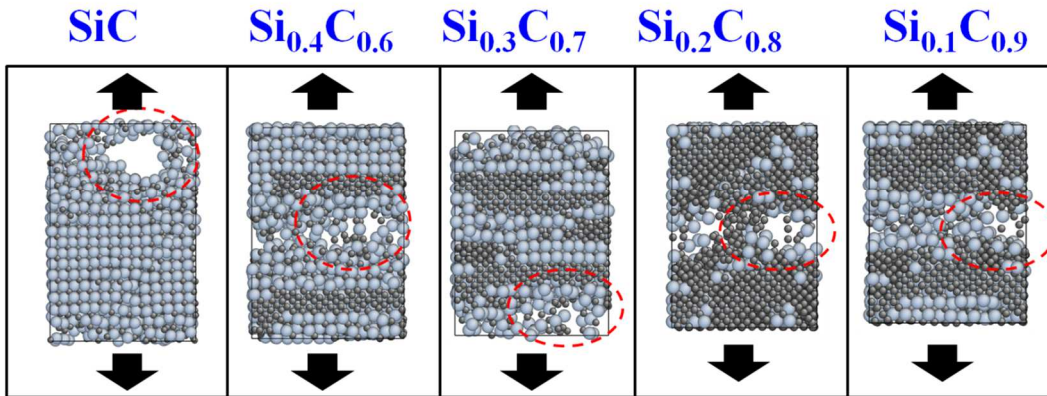


Figure 6-3 Tensile failure snapshots for different “C” enriched models

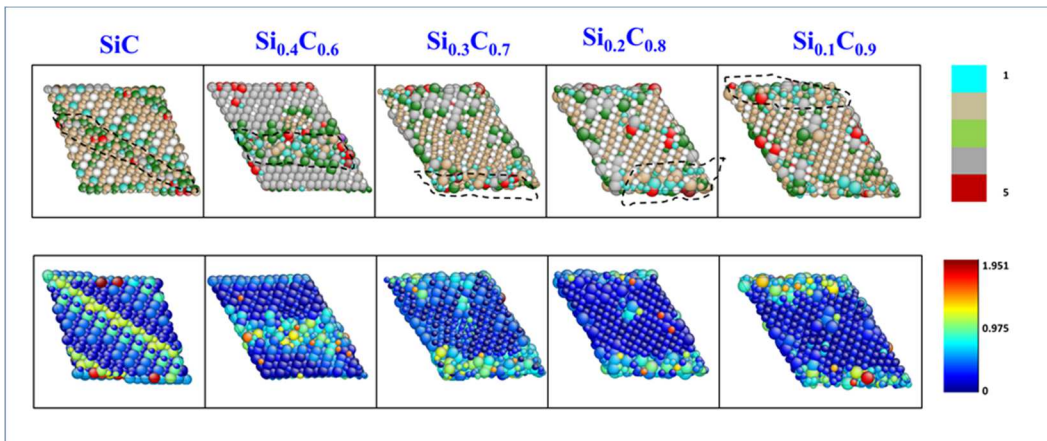
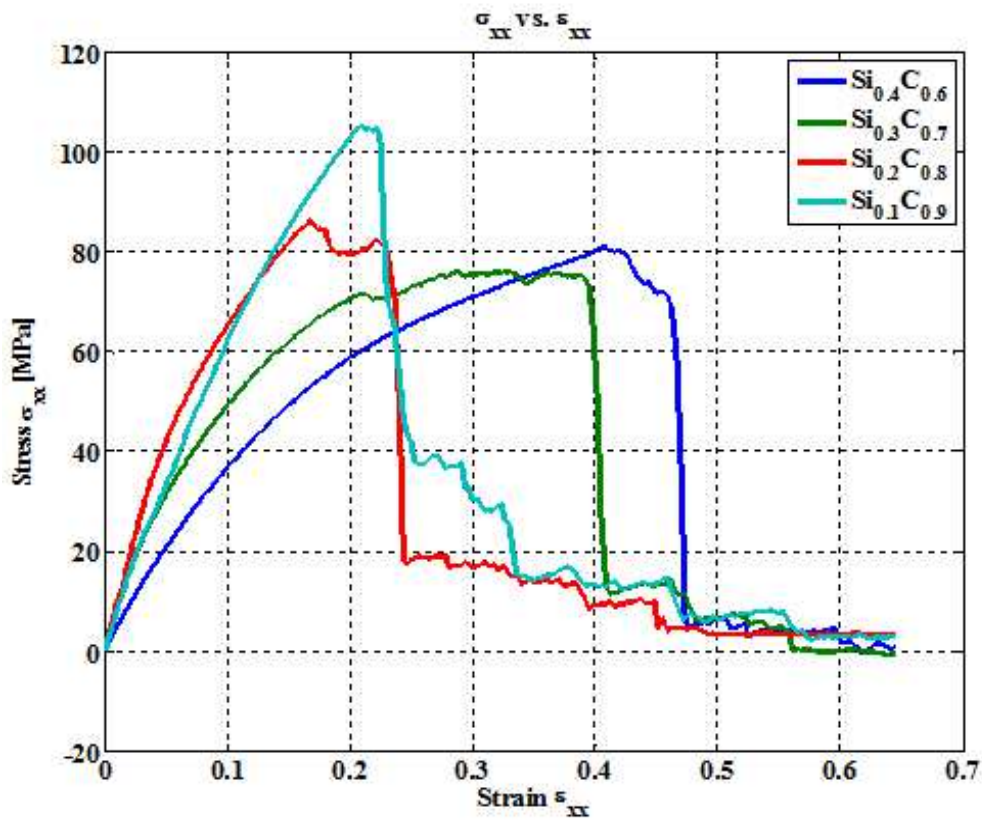


Figure 6-4 Shear failure snapshots for different “C” enriched models. To clearly identify shear failure locations, atoms are colored by coordination number and von-mises shear strain at the top and bottom figures

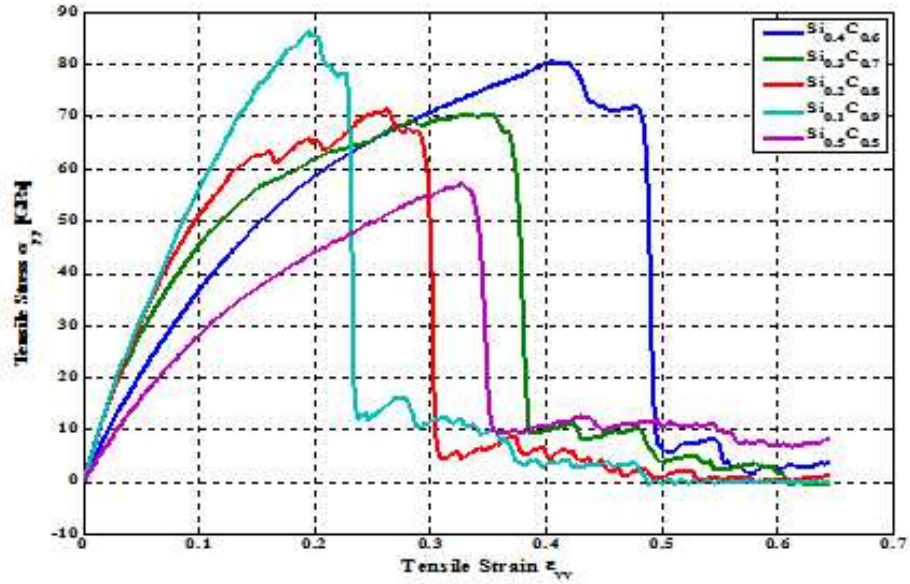
### 6.3.2 Effect of Loading Direction.

The results reported in Section 6.3.1 are based on the tensile responses along one direction (along y-direction) only. Following identical procedure, we generated tensile stress strain curves for other two directions (along x and z) for those models (2744 atoms) we studied earlier. Results are shown in Fig. 6-5. It is evident that the charts are

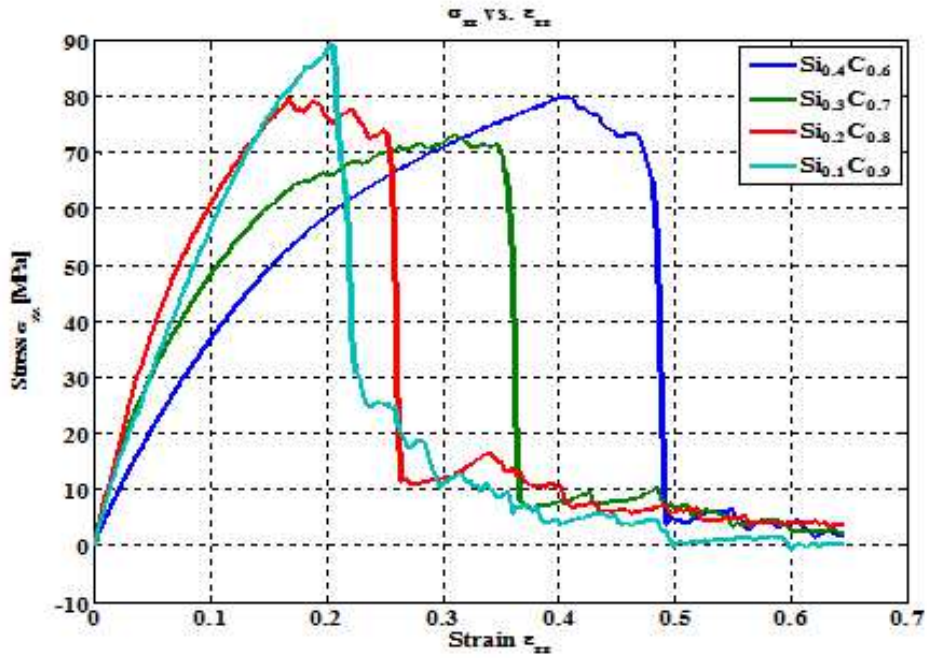
not identical but overall trends remain the same as described in Section 6.3.1. In general, the  $\text{Si}_{0.4}\text{C}_{0.6}$  systems appear to be the toughest and the  $\text{Si}_{0.1}\text{C}_{0.9}$  systems are the strongest. Both these models exhibit better strength and toughness properties than pure SiC. To further understand the matter, we developed larger models containing  $\sim 20$  times more atoms than the existing models and separately obtained their tensile responses along the three coordinate directions, as shown in Fig. 6-6. Results are very consistent compared to the results obtained for the smaller models. This part of the study suggests that the size of models were large enough and can be considered representative for each carbon enriched models.



(a)

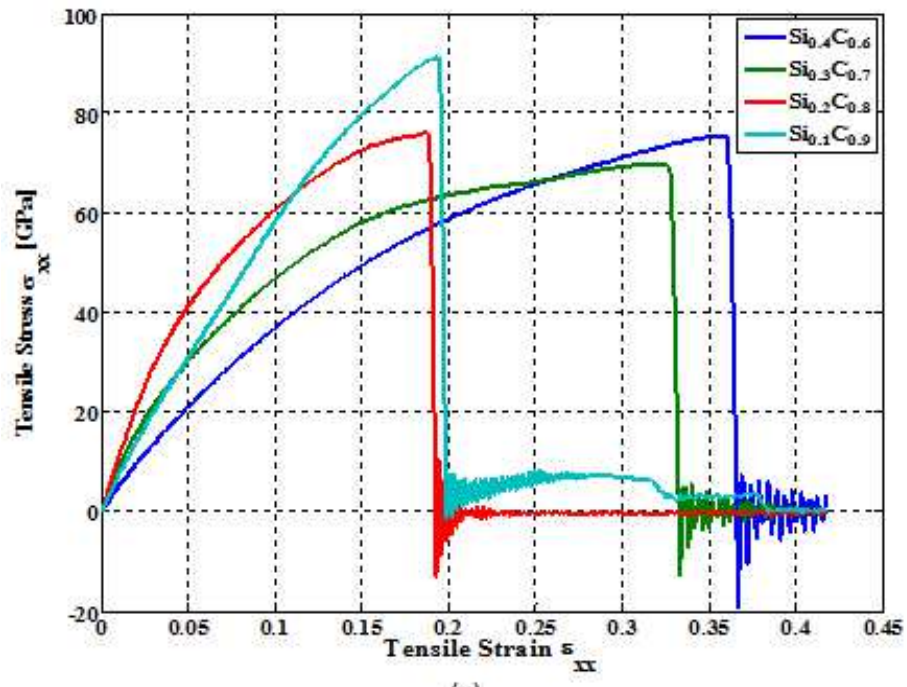


(b)

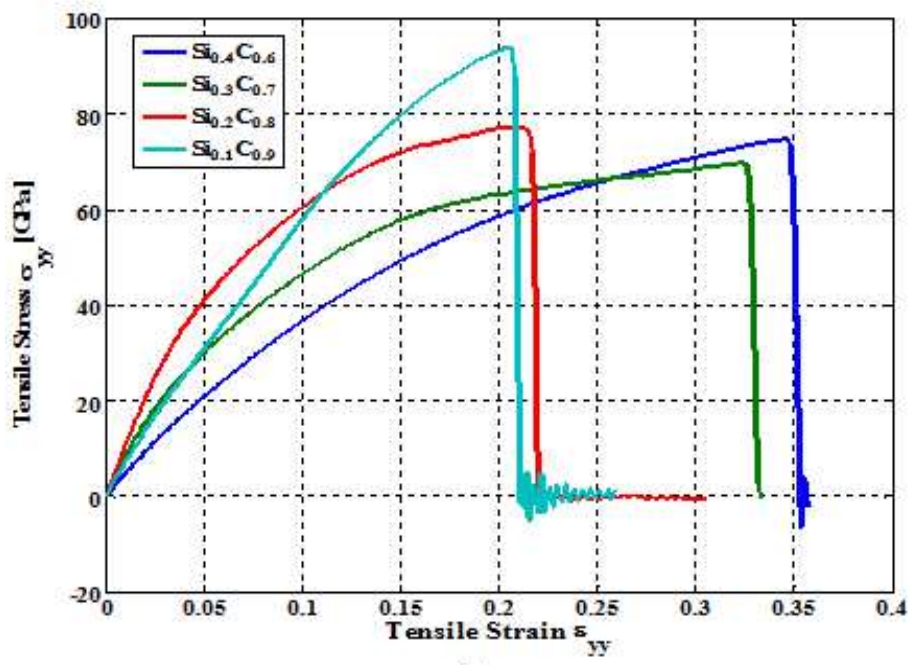


(c)

Figure 6-5 Tensile response of “small” models (total 2744 atoms) along (a) x, (b) y and (c) z directions



(a)



(b)

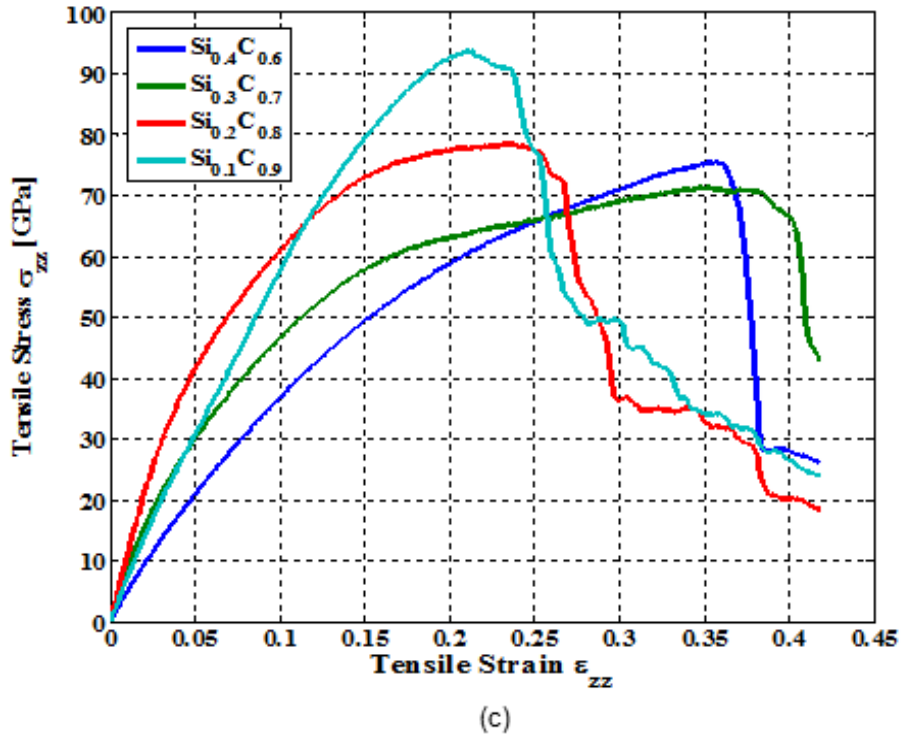


Figure 6-6 Tensile response of “large” models (total 57600 atoms) along (a) x, (b) y and (c) z directions

### 6.3.3 Effect of Random Distribution

Since the carbon atoms are randomly substituting Si atoms from SiC, it is not obvious whether strengths of the carbon enriched models would fluctuate from sample to sample. To quantitatively determine the effect of randomness on the overall properties, we freshly developed models made out of 20 times more atoms (57600 atoms) than the original model and investigated their tensile responses. Stress strain responses of these models have been obtained using the method described earlier. In essence, the new models have different randomness as evident from Fig. 6-7 that shows the comparative MD snapshots of three different models having same amount of carbon enrichment (20%

excess carbon) but different random distributions. The tensile responses, however, are very consistent, as shown in Fig. 6-8

This part of the study certainly suggests that the size of models we studied were large enough such that the local microstructural variations due to different random distributions of carbon atoms in the same type of carbon enriched systems of local cannot make any difference.

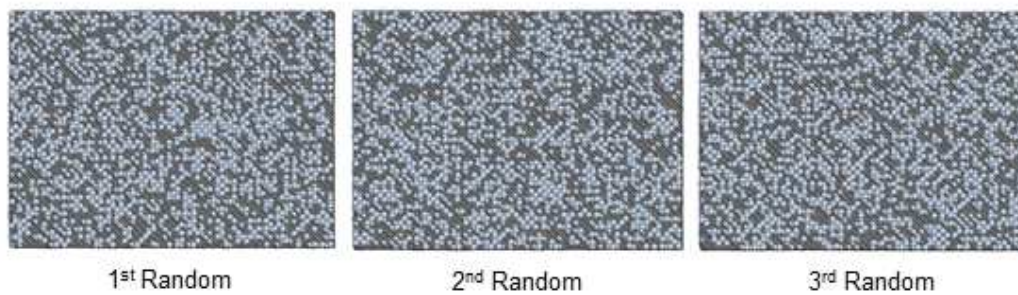
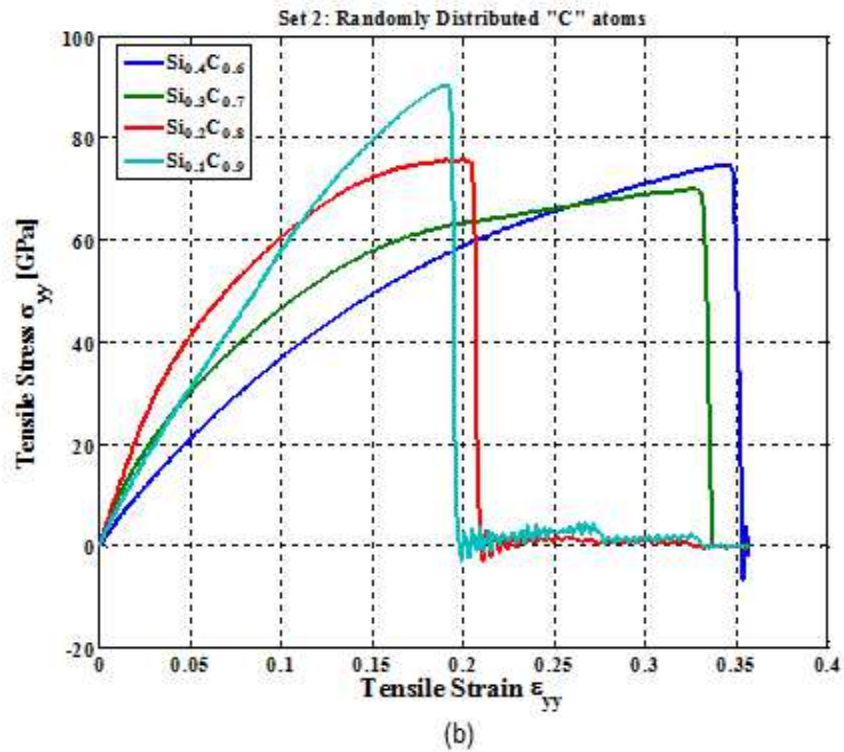
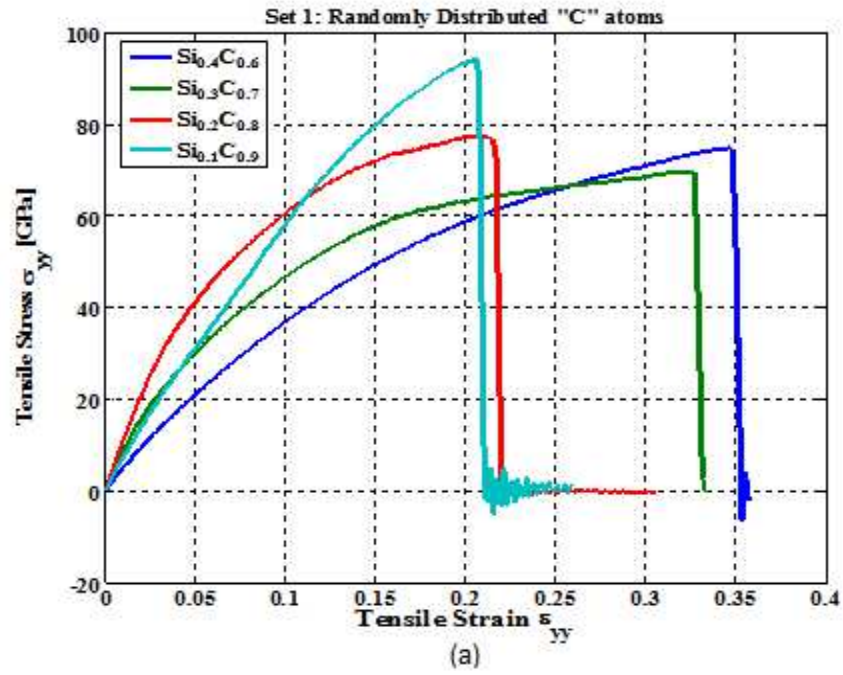


Figure 6-7 Equilibrium MD snapshots of three independently created  $\text{Si}_{0.2}\text{C}_{0.8}$  samples (each system contains 57600 atoms). The circles with light blue color and grey color represent Si and C atoms respectively.



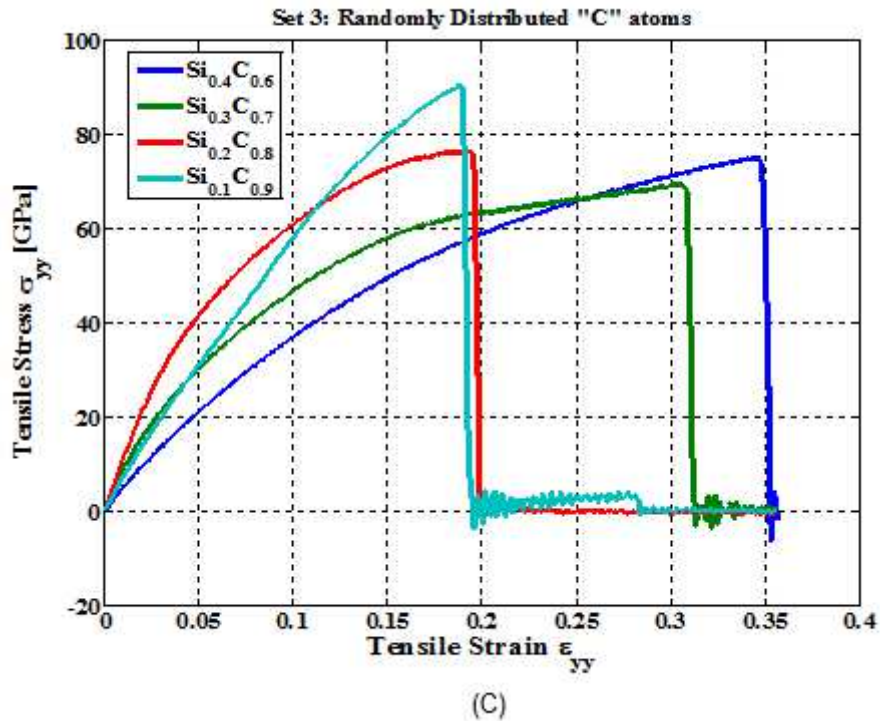


Figure 6-8 Effect of random distributions on the tensile response of carbon enriched models. Figures (a) to (c) represent responses of three different set of models

#### 6.3.4 Effect of Free Surface

In our simulations, we employed periodic boundary conditions for all carbon enriched models as well as for pure SiC model. The failure modes for the enriched systems were generally “cavitation” type. We argued that the bond energies of “Si” rich zones are less than any other zones within the entire volume. As such, these locations acted as the “weakest links” for the whole system. It is known that the strength of materials depends on the distributions of flaws, defects, free surfaces as well as on the flaw tolerant capabilities of materials [37]. In our study, we did not include any defects or flaws in the models. Due to periodic conditions, systems were also free from “free

surfaces". It can be suspected that the absence free surfaces in the geometries used may misrepresent the strengths of the materials we predicted.

In order to check whether there are any differences in the failure modes when the models are simulated with non-periodic boundary conditions, we have conducted additional simulations by modifying the boundary conditions of the existing models. In the new simulations, we removed the periodic conditions in the lateral directions and applied tensile loading along the longitudinal directions. As such, four lateral surfaces remained exposed during mechanical loading. Post-failure MD snapshots were taken (as shown in Fig. 6-9 and compared with the models shown in Fig. 6-3. It is evident from the new simulations that all "C" enriched systems have essentially failed via "cavitation" type failure. We did not notice any cavitation in pure SiC sample when simulated without periodic condition. As shown in Fig. 6-3, pure SiC simulated with periodic conditions displays both shear failure (making approximately 45° with the horizontal/vertical axis) and cavitation failure modes. According to Fig. 6-9 below, it is apparent that pure SiC failed via "shear" when simulated without periodic conditions. Figure 6-10 shows the comparative stress strain response of different carbon enriched models simulated with and without periodic boundary conditions. As expected, the maximum  $\sigma_{yy}$  of models simulated with periodic conditions are higher than the maximum  $\sigma_{yy}$  of models simulated without periodic conditions. This is because of Poisson's effect.

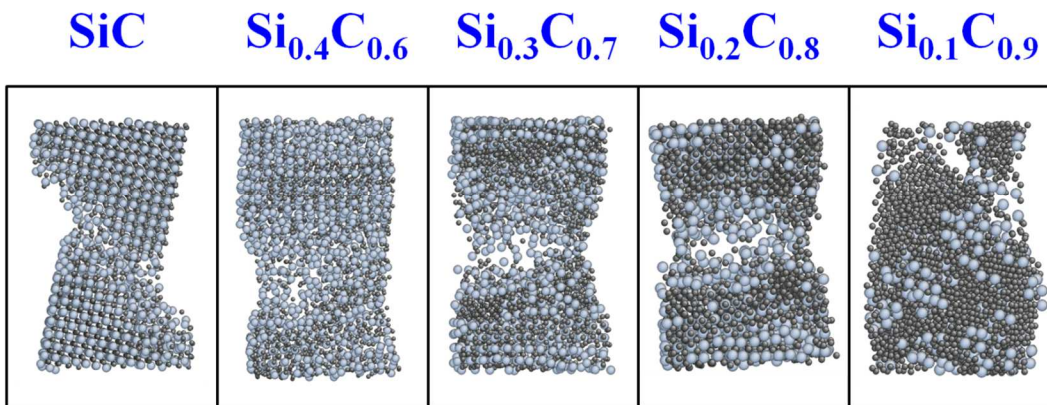


Figure 6-9 Tensile failure snapshots for different “C” enriched models simulated without any periodic boundary conditions in the lateral directions

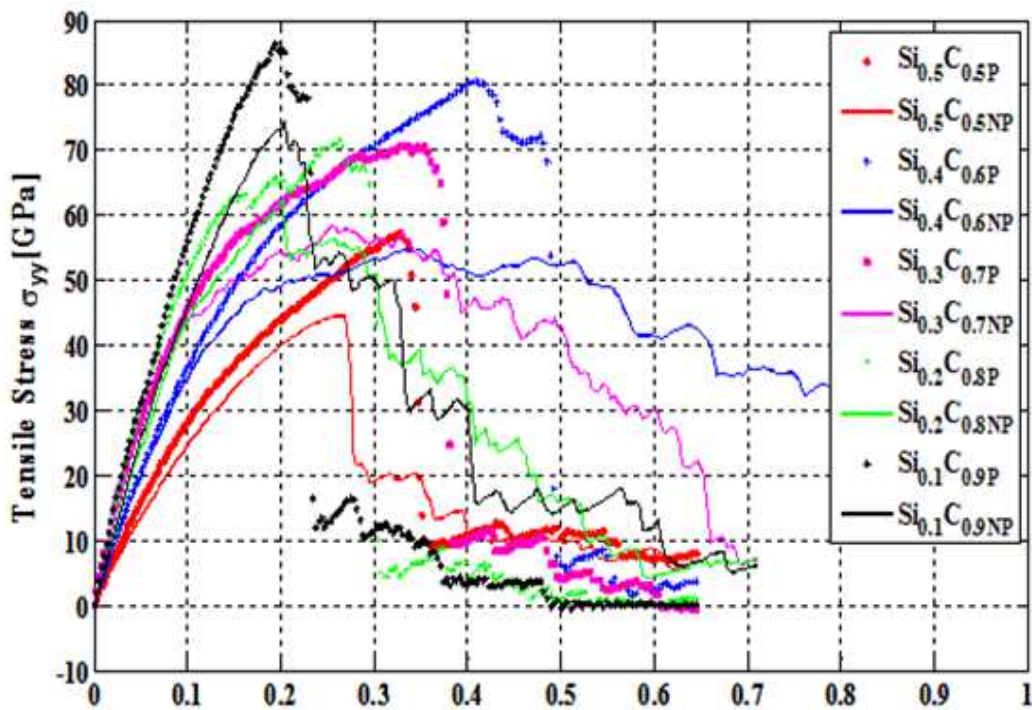


Figure 6-10 comparative Tensile Stress-Strain curves for different carbon enriched models simulated with and without periodic boundary conditions in the lateral directions

## 6.4 Summary and Conclusions

A brief summary of our study is presented below:

- In this study, we have investigated tensile and shear behavior of a new type of “C” enriched SiC ceramics using classical molecular dynamics simulations. We studied four different systems with different fraction of “C” enrichments, namely 10, 20%, 30%, 40, and 50%.
- Our study was based on the hypothesis that if “Si” atoms from SiC are randomly substituted by “C” atoms, then the bond lengths in the vicinities of the newly formed “C-C” bonds (in place of “Si-C” bonds) will be shortened but the overall crystal structure may not change significantly because both “C-C” and “Si-C” bonds are  $sp^3$  type. Because of bond-length mismatch in several locations (in the vicinity where Si substitution takes place), the final materials will be structurally disordered but will remain stable [125].
- Significant role of “C” enrichments on the tensile properties (strength, stiffness, toughness and failure strain) of the “C” enriched systems has been observed. Failure appears to nucleate from “C” leaned zones, possibly because Si-C or Si-Si bond energy is less than C-C energy. The 10% “C” enriched appears to be best performing in terms of tensile strength and toughness compared to pure SiC.
- Significant role of “C” enrichments on the shear properties (strength, stiffness, toughness and failure strain) of the “C” enriched systems has also been observed. Failure mode of “C” enrichment system along (100 direction) is different from the failure mode of pure SiC (along (110

direction). This is probably the reason why shear toughness of enriched systems are very high compared to pure SiC.

- The 40% “C” enriched appears to be best performing in shear when compared with pure SiC. For lower fraction of “C” enrichment, toughness increases but strength reduces.
- The failure strengths and trends in properties with respect to carbon enrichment fractions do not change significantly with the change in loading directions and model sizes.
- Microstructures of carbon enriched systems for same level of carbon fractions are not unique because Si substitution by C atoms was done randomly. In other words, microstructure of same carbon enriched system would vary in sample to sample. In our study, the size of the models was large enough so that properties remain invariant despite the unique “random” microstructure.
- Due to Poisson’s effect, the presence of free surface alters the failure strengths. The failure modes of the enriched system generally remain unchanged.

## Chapter 7

### Improving Fracture Toughness of Silicon Carbide Ceramics with Nanodiamond

#### Reinforcements and via Nanoscale Multilayer Ceramics

#### 7.1 Fracture Toughness Improvement via Reinforcement

Silicon Carbide (SiC) is a superhard and strong material applied for many engineering applications including abrasives, rotating disks, bearing, high temperature coatings etc. Poor fracture toughness due to brittleness is one of the limitations that keeps SiC from widespread applications. Over the last few years, scientific and industrial interests on nanoparticle reinforced Silicon Carbide materials have grown extensively primarily because of their immense potential to improve the fracture toughness without sacrificing strengths. In this study, we have investigated the reinforcement efficiency of nanodiamond and Silicon nanoparticles in Silicon Carbide using molecular dynamics simulation. Two different arrangements of nanoparticles have been considered: (a) clustered particles ahead of the crack tip and (b) uniformly distributed particles. Mode I and Mode II fracture toughness were measured. It has been observed that infusion of nanodiamonds in Silicon Carbide improves the Mode II fracture toughness by ~100%. About ~25% improvement is observed for Mode I fracture toughness. Details will be discussed in the paper.

##### *7.1.1 Introduction and Background*

Silicon Carbide (SiC) is a superhard and strong material applied for many engineering applications including abrasives, rotating disks, bearing, high temperature coatings etc. However, like most ceramic materials, Silicon Carbide exhibits high yield strength (~9 GPa) and high hardness (~2800 kg/mm<sup>2</sup>) but low toughness (~4.6 MPa.m<sup>0.5</sup>)

properties [1]. The strong covalent and ionic bonds that form the microstructure of SiC are responsible for such mechanical responses of SiC. Unfortunately, the low-toughness characteristics of SiCs significantly limit their wide-spread structural applications. Therefore, improving toughness of ceramic material is highly desirable. In principle, the property of toughness implies a combination of strength and deformability (ductility). A high in strength but low in ductility type materials are overall low in toughness. There are mostly two different ways toughness can be enhanced - either by using "Extrinsic" or "Intrinsic" mechanisms [1, 162]. However, in ceramics, toughening is mainly possible via extrinsic mechanisms. Some commonly employed ceramic material toughening methods are (1) ductile phasing [163, 164, 165, 166, 167] where fracture toughness in ceramic materials can be increased by strain relaxation around crack tip through large scale ductile phase deformation or crack blunting, bridging of cracks via ductile phase stretching behind the advancing crack tip, resisting crack initiation and propagation, (2) nano-graining [168, 169, 170, 171, 172, 173] where strengthening occurs at the grain boundary to reduce crack concentration, (3) multi-layering [174, 175, 176, 177, 178, 179, 61, 62, 180, 63] to enhance adhesion between film and substrate [64, 65, 66, 67], (4) nanofiber reinforcing [68] where cracks are deflected at the fiber/matrix interface, (5) diamond sintering [181] etc. to bridge cracks etc. Regardless what toughening mechanisms are followed, they all happen via extrinsic sources.

In this work, we have studied toughening of SiC ceramics by reinforcing it with Nanodiamond (ND) nanoparticles via classical molecular dynamics simulations which is already published in conference proceedings [182]. The unique feature of Nanodiamond is that it possesses identical crystal structure with SiC. As a result, we hypothesize that the interface of SiC and ND will create a transformed layer (with lattice constants in between SiC and ND) of some nanoscale thickness. We believe, overall stress-strain

response of the nanocomposite will be dictated by the new nanocomposite morphology. Two different arrangements of nanoparticles have been considered: (a) clustered particles ahead of the crack tip and (b) uniformly distributed particles. Mode I and Mode II fracture toughness were measured. Details are discussed in the remainder of the paper.

### 7.1.2 Molecular Modeling of Structure

Molecular models of SiC are developed from SiC unit cell as shown in Fig. 7-1.

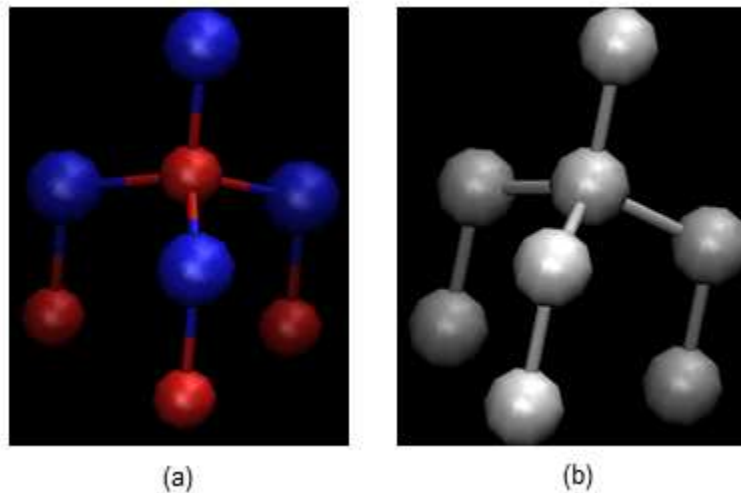


Figure 7-1 a) Pure SiC structure (Blue = Si, Red = Carbon), b) Pure ND structure

The pure SiC model (referred as SiC-WND) contains 68,832 number of atoms. A center crack of length  $a = 2.62$  nm is then created in the WND model by removing atoms from the perfect crystal. Several nanocomposite models were also developed in a similar manner. In type 1, eight solid nanodiamond (ND) nanoparticles are infused in SiC matrix. In type 2, two clustered ND particles are infused where each cluster contains four ND particles. In type 3, solid ND particles are replaced by hollow ND particles. In type 4, ND nanoparticles are modeled as non-deformable rigid particles. In addition, one model was

created where ND particles are replaced with Si nanoparticles. All nanocomposites and the pure models are shown in Fig.7-2. The shape of each nanoparticle was assumed square with each side = 0.357 nm for ND and 0.43597 nm for SiC. For all models, the interactions between atoms were based on Tersoff potential [82].

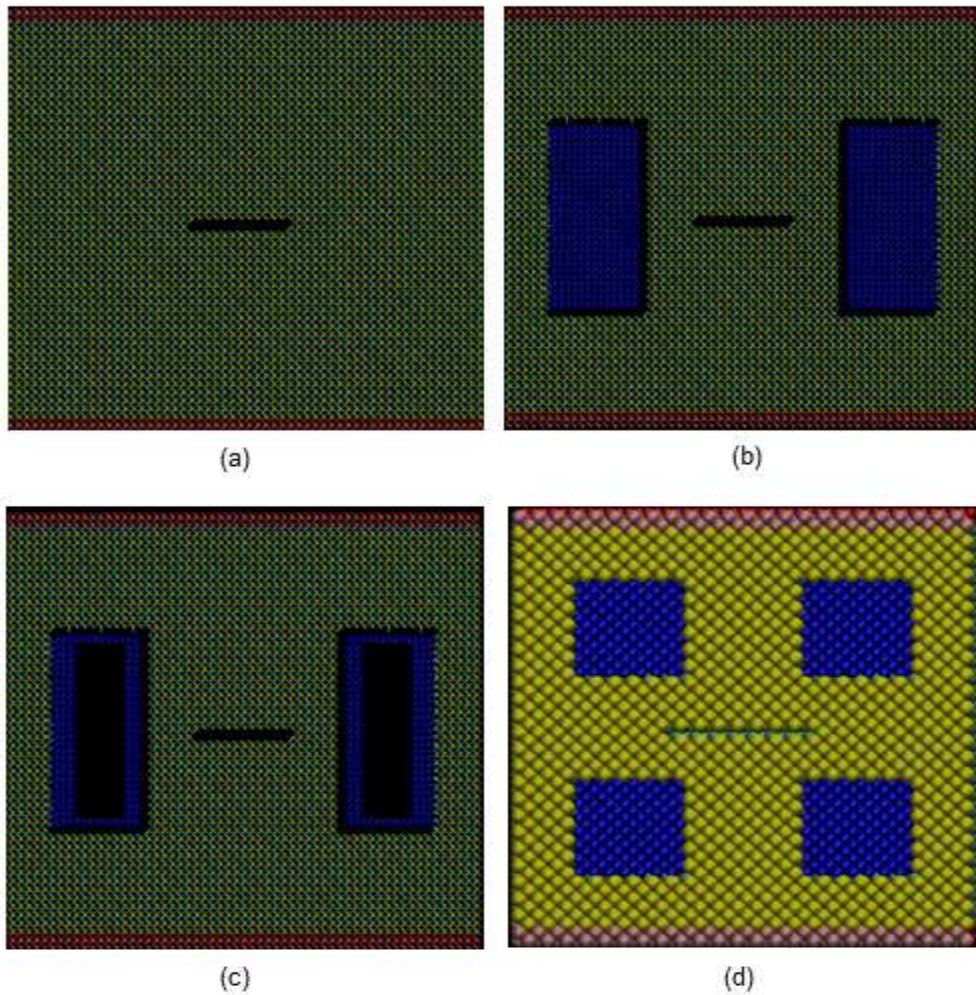


Figure 7-2 a) Pure SiC with crack b) A sliced view of ND reinforced SiC with crack. c) A sliced view of hollow ND reinforced SiC with crack, d) A sliced view of uniformly dispersed ND reinforced SiC with crack

### 7.1.3 Molecular Simulation of Structure

DL-POLY (version 2.20) developed by Daresbury Laboratory (Daresbury, Warrington, Cheshire, UK) is used to perform all the simulations [80, 81]. All simulations are carried out at 300K with 0.5 fs time step. Two steps are followed to observe the mechanical property. Atomistic models are equilibrated in the first step. In the next step, the models were subjected to incremental axial mechanical loading.

#### 7.1.3.1 Equilibrium State

It is done with combination of ensemble NPT and NVT. At first the model was run upto 30,000 time-steps in NPT condition to make the model stress free. Then mechanical loading was applied in NVT condition.

#### 7.1.3.2 Stress Strain Curve from Simulation

Stress–strain curves were generated for tensile and shear test of MD simulation. For all models, the axial tension test is simulated by applying incremental strain field to these models.

A uniform strain is applied by uniformly scaling (expanding) the dimensions of the MD cell in the direction of the deformation and re-scaling the new coordinates of the atoms to fit within the new dimensions. After this initial deformation, the MD simulation was continued and the atoms were allowed to equilibrate within the new MD cell dimensions. This process is repeated for the subsequent increments of deformation. The applied-strain increment, in the axial tension direction, is 0.25%. After that, the system was relaxed for 0.1ps, and then the stress on the system was averaged over an interval of 0.1 ps. Periodic boundary condition is applied.

The response of the nanocomposite structures under different applied displacement (strain) field is monitored by computing the developed “engineering virial” stresses in these systems [83].

#### 7.1.4 Results and Discussions

Stress strain curves are generated for tensile (Mode I) and shear (Mode II) in all cases. The stress-strain responses for each nanocomposite models are described below.

##### 7.1.4.1 Mode-I Fracture

Figure 7-3 shows the stress-strain response of center-cracked cluster ND reinforced nanocomposites and pure SiC ceramics. Figure 7-4 shows the corresponding MD snapshots.

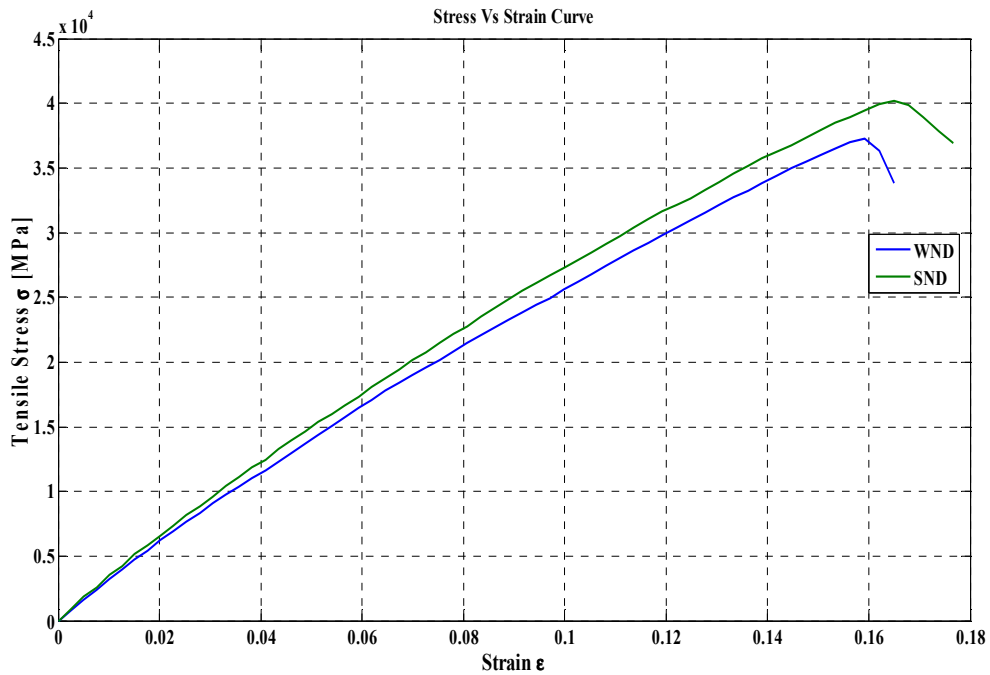


Figure 7-3 Stress-strain curve when pure ND is inserted as nanoparticle

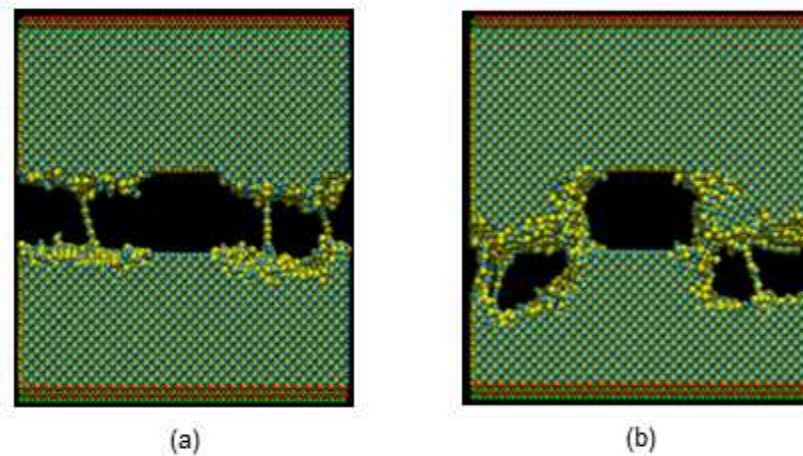


Figure 7-4 Failure snapshots of a) Pure SiC with crack. b) ND reinforced SiC with crack

It is evident from Fig. 7-4 that the presence of ND particle in clustered from where ND particles are located few nano meters ahead of the cracktips, increases the Mode I toughness and strength compare to the pure SiC structure with crack. As evident from Fig. 7-5, the presence of ND particle resists the crack to propagate through, which in turn causes delay in crack propagation. As such, overall toughness was improved.

To see the role of ND particle deformability on the overall stress-strain response, we carried out another simulation where ND was assumed non-deformable. The curve is shown in Fig. 7-5. Figure 7-6 shows the corresponding MD snapshots. It is evident that the non-deformable ND degrades overall strength and toughness behavior. Such behavior is somewhat counterintuitive in that the MD snapshot shown in Fig. 7-6 suggests a trace of crack deflection which would imply increase in toughness. Since the ND is non-deformable, there is no energy dissipation when the crack hits the ND-SiC interface. We believe the local strain energy became very intense which causes a “yielding” like behavior. It is evident from Fig. 7-5 that there is “kink” in the stress-strain curve at 10% strain.

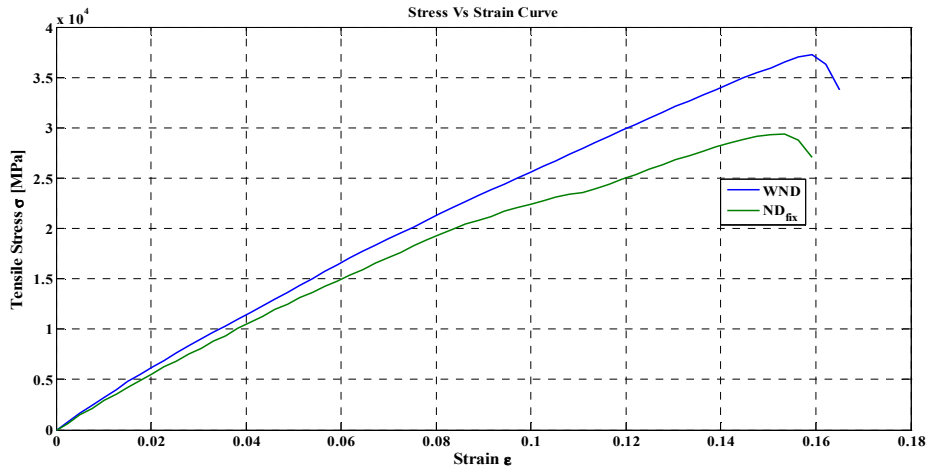


Figure 7-5 Stress-strain curve when pure ND as frozen is inserted as nanoparticle

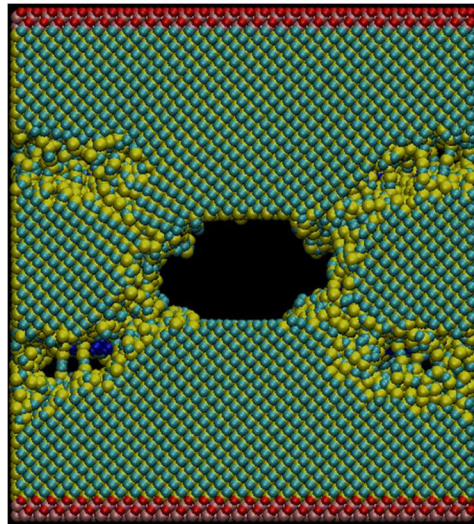


Figure 7-6 Failure snapshots of rigid ND reinforced SiC with crack

In order to understand whether the core of ND has any role on the stress-strain response, we developed a hollow ND reinforced model. We intended to observe if there is any effect of particle thickness on crack propagation. The curve is shown in Fig. 7-7. Figure

7-8 shows the corresponding MD snapshots. As the Fig. 7-7 indicates, we observed that a hollow reinforced ND doesn't increase the mechanical properties of SiC. It is also seen that the hollow deformable ND can not resist crack propagation through it. Therefore, a little difference in the stress-strain response is observed when compared with WND stress-strain curve.

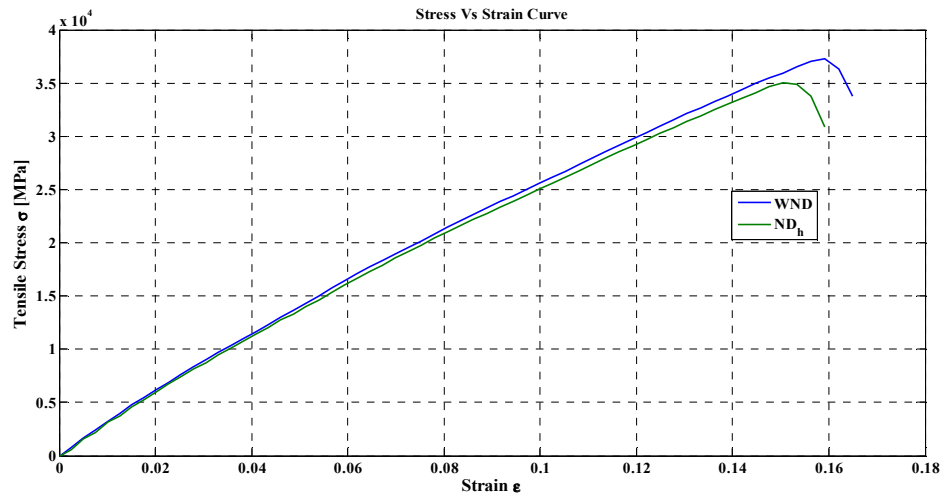


Figure 7-7 Stress-strain curve when pure ND as frozen is inserted as nanoparticle

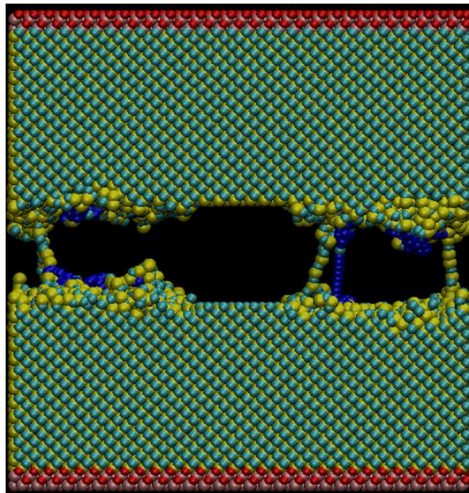


Figure 7-8 Failure snapshots of hollow ND reinforced SiC with crack

To complete our assesment on nanoparticle reinforcement effect, we also investigated a case where the hollow ND is non-defromatble. The curve is shown in Fig. 7-9 .Figure 7-10 shows the corresponding MD snapshot. As the Fig. 7-9 indicates, the overall stress-strain properties degrades when non-defomrable hollow ND is infused. Figure 7-10 shows similar trends when rigid ND is used. This result suggest that the same mechanism of deformation compared with rigid ND reinforced system. It can be concluded that super hard reinforced nanoparticle doesn't increase the mechanical properties.

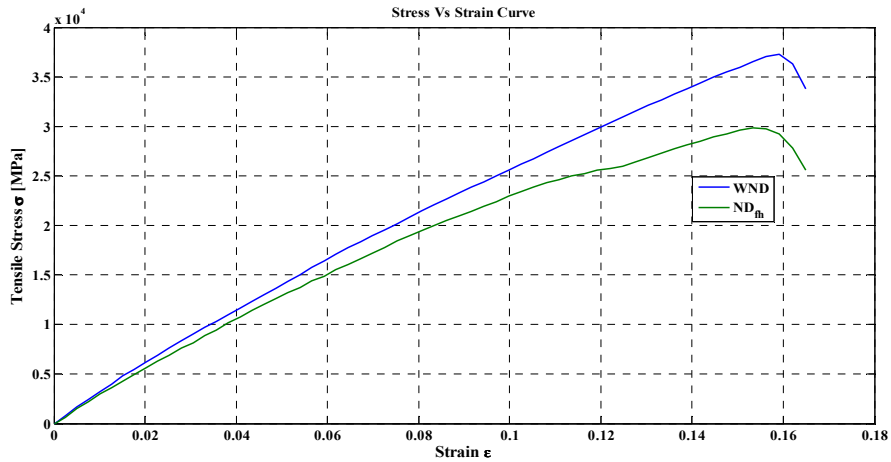


Figure 7-9 Stress-strain curve when frozen hollow ND is inserted as nanoparticle

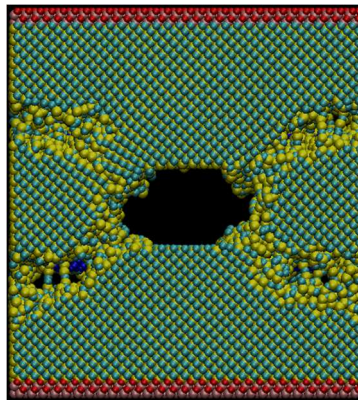


Figure 7-10 Failure snapshots of rigid ND reinforced SiC with crack

In order to investigate the effect of nanoparticle properties relative to SiC matrix, we replaced ND with Si nanoparticle of same dimension. We incorporated pure Si as nanoparticle to see the change in property in pure SiC structure. Note that Si is not harder than SiC and we put it in the path of crack. The curve is shown in Fig. 7-11. It is evident that the overall stress-strain property doesn't improve when Si is infused as reinforcing particles.

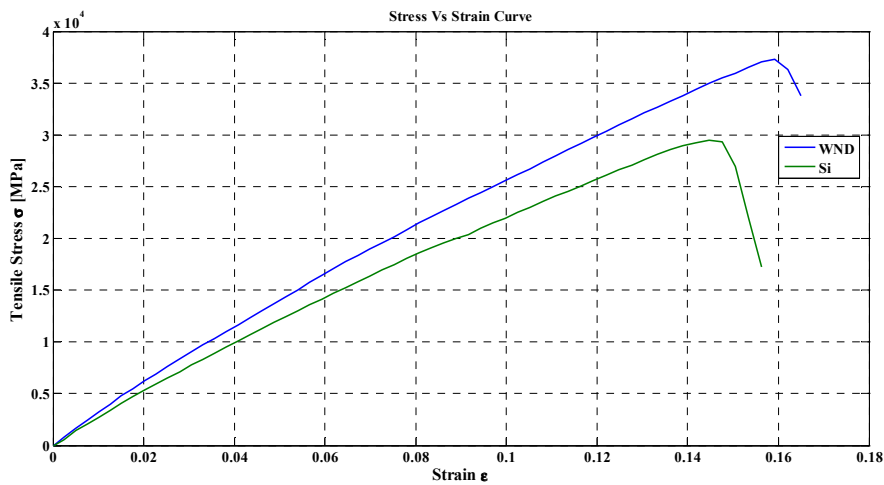


Figure 7-11 Stress-strain curve when pure Si is inserted as nanoparticle

#### 7.1.4.2 Mode-II Fracture

We concluded from tensile test that strength and toughness properties of SiC can only be improved when reinforced NDs are not super hard (i.e deformable). In order to confirm our hypothesis, we performed shear test in all cases and observed that reinforced ND increase the toughness more in under shear load. Results in shear are shown in Fig. 7-12. Fig. 7-13 shows the corresponding MD snapshots. We believe significant plastic deformation takes place during shear loading due to nucleation of

dislocation. More studies are ongoing to quantify degree of dislocation during shear deformation.

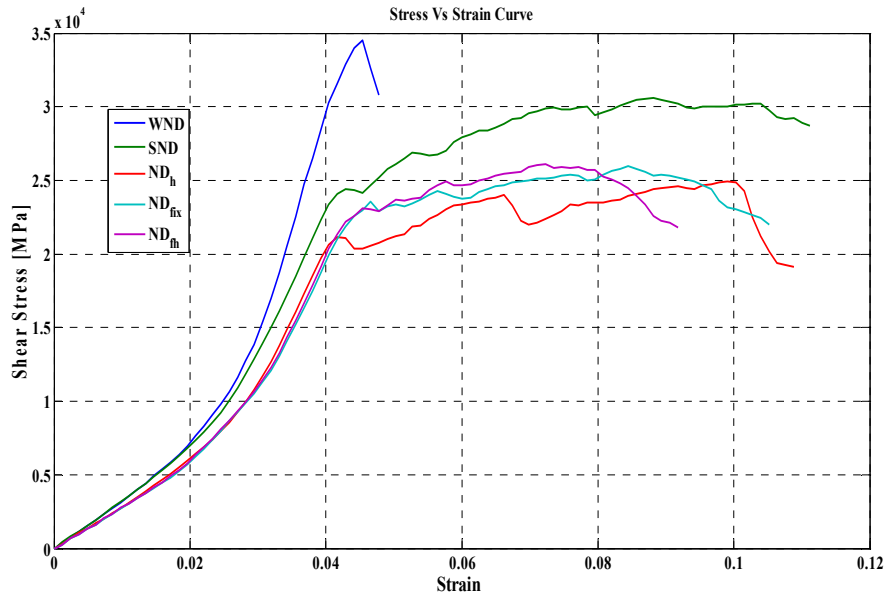


Figure 7-12 Stress-strain curve for shear load in all cases

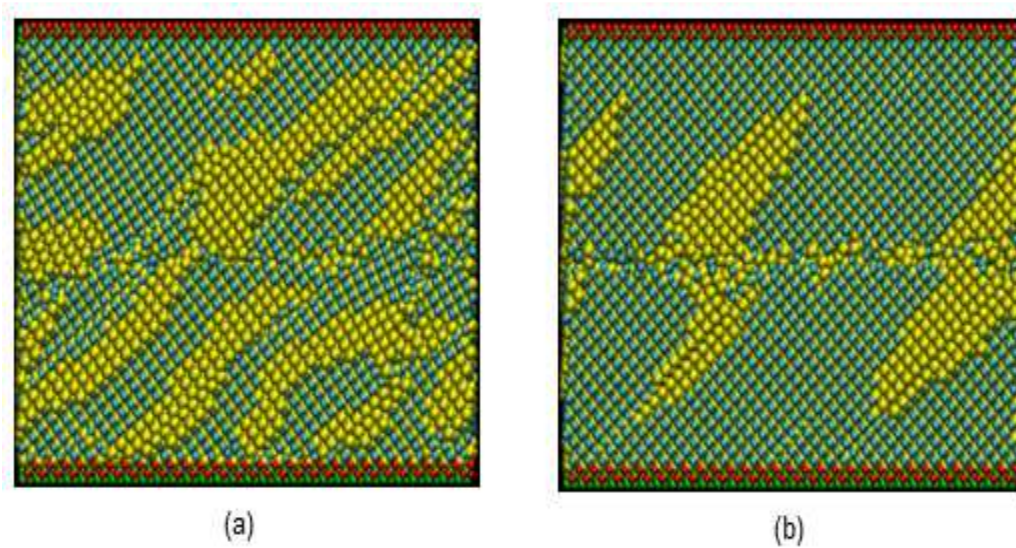


Figure 7-13 Failure snapshots of shear failed (a) ND-SiC composites, (b) Pure SiC

## 7.2 Fracture Toughness Improvement via Nanoscale Multilayer Ceramics

Silicon Carbide (SiC) is a superhard and strong material applied for many engineering applications including abrasives, rotating disks, bearing, high temperature coatings etc. However, like most ceramic materials, Silicon Carbide exhibits high yield strength (~9 GPa) and high hardness (~2800 kg/mm<sup>2</sup>) but low toughness (~4.6 MPa.m<sup>0.5</sup>) properties. The strong covalent (88%) bonds along with ionic bonds that form the microstructure of SiC are responsible for such mechanical responses. Unfortunately, the low-toughness characteristics of SiCs significantly limit their wide-spread structural applications. Therefore, improving toughness of ceramic material is highly desirable. In this study, we have computationally developed a nanoscale multilayer ceramic film where SiC and diamond crystals are arranged at an alternating sequence. The thickness of the nanodiamond film layers are varied between 2 nm and 10 nm. Center crack was created in the SiC layer and the corresponding fracture toughness was measured using integrated MD simulation. We have observed the fracture toughness of the multilayer film can be modulated by varying the SiC layer thickness. In particular, the mode-I fracture toughness can be increased by at least 20% when SiC layer thickness changes from 2 nm to 5 nm. The trend under mode-II fracture is opposite to mode-I.

### *7.2.1 Introduction and Background*

Ceramic materials have numerous applications in aerospace, automotive, electronics, medical, military, consumer use and other fields. They are generally classified as Oxides, Borides, Carbides, Nitrides and Oxynitrides. A few of them are nonmetallic, inert, crystalline or non-crystalline materials composed of metals and non-metals. It has wide variety of properties and numerous applications due to their strength,

stiffness, brittleness, high temperature stability and other properties. Unfortunately, fracture toughness of ceramics is typically very low, which is a major limitation for structural applications. Fracture toughness can be defined as resistance to failure of a material containing a crack. High toughness implies durability and resistance to catastrophic failure of a material. Therefore, ceramic materials can be a best candidate for applying them in more fields if the fracture toughness property can be enhanced.

Crack is nucleated under loading conditions in every materials and propagation of crack causes disaster for entire structure. So it is generally expected higher fracture toughness property in a material. A bunch of work has been already referred related to process and enhancement from chapter 2 to chapter 6.

In this work, we have studied toughening of SiC ceramics by multi-layering Silicon Carbide (SiC) and Nanodiamond (ND) films via classical molecular dynamics simulations which is published in conference proceedings [183]. The structure of SiC and ND are identical zinc blend structure. So the interface of SiC and ND create a lattice mismatch which may contribute in dissipating strain energy in this new morphology area. Initially, we started with same height layer of SiC and ND and further we changed the height of SiC layer as two and three times of ND layer. A crack is created in the middle of SiC layer. Mode I and Mode II fracture toughness were measured. Details are discussed in the next part of this chapter.

### *7.2.2 Molecular Modeling of Structure*

Molecular models started with the unit cell of SiC and ND. Lattice constant of SiC and ND are 0.4359 nm and 0.357 nm, respectively. We made two layers of ND and single layer of SiC where SiC is sandwiched in the middle containing a center crack of length 1.74 nm. The model has a total 13,320 atoms. The dimensions are length = 7.85

nm, thickness = 2.18 nm and each layer has 1.74 nm height. Another two models were created by doubling and tripling (as SiC:ND=2:1 and SiC:ND=3:1) the height of SiC. The next two models contain 16,200 and 19,080 atoms, respectively. All the models are shown in Fig. 7-14. Tersoff potential [82] is used to define the interactions between atoms.

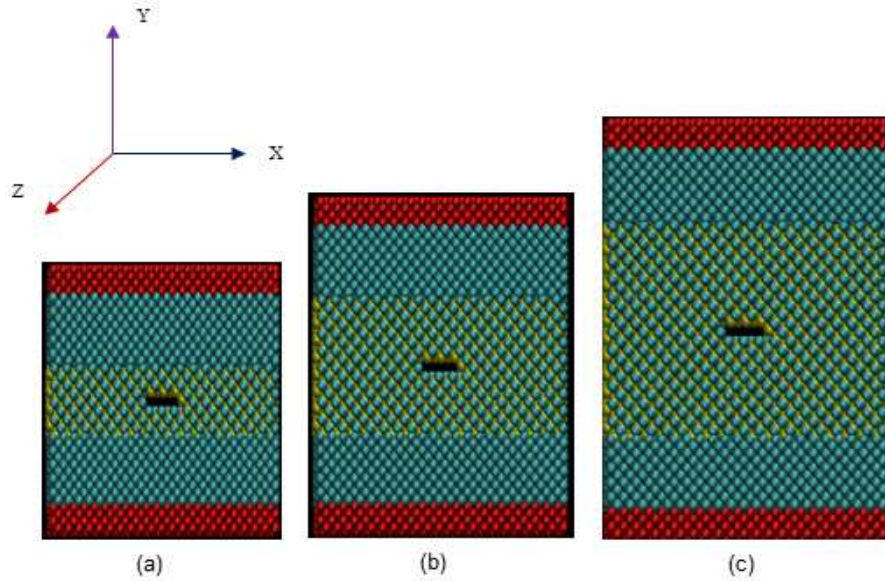


Figure 7-14 SiC in the middle containing crack and ND are on the both side of SiC. Upper and lower layers are created for applying load a) SiC:ND=1:1, b) SiC:ND=2:1, c) SiC:ND=3:1

### 7.2.3 Molecular Simulations of Structure

All simulations are performed at 300K with 0.5 fs time step. Models are equilibrated first to create a stress free system. Loading is applied subsequently to generate the stress strain curve. DL-POLY (version 2.20) developed by Daresbury Laboratory (Daresbury, Warrington, Cheshire, UK) is used to perform all the simulations [65, 66]. Periodic boundary condition along X and Z directions are enforced.

#### 7.2.3.1 Equilibrium State

NPT and NVT conditions are used. All models are equilibrated in NPT for 20,000 steps for 10 ps. Then mechanical loading is applied in NVT condition after making the models stress free.

#### 7.2.3.2 Stress Strain Curve from Simulation

Stress–strain curves were generated for Mode I (tensile) and Mode II (shear) fracture using MD simulation. A uniform state of strain is applied along the Y-direction by re-scaling the co-ordinates of atoms. This process is repeated until the fracture happens. The applied-strain increment is 0.25%. The system is relaxed during the first half of each increment and the data is taken during the rest of half interval. The taken data is averaged to generate stress strain curve by converting them into developed “engineering virial” stresses in these systems corresponding to applied strains.

### 7.2.4 Results and Discussions

Stress strain curves are generated for tensile (Mode I) and shear (Mode II) to understand the mechanical behavior. The response is described below.

#### 7.2.4.1 Mode-I Fracture

Figure 7-15 shows the stress-strain response for all three systems. In mode I loading, the film with thinnes SiC layer is showing better mechanical property in terms of fracture toughness. There is difference in lattice constant of SiC and ND. The hypothesis is that the lattice mismatch between ND and SiC layer may allow dislocation type deformation which eventually alters the fracture toughness. The degree of dislocations control the energy dissipation of that area. We have also observed that there is a direct

relation between distance of ND from crack and the variation of mechanical properties. In the first model SiC:ND thickness ratio = 1:1. Here, the layer of SiC is so thin that the crack reaches close to the nanodiamond.

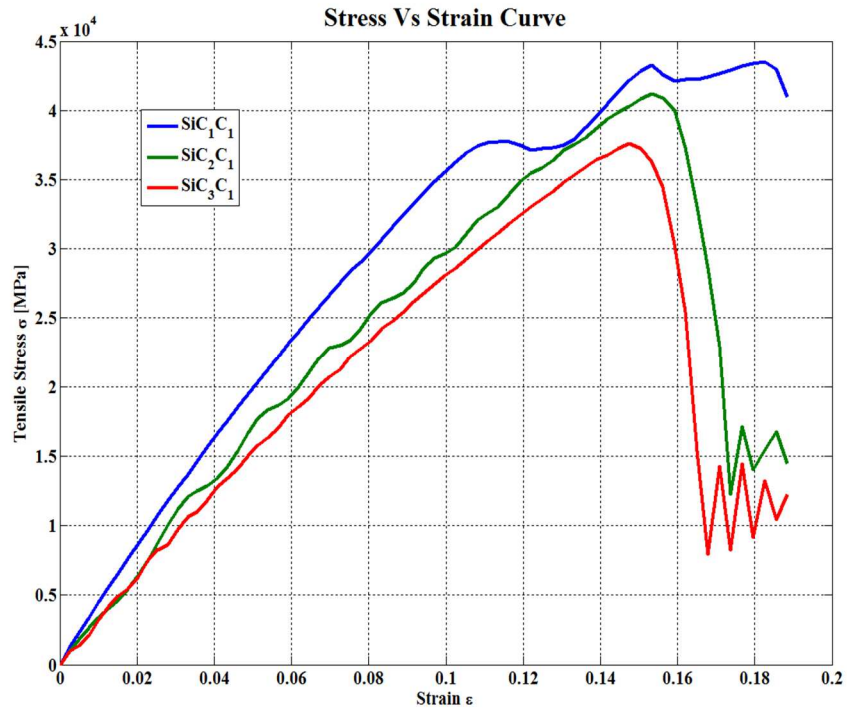


Figure 7-15 Stress-strain curve for tensile loading

The failure snapshots for mode 1 loadings are shown in Fig.7-16. with the increase in thickness, the layer height of SiC is increased and the crack is far away from ND. As the distance from crack to ND is increased the fracture toughness is decreased.

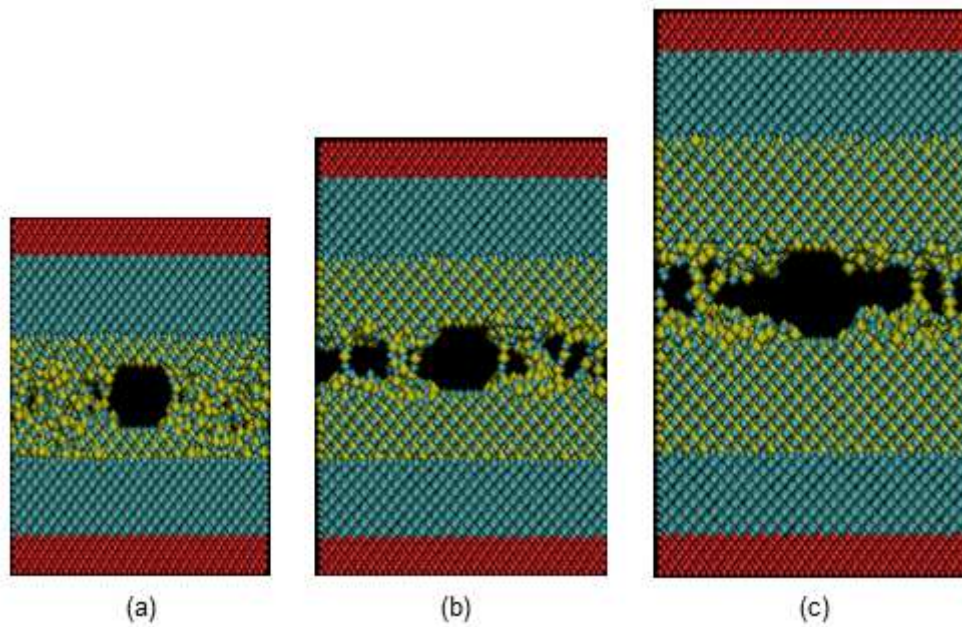


Figure 7-16 Failure snapshots of tensile failure

#### 7.2.4.2 Mode-II Fracture

Stress strain response for mode II is shown in Fig. 7-17 and snapshots are shown in Fig. 7-18. We concluded from mode I fracture that the fracture toughness is increased if the distance from ND to crack is decreased in other word, fracture toughness is maximum for lowest height of SiC. This is not very obvious in mode two fracture. It is showing an opposite trend compared to mode I fracture.

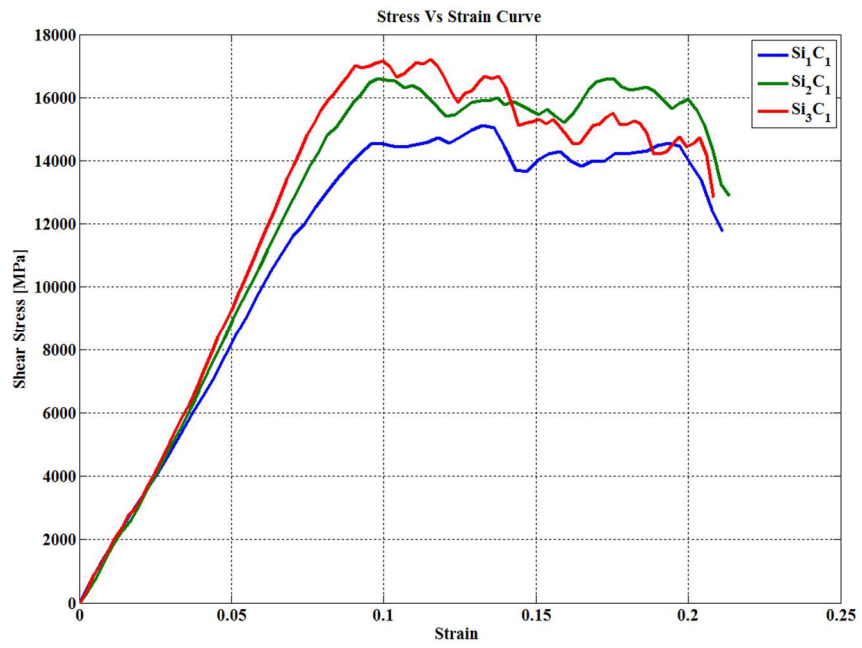


Figure 7-17 Stress-strain curve for mode II fracture

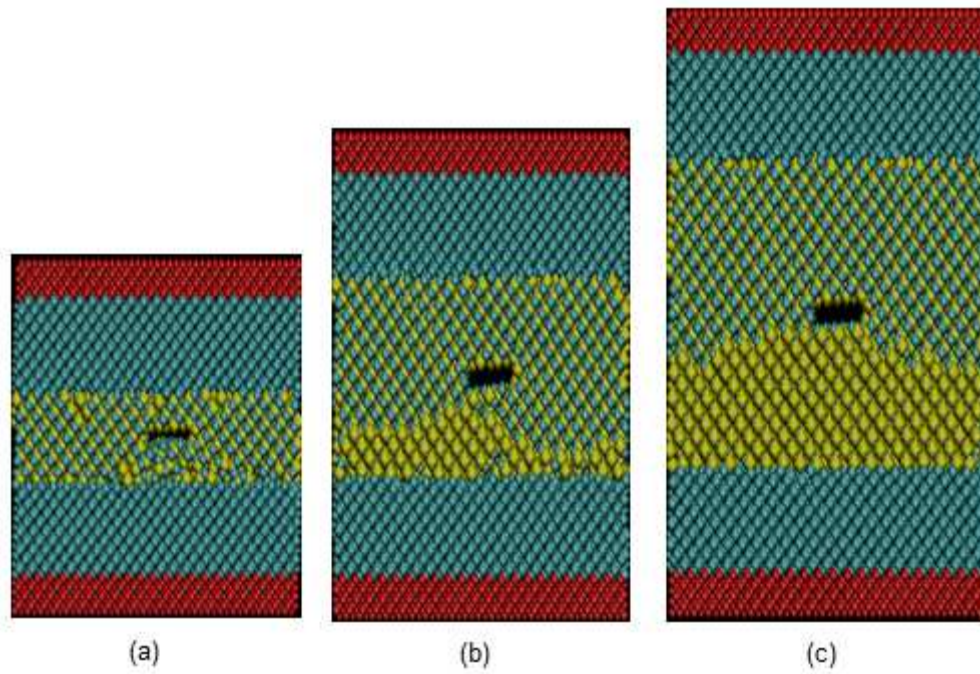


Figure 7-18 Failure snapshots of mode II fracture

### 7.2.5 Crack at Interface

Fracture toughness is not improved in tensile loading as expected in the model described previous sections. New models are made to see the effect of interface crack. Crack present this time at interphase of Nanodiamond and Silicon Carbide. We have seen that the crack deflects and it's not propagating as such as pure mode I fracture. Individual Nanodiamond, Silicon Carbide, and their interphase models were made to see the crack propagation feature. Crack deflection indicates that interphase is strong and its not breaking even a crack is present. Figure 7-19 shows the snapshot of models.

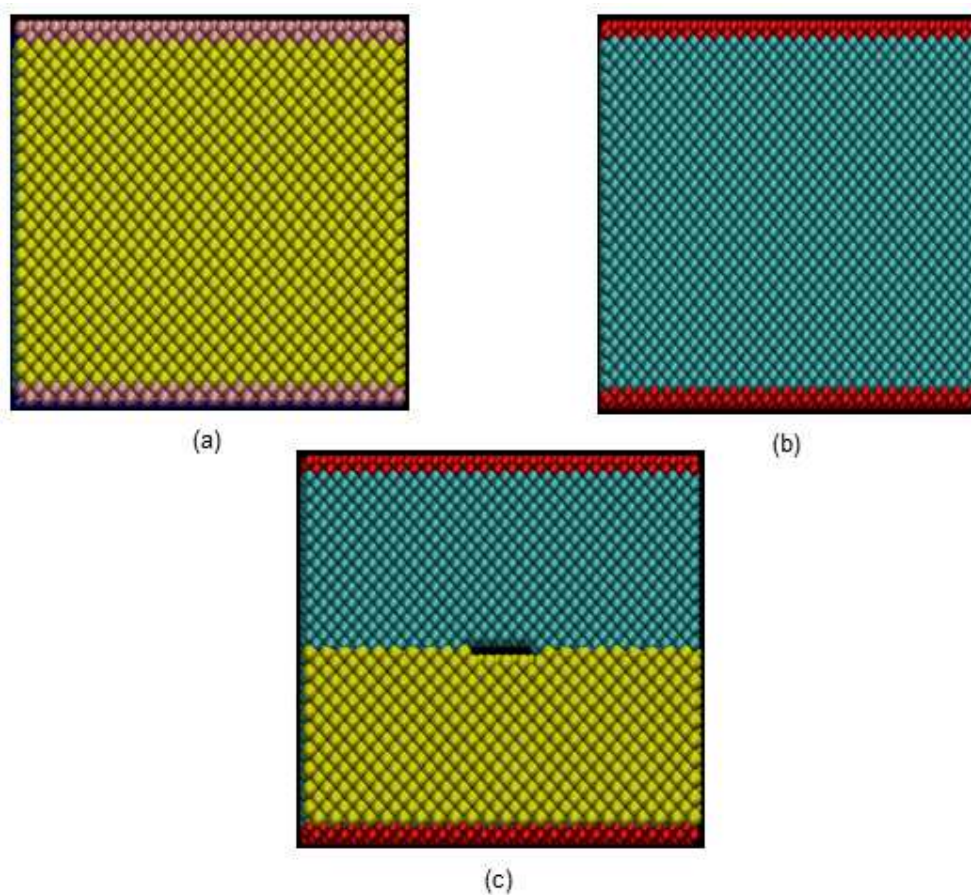


Figure 7-19 Snapshots for Models a) ND, b) SiC, c) Interphase

Figure 7-20 shows the failure snapshots and we can clearly observe that crack deflect at the interphase. Nanodiamond and Silicon carbide represent exact mode I fracture but interphase model not. We are trying to quantify the fracture toughness value as here mix mode works.

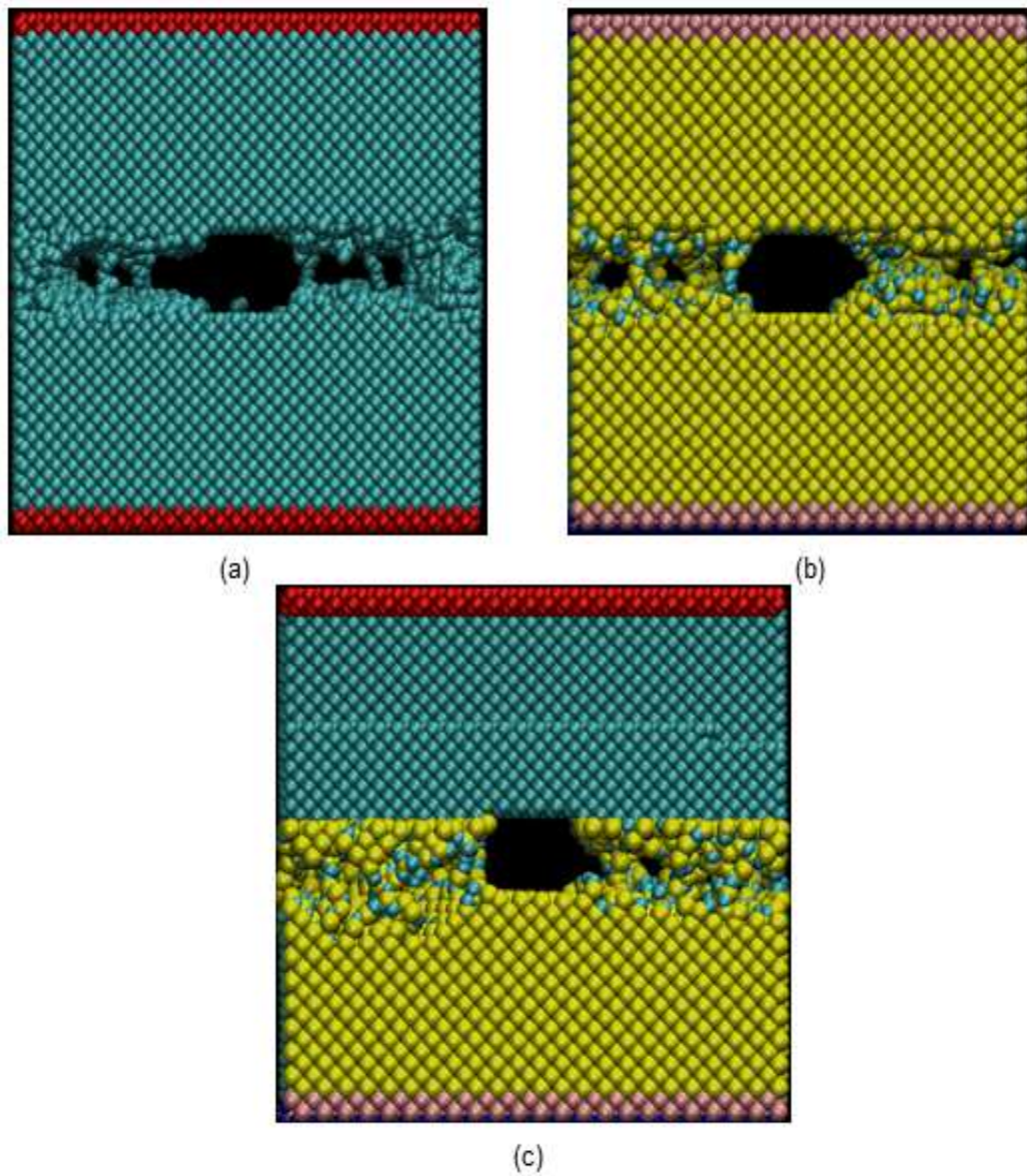


Figure 7-20 Failure Snapshots for ND, SiC, Interphase

### 7.2.5.1 Crack at Interface in Different Orientation

Crystal orientation of Silicon Carbide has been studied as the crack is propagated through Silicon Carbide. We changed the crystal orientation as (110) and (111) of Silicon Carbide and remained the orientation of Nanodiamonds as (100). Figure 7-21 shows the corresponding stress strain curve. Crystal orientation of (111) seems failing at lower strength but withstand at higher strain to failure ratio.

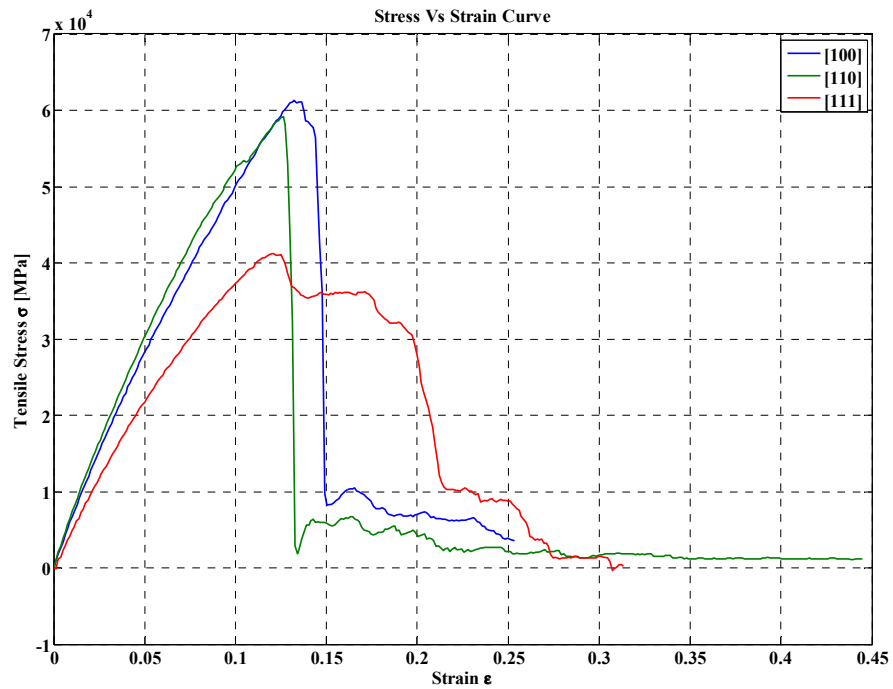


Figure 7-21 Curves for different crystal orientation of Silicon Carbide

### 7.3 Conclusion

A first order approximation to increase the toughness of SiC structure is clearly described. We could conclude that the ND should be in the path of crack to increase the toughness and very super hard reinforcement does not help to increase fracture toughness. An inclusion has not to present all through the thickness but only presence of it can deviate the path crack propagation. In later part of study, we have seen that fracture toughness of layering of ceramic materials depends on crack presence position and the crystal orientation.

## Chapter 8

### Summary and Conclusion

#### 8.1 Summary

Ceramic materials are considered as next generation material for their incomparable properties. The only limiting parameter is the fracture toughness which can be described as the shattering of ceramic bowl if dropped on floor. Ceramic materials will become one of the best candidates for structural applications even in harsh environment such as high temperature if this limiting property can be enhanced. Several ideas have been proposed in this study and a way to estimate fracture toughness in multiscale approach. The core findings reveal in this study is furnished below

- ✓ The main idea is blending of two identical ceramic structures to increase the fracture toughness without sacrificing the strength.
- ✓ The interphase of Silicon Carbide (SiC) and Nanodiamond (ND) acted as toughened interphase.
- ✓ Multi-layering of ceramic nanofilm can be a good candidate with enhanced properties.
- ✓ Volume fraction of ceramic material has also effect on fracture toughness.
- ✓ Determination of fracture toughness at nanoscale considering diamond as candidate.

#### 8.2 Conclusion

The study is an effort to induce dislocations in ceramic structure. The ultimate target is that these dislocations will increase the ductility in ceramic materials. Potential models and measurement procedures have been furnished in this study.

### 8.3 Future Recommendations

An attempt has taken to induce dislocations in ceramic materials though it is very hard job. Some recommendations are furnished below to take this work in next level for the future researchers are:

- ✓ Generate poly-crystal model
- ✓ Using different blend of ceramic materials
- ✓ High temperature study
- ✓ Crystal orientation study
- ✓ Experimental works

## References

- [1] Robert O Ritchie, "The Conflicts Between Strength and Toughness," *Nature Material*, vol. 10, pp. 817-822, 2011.
- [2] Sam Zhang, Deen Sun, et al., "Toughening of Hard Nanostructural Thin Films: A Critical Review," *Surface & Coatings Technology*, vol. 198, pp. 2-8, 2005.
- [3] A M Kueck, Q M Ramasse, et al., "Atomic Scale Imaging and the Effect of Yttrium on the Fracture Toughness of Silicon Carbide Ceramics," *Acta Materialia*, vol. 58, pp. 2999-3005, 2010.
- [4] Jumpei Kita, Hiroshi Suemasu, et al., "Fabrication of Silicon Carbide Composites with Carbon Nanofiber Addition and their Fracture Toughness," *Journal of Material Science*, vol. 45, pp. 6052-6058, 2010.
- [5] Edwin H Craft and Richard H. Smoak, "Crack Propagation in Sintered Alpha Silicon Carbide," in *American Ceramic Society*, 1977.
- [6] V Hatty, H Kahn, et al., "Fracture Toughness of Low-Pressure Chemical-Vapor-Deposited Polycrystalline Silicon Carbide Thin Film," *Journal of Applied Physics*, vol. 99, p. 013517, 2006.
- [7] Yusheng Zhao, Jiang Qian, et al., "Enhancement of Fracture Toughness in Nanostructured Diamond-SiC Composites," *Applied Physics Letters*, vol. 84, no. 8, 2004.
- [8] J Yi, W J Xue, et al. "Enhanced Toughness and Hardness at Cryogenic Temperatures of Silicon Carbide Sintered by SPS," *Materials Science & Engineering A*, vol. 569, pp. 13-17, 2013.
- [9] Chonghai Xu, Chuanzhen Huang, and Xing Ai "Effects of Carbon on the

- Microstructure and Fracture Toughness of Composite Ceramic Materials," *Journal of Materials Science*, vol. 40, pp. 4419-4421, 2005.
- [10] R Yuan, J J Kruzic, et al., "Ambient to High-Temperature Fracture Toughness and Cyclic Fatigue Behavior in Al-Containing Silicon Carbide Ceramics," *Acta Materialia*, vol. 51, pp. 6477-6491, 2003.
- [11] Rajiv K Kalia, Aiichiro Nakano, et al., "Multiresolution Atomistic Simulations of Dynamic Fracture in Nanostructured Ceramics and Glasses," *International Journal of Fracture*, vol. 121, pp. 71-79, 2003.
- [12] Yifei Mo and Izabela Szlufarska, "Simultaneous Enhancement of Toughness, Ductility and Strength of Nanocrystalline Ceramics at High Strain Rate," *Applied Physics Letter*, vol. 90, p. 181926, 2007.
- [13] S R Wylie, A I Al-Shamma, et al., "An Atmospheric Microwave Plasma Jet for Ceramic Material Processing," *Journal of Materials Processing Technology*, Vols. 153-154, pp. 288-293, 2004.
- [14] Yury G Gogotsi, In Deok Jeon, and Michael J McNallan, "Carbon Coatings on Silicon Carbide by Reaction with Chlorine-Containing Gases," *J. Mater. Chem.*, vol. 7, pp. 1841-1848, 1997.
- [15] Narasimha S Prasad, Sudhir B Trivedi, et al., "Development of Solid-State Ceramic Laser Material using Nd:Yttria," in *SPIE- The International Society for Optical Engineering*, West Virginia, 2006.
- [16] D Njoya, M Hajjaji, et al., "Effects of Some Processing Factors on Technical Properties of a Clay-Based Ceramic Material," *Applied Clay Science*, Vols. 65-66, pp. 106-113, 2012.

- [17] Stephen T Rasmussen, Walter Ngaji-Okumu, et al. "Optimum Particle Size Distribution for Reduced Sintering Shrinkage of a Dental Porcelain," *Dent. Mater.*, vol. 13, pp. 43-50, 1997.
- [18] J. S. Reed, *Principles of Ceramic Processing*, New York: Wiley, 1995.
- [19] C. J. Brinker and G. W. Scherer, *Sol-Gel Science, The Physics and Chemistry of Sol-Gel Processing*, New York: Academic Press, 1990.
- [20] T Nishimura, K Jinbo, et al., "Forming of Ceramic Powders by Cyclic-CIP," *J. Ceram. Soc. Jpn.*, vol. 98, pp. 735-738, 1990.
- [21] W. M. Sigmund, "Novel Powder-Processing Methods for Advanced Ceramics," *J. Am. Ceram. Soc. A*, vol. 83, no. 7, pp. 1557-1574, 2000.
- [22] P. Colombo, "Conventional and Novel Processing Methods for Cellular Ceramics," *Phil. Trans. R. Soc. A*, vol. 364, pp. 109-124, 2006.
- [23] Jon Binner, Hong Chang, et al., "Processing of Ceramic-Metal Interpenetrating Composites," *Journal of the European Ceramic Society*, vol. 29, pp. 837-842, 2009.
- [24] F F Langa, W C Tu, and A G Evans, "Processing of Damage-Tolerant, Oxidation-Resistant Ceramic Matrix Composites by a Precursor Infiltration and Pyrolysis Method," *Material Science and Engineering A*, vol. 195, pp. 145-150, 1995.
- [25] S. J. Glass and D. J. Green, "Surface Modification of Ceramics by Partial Infiltration," *Adv. Ceram. Mater.*, vol. 2, pp. 129-131, 1987.
- [26] B. R. Marple and D. J. Green, "Incorporation of Mullite as a Second Phase Into Alumina by An Infiltration Technique," *J. Am. Ceram. Soc.*, vol. 71, no. 11, pp. C471-C173, 1988.
- [27] B E Walker, et al. "Preparation and Properties of Monolithic and Composite

- Ceramics Produced by Polymer Pyrolysis," *Am. Ceram. Soc. Bull.*, vol. 62, no. 8, pp. 916-923, 1983.
- [28] D Hotza and P Greil "Review: Aqueous Tape Casting of Ceramic Powders," *Materials Science and Engineering A*, vol. 202, pp. 206-217, 1995.
- [29] J. C. Williams, "Doctor Blade Process," in *Treatise on Material Science and Technology, Ceramic Fabrication Processes*, New York, Academic Press, 1976.
- [30] R E Mistler, D J Shanefield, and R B Runk, "Tape Casting of Ceramics," in *Ceramic Processing Before Firing*, New York, John Wiley and Sons, 1978, pp. 411-448.
- [31] R. Moreno, "The Role of Slip Additives in Tape Casting Technology: Part I-Solvent and Dispersants," *Am. Ceram. Soc. Bull.*, vol. 71, no. 10, pp. 1521-1531, 1992.
- [32] R Chaim, M Levin, et al., "Sintering and Densification of Nanocrystalline Ceramic Oxide Powders: A Review," *Advances in Applied Ceramics*, vol. 107, no. 3, pp. 159-169, 2008.
- [33] W. D. Kingery and B. Francois, "Sintering and Related Phenomena," New York, Gordon and Beach, 1967, pp. 471-498.
- [34] M. J. Bannister, "Sintering and Related Phenomena," New York, Gordon and Breach, 1967, pp. 581-605.
- [35] Sheikh F Ferdous, Md Sarker, and A Adnan, "Role of Nanoparticle Dispersion and Filler Matrix Interface on the Matrix Dominated Failure of Rigid C60-PE Nanocomposites: A Molecular Dynamics Simulation Study," *Polymer*, vol. 54, pp. 2565-2576, 2013.
- [36] Sheikh F Ferdous and Ashfaq Adnan, "The Effects of Filler-Matrix Interface Strength, Filler Shape, and Filler Dispersion on the Mechanical Properties of

- Polymer Nanocomposites," in *American Society for Composites*, Arlington, TX, 2012.
- [37] Sheikh F Ferdous, Ashfaq Adnan, "Role of a Single Surface Vacancy on the Tensile Stress-Strain Relations of Single Crystal Ni Nanowire," *Computational Materials Science*, vol. 90, pp. 221-231, 2014.
- [38] M A Bhatia, K N Solanki, et al., "Investigating Damage Evolution at the Nanoscale: Molecular Dynamics Simulations of Nanovoid Growth in Single Crystal Aluminum," *Metallurgical and Materials Transactions A*, vol. 44, no. 2, pp. 617-626, 2013.
- [39] M A Bhatia, S Groh, et al., "Atomic Scale Investigation of Point Defects and Hydrogen Solute Atmospheres on the Edge Dislocation Mobility in Alpha Iron," vol. 116, p. 064302, 2014.
- [40] Kiran N Solanki, Mark A Tschopp, et al., "Atomic Investigation of the Role of Grain Boundary Structure on Hydrogen Segregation and Embrittlement in alpha Fe," *Metallurgical and Materials Transactions*, vol. 44, no. 3, pp. 1365-1375, 2013.
- [41] Fazle R Ahad, K Enakoutsa, et al. "Modeling the Dynamic Failure of Railroad Tank Cars Using a Physically/Damage Nonlocal Model," *Modeling and Simulation in Engineering*, vol. 2013, p. 815158, 2013.
- [42] Fazle R Ahad, K Enakoutsa, et al., "Nonlocal Modeling in High-Velocity Impact Failure of 6061-T6 Aluminum," *International Journal of Plasticity*, vol. 55, pp. 108-132, 2014.
- [43] Koffi Enakoutsa, Fazle R Ahad, et al., "Using Damage Delocalization to Model Localization Phenomena in Bammann-Chiesa-Johnson Metals," *Journal of Engineering Materials and Technology*, vol. 134, pp. 041014-1, 2012.

- [44] Koffi Enakoutsa, Fazle R Ahad, et al., "Localization Effects in Bammann-Chiesa-Johnson Metals with Damage Delocalization," in *American Society of Mechanical Engineers*, Denver,CO, 2011.
- [45] Fazle R Ahad,K Enakoutsa, et al., "A Physically Motivated Internal State Variable Plasticity/Damage Model Embedded with a Length Scale for Hazmat Tank Cars' Structural Integrity Applications," in *American Society for Mechanical Engineers*, Pueblo, CO, 2011.
- [46] Fazle R. Ahad, Modified Internal State Variable Models of Plasticity Using Nonlocal Integrals in Damage and Gradients in Dislocation Density, Starkville, Mississippi: Proquest Dissertation and Thesis, 2014.
- [47] Ashfaq Adnan,Md Sarker, and Sheikh F Ferdous, "Biomechanics of Mineralized Collagens," in *Multiscale Simulations and Mechanics of Biological Materials*, John Wiley & Sons, 2013, pp. 435-447.
- [48] Sheikh F Ferdous, A R N Sakib, and A Adnan, "pH Dependent Interfacial Adhesion Between Collagen and Hydroxyapatite in the Mineralized Collagen Fibril," in *SAMPE TECH*, Fort Worth, TX, 2011.
- [49] Florian Bouville,Eric Maire, et al., "Strong, Tough and Stiff Bio-inspired Ceramics from Brittle Constituents," *Nature Materials*, vol. 13, pp. 508-514, 2014.
- [50] R H J Hannink, M V Swain, "Progress in Transformation Toughening of Ceramics," *Annual Review of Materials Science*, vol. 24, pp. 359-408, 1994.
- [51] R H J Hannink,P M Kelly, et al., "Transformation Toughening in Zirconia Containing Ceramics," *Journal of the American Ceramic Society*, vol. 83, pp. 461-487, 2000.
- [52] B. Basu, "Toughening of Ytria-Stabilised Tetragonal Zirconia Ceramics,"

- International Materials Review*, vol. 50, pp. 239-256, 2005.
- [53] W. M. Kriven, "Martensitic Toughening of Ceramics," *Materials Science and Engineering A*, vol. 127, pp. 249-255, 1990.
- [54] A H Heuer, "Transformation Toughening in ZrO<sub>2</sub>-Containing Ceramics," *Journal of the American Ceramic Society*, vol. 70, pp. 689-698, 1987.
- [55] F. E. Buresch, "A Structure Sensitive K<sub>IC</sub>-Value and Its Dependence on Grain Size Distribution, Density and Microcrack Interaction," *Fracture Mechanics of Ceramics*, vol. 4, pp. 835-847, 1978.
- [56] M Ruhle, A G Evans, et al. "Microcrack Toughening in Alumina/Zirconia," *Acta Metall.*, vol. 35, pp. 2701-2710, 1987.
- [57] B R G Hoagland, J D Embury, and D J Green, "On The Density of Microcracks Formed During the Fracture of Ceramics," *Scr. Metall.*, vol. 9, no. 9, pp. 907-909, 1975.
- [58] A. G. Evans, "On The Formation of a Crack Tip Microcrack Zone," *Scr. Metall*, vol. 10, p. 93, 1976.
- [59] J. A. Yeomans, "Ductile Particle Ceramic Matrix Composites-Scientific Curiosities or Engineering Materials?," *Journal of the European Ceramic Society*, vol. 28, no. 7, pp. 1543-1550, 2008.
- [60] Rodriguez Suarez, T Bartolome, et al. "Mechanical and tribological properties of ceramic/metal composites: A Review of Phenomena Spanning from the Nanometer to the Micrometer Length Scale," *Journal of the European Ceramic Society*, vol. 32, no. 15, pp. 3887-3898, 2012.
- [61] S Ulrich, et al., "Correlation Between Constitution, Properties and Machining

- Performance of TiN/ZrN Multilayers," *Surface and Coatings Technology*, Vols. 188-189, pp. 331-337, 2004.
- [62] J. H. Hsieh, et al., "Deposition and Characterization of TiAlN and Multi-layered TiN/TiAlN Coatings Using Unbalanced Magnetron Sputtering," *Surface and Coatings Technology*, Vols. 108-109, pp. 132-137, 1998.
- [63] M Berger, et al., "The Multilayer Effect in Abrasion — Optimising the Combination of Hard and Tough Phases," *Surface and Coatings Technology*, Vols. 116-119, pp. 1138-1144, 1999.
- [64] Q Yang, D Y Seo, and L R Zhao, et al., "Multilayered Coatings with Alternate Pure Ti and TiN/CrN Superlattice," *Surface and Coatings Technology*, Vols. 177-178, pp. 204-208, 2004.
- [65] C. J. Tavares, et al., "A Structural and Mechanical Analysis on PVD-Grown (Ti,Al)N/Mo Multilayers," *Thin Solid Films*, Vols. 377-378, pp. 425-429, 2000.
- [66] A A Voevodin, S D Walck, and J S Zabinski, "Architecture of Multilayer Nanocomposite Coatings with Super-hard Diamond-like Carbon Layers for Wear Protection at High Contact Loads," *Wear*, Vols. 203-204, pp. 516-527, 1997.
- [67] H Holleck, M Lahres, and P Woll, "Multilayer Coatings—Influence of Fabrication Parameters on Constitution and Properties," *Surface and Coatings Technology*, vol. 41, no. 2, pp. 179-190, 1990.
- [68] S. Logothetidis, et al. "Comprehensive Study on the Properties of Multilayered Amorphous Carbon Films," *Diamond and Related Materials*, vol. 9, no. 3-6, pp. 756-760, 2000.
- [69] Xia Kenong, T G Langdon, et al., "Toughening and Strengthening of Ceramic

- Materials Through Discontinuous Reinforcement," *Journal of Materials Science*, vol. 29, no. 20, pp. 5219-5231, 1994.
- [70] C. H. Hsueh, "Toughening Behavior and Interfacial Properties of Fiber-Reinforced Ceramic Composites," *Journal of Energy Resources Technology*, vol. 113, no. 3, pp. 197-203, 1991.
- [71] A E Giannakopoulos, K Breder, et al., "Synergism of Toughening Mechanisms in Whisker-Reinforced Ceramic-Matrix Composites," *Journal of the American Ceramic Society*, vol. 74, no. 1, pp. 194-202, 1991.
- [72] J D Kuntz, G D Zhan, et al., "Nanocrystalline-Matrix Ceramic Composites for Improved Fracture Toughness," *MRS Bulletin*, vol. 29, no. 1, pp. 22-27, 2004.
- [73] Shantikumar V Nair, Tsung Ju Gwo, "Role of Crack Wake Toughening on Elevated Temperature Crack Growth in a Fiber Reinforced Ceramic Composite," *Journal of Engineering Materials and Technology*, vol. 115, no. 3, pp. 273-280, 1993.
- [74] C. H. Hsueh, "Toughening Behavior and Interfacial Properties of Fiber-Reinforced Ceramic Composites," *American Society of Mechanical Engineers*, vol. 32, pp. 119-126, 1990.
- [75] J Cho, A R Boccaccini, et al., "Ceramic Matrix Composites Containing Carbon Nanotubes," *Journal of Materials Science*, vol. 44, no. 8, pp. 1934-1951, 2009.
- [76] B Zhao, G F Gao, et al., "Study on Toughening Mechanism of Nano-composite Ceramics Prepared by Mixed Coagulative Method," *Materials Science Forum*, Vols. 561-565, no. 1, pp. 737-742, 2007.
- [77] M Rajagopalan, M A Bhatia, et al., "Atomic Scale Analysis of Liquid Gallium Embrittlement of Aluminum Grain Boundaries," *Acta Materialia*, vol. 73, pp. 312-

325, 2014.

- [78] I Adlakha, M A Bhatia, et al., "Atomic Scale Investigation of Grain Boundary Role on Intergranular Deformation in Aluminum," *Philosophical Magazine*, vol. 94, no. 30, pp. 3445-3466, 2014.
- [79] M A Bhatia and K. N. Solanki, "Energetics of Vacancy Segregation to Symmetric Tilt Grain Boundaries in Hexagonal Closed Pack Materials," *Journal of Applied Physics*, vol. 114, no. 24, p. 244309, 2013.
- [80] W Smith and T R Forester, "DL\_POLY\_2.0: A General-Purpose Parallel Molecular Dynamics Simulation Package," *Journal of Molecular Graphics*, vol. 14, pp. 136-141, 1996.
- [81] W Smith, T R Forester, and I T Todorov, "DLPOLY (version-2.20).STFC Daresbury Laboratory," no. 1.2.5.2,2.5,4.1.1.
- [82] J. Tersoff, "New Empirical Approach for the Structure and Energy of Covalent Systems," *Phys. Rev. B*, vol. 37, pp. 6991-7000, 1988.
- [83] AK Subramaniyan and CT Sun, "Physical Interpretation of the Virial Stress," *International Journal of Solid Sand Structures*, vol. 45, pp. 4340-4346, 2008.
- [84] T L Anderson, *Fracture Mechanics: Fundamentals and Applications*, New York: CRC Press, 2005.
- [85] ANSYS Inc., [Online]. Available: <http://www.ansys.com/>.
- [86] A. Stukowski, "Structure Identification Methods for Atomistic Simulations of Crystalline Materials," *Modeling and Simulation in Materials Science and Engineering*, vol. 20, p. 045021, 2012.
- [87] C L Kelchner, S J Plimpton, et al., "Dislocation Nucleation and Defect Structure

- During Surface Indentation," *Phys. Rev. B*, vol. 58, no. 17, p. 11085, 1998.
- [88] J. Li, "AtomEye:An Efficient Atomistic Configuration Viewer," *Modelling Simul. Mater. Sci. Eng.*, vol. 11, pp. 173-177, 2003.
- [89] [Online]. Available: <http://www.ks.uiuc.edu/>.
- [90] C. T. Sun and Z. H. Jin, *Fracture Mechanics*, New York: Academic Press, 2012.
- [91] X. K. Zhu and J. A. Joyce, "Review of Fracture Toughness (G, K, J, CTOD, CTOA) Testing and Standardization," *Engineering Fracture Mechanics*, vol. 85, pp. 1-46, 2012.
- [92] H. Gao and B. Ji, "Modeling Fracture in Nanomaterials Via a Virtual Internal Bond Method," *Engineering Fracture Mechanics*, vol. 70, no. 14, pp. 1777-1791, 2003.
- [93] M Karimi and T Roarty, "Molecular Dynamics Simulations of Crack Propagation in Ni With Defects," *Modeling and Simulation in Materials Science and Engineering*, vol. 14, pp. 1409-1420, 2006.
- [94] J G Swadener, M I Baskes, and M Nastasi, "Molecular Dynamics Simulation of Brittle Fracture in Silicon," *Physical Review Letters*, vol. 89, p. 085503, 2002.
- [95] H Kikuchi, R V Kalia, et al., "Brittle Dynamic Fracture of Crystalline Cubic Silicon Carbide (3C-SiC) Via Molecular Dynamics Simulation," *Journal of Applied Physics*, vol. 98, p. 103524, 2005.
- [96] S Zhang, T Zhu, et al., "Atomistic and Multiscale Analyses of Brittle Fracture in Crystal Lattices," *Physical Review B*, vol. 76, pp. 94-114, 2007.
- [97] N. M. Pugno and R. S. Ruoff, "Quantized Fracture Mechanics," *Philosophical Magazine*, vol. 84, no. 27, pp. 2829-2845, 2004.
- [98] A Mattoni, L Colombo, et al., "Atomic Scale Origin of Crack Resistance in Brittle

- Fracture," *Physical Review Letters*, vol. 95, pp. 115501-115504, 2005.
- [99] M H Buehler, H Yao, et al., "Cracking and Adhesion at Small Scales: Atomistic and Continuum Studies of Flaw Tolerant Nanostructures," *Modeling and Simulation in Materials Science and Engineering*, vol. 14, pp. 799-816, 2006.
- [100] S Kumar, X Li, et al., "Is Stress Concentration Relevant for Nanocrystalline Metals?," *Nanoletters*, vol. 11, no. 6, pp. 2510-2516, 2011.
- [101] S G Kravchenko, O G Kravchenko, and C T Sun, et al., "A Two-Parameter Fracture Mechanics Model for Fatigue Crack Growth in Brittle Materials," *Engineering Fracture Mechanics*, vol. 119, pp. 132-147, 2014.
- [102] S H Cheng and C T Sun, "Size-Dependent Fracture Toughness of Nanoscale Structures: Crack-Tip Stress Approach in Molecular Dynamics," *Journal of Nanomechanics and Micromechanics*, vol. 4, no. 4, pp. A4014001-8, 2014.
- [103] A R Nazmus Sakib, Narendra De, Ashfaq Adnan, "Effect of Nanoscale Confinement on the Mode II Fracture of Confined Nanosolids," *Computational Materials Science*, vol. 68, pp. 271-279, 2013.
- [104] A R Nazmus Sakib, Ashfaq Adnan, "On the Size-Dependent Critical Stress Intensity Factor of Confined Brittle Nanofilms," *Engineering Fracture Mechanics*, vol. 86, pp. 13-22, 2012.
- [105] Ashfaq Adnan and C T Sun, "Evolution of Nanoscale Defects to Planar Cracks in a Brittle Solid," *Journal of Mechanics and Physics of Solids*, vol. 58, no. 7, pp. 983-1000, 2010.
- [106] Priya Vashishta, Rajiv K Kalia, et al., "Interaction potential for silicon carbide: A molecular dynamics study of elastic constant and vibrational density of states for

- crystalline and amorphous siliconcarbide," *Journal of Applied Physics*, vol. 101, p. 103515, 2007.
- [107] H Tanei, N Nakamura, et al., "Unusual Elastic Behavior of Nanocrystalline Diamond Thin Films," *Physical Review Letters*, vol. 100, p. 016804, 2008.
- [108] James E Butler and Anirudh V. Sumant, "The CVD of Nanodiamond Materials," *Chem Vapor Deposition*, vol. 14, pp. 145-160, 2008.
- [109] Anirudha V Sumant, Orlando Auciello, et al., "Ultrananocrystalline and Nanocrystalline Diamond Thin Filmsfor MEMS/NEMS Applications," *MRS Bulletin*, vol. 35, 2010.
- [110] Markus Mohr, Arnaud Caron, et al., "Young's Modulus, Fracture Strength, and Poisson's Ratio of Nanocrystalline Diamond Films," *Journal of Applied Physics*, vol. 116, p. 124308, 2014.
- [111] Claude A Klein and G. F. Cardinate, "Young's Modulus and Poisson's Ratio of CVD Diamond," *Diamond and Related Materials*, vol. 2, no. 5-7, pp. 918-923, 1993.
- [112] P. Hess, "The Mechanical Properties of Various Chemical Vapor Deposition Diamond Structures Compared to the Ideal Single Crystal," *J. Appl. Phys.*, vol. 111, p. 051101, 2012.
- [113] G C Sih, P C Paris, et al., "On Cracks in Rectilinearly Anisotropic Bodies," *International Journal of Fracture*, vol. 1, no. 3, pp. 189-203, 1965.
- [114] J. Rice, "A Path Independent Integral and the Approximate Analysis of Strain Concentration by Notches and Cracks," *J. Appl. Mech.*, vol. 35, pp. 379-386, 1968.
- [115] D. Dugdale, "Yielding of Steel Sheets Containing Slits," *J. Mech. Phys. Solids*, vol. 8, pp. 100-108, 1960.

- [116] JR Rice and GF Rosengren, "Plane Strain Deformation Near a Crack Tip in a Power Law Hardening Material," *J. Mech. Phys. Solids*, vol. 16, pp. 1-12, 1968.
- [117] Z Feng and J. E. Field, "Dynamic Strengths of Diamond Grits," *Ind. Diamond Rev.*, vol. 49, pp. 104-108, 1989.
- [118] R H Telling, C J Pickard, et al., "Theoretical Strength and Cleavage of Diamond," *Physical Review Letters*, vol. 84, no. 22, pp. 5160-5163, 2000.
- [119] E. F. Rybicki and M. F. Kanninen, "A Finite Element Calculation of Stress Intensity Factors by a Modified Crack Closure Integral," *Engineering Fracture Mechanics*, vol. 9, pp. 931-938, 1977.
- [120] G A Voronin, T W Zerda, et al., "Diamond– SiC Nanocomposites Sintered from a Mixture of Diamond and Silicon Nanopowders," *Diamond and Related Materials*, vol. 12, pp. 1477-1481, 2003.
- [121] Qi Liang, C S Yan, et al., "Enhancing the Mechanical Properties of Single-Crystal CVD Diamond," *J. Phys. Condens. Matter*, vol. 21, p. 364215, 2009.
- [122] M A Prelas, G Popovici, and L K Bigelow, *Handbook of Industrial Diamond and Diamond Films*, New York: Marcel Dekker, 1998.
- [123] H D Espinosa, B Peng, et al., "Elasticity, Strength, and Toughness of Single Crystal Silicon Carbide, Ultrananocrystalline Diamond, and Hydrogen-free Tetrahedral Amorphous Carbon," *Appl. Phys. Lett.*, vol. 89, p. 073111, 2006.
- [124] O Auciello, J Birrell, et al., "Materials Science and Fabrication Processes for a New MEMS Technology Based on Ultrananocrystalline Diamond Thin Films," *J. Phys. Condens. Matter*, vol. 16, p. R539, 2004.
- [125] Ashfaq Adnan and Sheikh F Ferdous, "Computational Design of Novel Carbon

- Enriched  $\text{Si}_{1-x}\text{C}_x$  Ceramics: A Molecular Dynamics Simulation Study," *Computational Materials Science*, vol. 96, pp. 354-359, 2015.
- [126] D N Buckley and K. Miyoshi, "Fundamental Tribological Properties of Ceramics," *Cera. Eng. Sci. Proc.*, vol. 93, pp. 347-349, 1983.
- [127] X. Li and B. Bhushan, "Micro/Nanomechanical Characterization of Ceramic Films for Microdevices," *Thin Solid Films*, vol. 340, no. 1-2, pp. 210-217, 1999.
- [128] G Gradinaru, T S Sudarshan, et al., "Electrical Properties of High Resistivity 6H-SiC Under High Temperature/High Field Stress," *Applied Physics Letter*, vol. 70, pp. 735-737, 1997.
- [129] H. Matsunami, "Current SiC Technology for Power Electronic Devices Beyond Si," *Microelectronic Engineering*, vol. 83, no. 1, pp. 2-4, 2006.
- [130] R G Azevedo, J Zhang, et al., "Silicon Carbide Coated Mems Strain Sensor for Harsh Environment Applications," in *IEEE 20th International Conference on Micro Electro Mechanical System (MEMS)*, Hyogo, Japan, 2007.
- [131] J B Watchman, W R Cannon, and M J Matthewson, *Mechanical Properties of Ceramics*, Wiley, 2009.
- [132] B. Basu and K. Balani, *Advanced Structural Ceramics*, Wiley, 2011.
- [133] H Park, H E Kim, et al., "Microstructure and High-Temperature Strength of  $\text{Si}_3\text{N}_4$ -SiC Nanocomposite," *Journal of European Ceramic Society*, vol. 18, no. 7, pp. 907-914, 1998.
- [134] Y S Oh, C S Kim, et al., "Fracture Strengths and Microstructures of  $\text{Si}_3\text{N}_4/\text{SiC}$  Nanocomposites Fabricated by in-situ Process," *Scripta Materialia*, vol. 44, no. 8-9, pp. 2079-2081, 2001.

- [135] T. Hirano and K. Niihara, "Microstructure and Mechanical Properties of Si<sub>3</sub>N<sub>4</sub>/SiC Composites," *Materials Letters*, vol. 22, pp. 249-254, 1995.
- [136] L Gao, X Jin, et al., "Microstructure and Mechanical Properties of SiC – Mullite Nanocomposite Prepared by Spark Plasma Sintering," *Materials Science and Engineering A*, vol. 334, pp. 262-266, 2002.
- [137] L Gao, X Jin, et al., ". Fabrication of YAG–SiC Nanocomposites by Spark Plasma Sintering," *Journal of European Ceramic Society*, vol. 22, pp. 785-789, 2002.
- [138] Y Luo, S Li, et al., "Fabrication and Mechanical Evaluation of SiC-TiC Nanocomposites by SPS," *Materials Letters*, vol. 58, pp. 150-153, 2003.
- [139] J L Demenet, M Amer, et al., "Dislocations in 4H- and 3C-SiC Single Crystals in the Brittle Regime," *Phys. Status Solidi.*, vol. C10, no. 1, pp. 64-67, 2013.
- [140] S Hamada, H Yoshioka, et al., "Dislocation Conversion in 4H-SiC Crystals Grown by Metastable Solvent Epitaxy.," *Journal of Solid State Science and Technology*, vol. 2, pp. N3092-97, 2013.
- [141] X. Ma, "Superscrew Dislocations in Silicon Carbide: Dissociation, Aggregation, and Formation," *J. Appl. Phys.*, vol. 99, p. 063513, 2006.
- [142] Y Gogotsi, S Welz, et al., "Conversion of Silicon Carbide to Crystalline Diamond-Structured Carbon at Ambient Pressure," *Nature*, vol. 411, pp. 283-287, 2001.
- [143] D Wittorf, W Jager, et al., "Electron Microscopy of Interfaces in Chemical Vapour Deposition Diamond Films on Silicon," *Diamond and Related Materials*, vol. 9, pp. 1696-1702, 2000.
- [144] X Shen, M P Oxley, et al., "Excess Carbon in Silicon Carbide," *Journal of Applied Physics*, vol. 108, p. 123705, 2010.

- [145] G Battistig, M P Oxley, et al., "Polarity Dependent Carbon Enrichment on 6H-SiC{0001} Due to Low Energy Ion Bombardment," *Surface Science*, vol. 526, pp. L133-L136, 2003.
- [146] A L Hurtado, D Morgan, et al., "Cs and Ag Co-Incorporation in Cubic Silicon Carbide," *Journal of Nuclear Materials*, vol. 439, pp. 65-71, 2013.
- [147] D Shrader, I Szulowska, et al., "Cs Diffusion in Cubic Silicon Carbide," *Journal of Nuclear Materials*, vol. 421, no. 1-3, pp. 89-96, 2012.
- [148] D Shrader, S Khalil, et al., "Ag Diffusion in Cubic Silicon Carbide," *Journal of Nuclear Materials*, vol. 408, no. 3, pp. 257-271, 2011.
- [149] R. I. Scace and G. A. Slack, "Solubility of Carbon in Silicon and Germanium," *The Journal of Chemical Physics*, vol. 30, p. 1551, 1959.
- [150] P Wernera, H J Gossmann, et al., "Carbon Diffusion in Silicon," *Applied Physics Letters*, vol. 73, no. 17, pp. 2465-2467, 1998.
- [151] R. C. Newman and J. Wakefield, "The Diffusivity of Carbon in Silicon," *J. Phys. Chem. Solids*, vol. 19, no. 3-4, pp. 230-234, 1961.
- [152] A L Ivanovskii, N I Medvedeva, et al., "Electronic Structure of Silicon carbide containing Superstoichiometric Carbon," *Russian Chemical Bulletin*, vol. 48, no. 3, pp. 612-615, 1999.
- [153] Y M Chiang and R P Messner, "Reaction Formed Silicon Carbide," *Materials Science and Engineering A*, vol. 144, no. 1-2, pp. 63-74, 1991.
- [154] C. A. Daniels, *Ceramics: Structure and Properties*, Abyss Books, 2002.
- [155] W. G. Hoover, "Canonical Dynamics: Equilibrium Phase-Space Distribution," *Physical Review A*, vol. 31, no. 3, pp. 1695-1697, 1985.

- [156] B. R. A. Nijboer and L Van Hove,, "Radial Distribution Function of a Gas of Hard Spheres and the Superposition Approximation," *Phys. Rev. Lett.*, vol. 85, no. 5, p. 777, 1952.
- [157] R. T. Sanderson, *Chemical Bonds and Bond Energy (Physical Chemistry)*, Academic Press, 1976.
- [158] M Mishra, C Tangpatjaroen, et al., "Plasticity Controlled Friction and Wear of Nanocrystalline SiC," *Journal of American Ceramic Society*, vol. 97, pp. 1194-1201, 2014.
- [159] F. A. Hummel, *Introduction to Phase Equilibrium in Ceramic Systems*, CRC Press, 1984.
- [160] F Kobayashi, K Ikawa, et al., "Formation of Carbon-Excess SiC from Pyrolysis of CH<sub>3</sub>SiCl<sub>3</sub>," *Journal of Crystal Growth*, vol. 28, no. 3, pp. 395-396, 1975.
- [161] O O Mykhaylyk and M. P. Gadzira, "Arrangement of C Atoms in the SiC-C Solid Solution," *Acta Crystallogr. B*, vol. 55, pp. 297-305, 1999.
- [162] R. O. Ritchie, "Mechanisms Of Fatigue Crack Propagation In Metals, Ceramics And Composites: Role Of Crack Tip Shielding," *Materials Science and Engineering A*, vol. 103, no. 1, pp. 15-28, 1988.
- [163] J Musil and H. Polakova, "Hard Nanocomposite Zr–Y–N Coatings, Correlation Between Hardness And Structure," *Surface and Coating Technoly*, vol. 127, no. 1, pp. 99-106, 2000.
- [164] J. Musil and J Vicek, "Magnetron Sputtering Of Films With Controlled Texture And Grain Size," 1998, vol. 54, no. 1-3, pp. 116-122, 1998.
- [165] A. Voevodin, "Supertough Wear-Resistant Coatings With 'Chameleon' Surface

- Adaptation," *Thin Solid Films*, vol. 370, no. 1-2, pp. 223-231, 2000.
- [166] Y Pauleau, F Thiery, et al., "Tribological Properties Of Copper/Carbon Films Formed By Microwave Plasma-assisted Deposition Techniques," *Surface and Coatings Technology*, Vols. 180-181, pp. 102-107, 2004.
- [167] H Dimigen, H Hubsch, and R Memming, "Tribological And Electrical Properties Of Metal Containing Hydrogenated Carbon Films," *Applied Physics Letters*, vol. 50, no. 16, pp. 1056-1058, 1987.
- [168] S. Veprek and S. Reiprich, "A Concept For The Design Of Novel Superhard Coatings," *Thin Solid Films*, vol. 268, no. 1-2, pp. 64-71, 1995.
- [169] S. Veprek, "Conventional And New Approaches Towards The Design Of Novel Superhard Materials," *Surface and Coatings Technology*, vol. 97, no. 1-3, pp. 15-22, 1997.
- [170] S. Veprek, "The Search For Novel, Superhard Materials," *Journal of Vacuum Science & Technology*, vol. 17, no. 5, pp. 2401-2420, 1999.
- [171] S Veprek, S Reiprich, and L Shizhi, "Super Hard Nanocrystalline Composite Materials: The TiN/Si<sub>3</sub>N<sub>4</sub> System," *Applied Physics Letters*, vol. 66, no. 20, pp. 2640-2642, 1995.
- [172] S Veprek, M Haussmann, and S Reiprich, "Superhard Nanocrystalline W<sub>2</sub>N/Amorphous Si<sub>3</sub>N<sub>4</sub> Composite Materials," *Journal of Vacuum Science & Technology*, vol. 14, no. 1, pp. 46-51, 1996.
- [173] P Karvankova, M G J Veprek-Heijman, et al., "Superhard nc-TiN/a-BN And nc-TiN/a-TiBx/a-BN Coatings Prepared By Plasma CVD And PVD: A Comparative Study Of Their Properties," *Surface and Coatings Technology*, Vols. 163-164, pp.

149-156, 2003.

- [174] P. Nesladek and S. Veprek, "Superhard Nanocrystalline Composites With Hardness of Diamond," *Physica Status Solidi (a)*, vol. 177, no. 1, pp. 53-62, 2000.
- [175] A A Voevodin, S V Prasad, and J S Zabinski, "Nanocrystalline Carbide/Amorphous Carbon Composites," *Journal of Applied Physics*, vol. 82, no. 2, pp. 855-858, 1997.
- [176] S Hogmark, S Jacobson, and M Larsson, "Design And Evaluation Of Tribological Coatings," *Wear*, vol. 246, no. 1-3, pp. 20-33, 2000.
- [177] G. S. Was and T. Foecke, "Deformation And Fracture In Micro-laminates," *Thin Solids Films*, vol. 286, no. 1-2, pp. 1-31, 1996.
- [178] H. Holleck, "Material Selection For Hard Coatings," *Journal of Vacuum Science & Technology*, vol. 4, no. 6, pp. 2661-2669, 1986.
- [179] M Nordin, R Sundstrom, et al., "Wear And Failure Mechanisms Of Multilayered PVD TiN/TaN Coated Tools When Milling Austenitic Stainless Steel," *Surface and Coatings Technology*, Vols. 133-134, pp. 240-246, 2000.
- [180] H G Prengel, P C Jindal, et al., "A New Class Of High Performance PVD Coatings For Carbide Cutting Tools," *Surface Coatings Technology*, vol. 139, no. 1, pp. 25-34, 2001.
- [181] H Holleck, A Kumar, et al., "Surface Engineering: Science And Technology I," *Minerals. Metals & Materials Society*, pp. 207-218, 1999.
- [182] Sheikh F Ferdous, Muhammad N Huda, and Ashfaq Adnan, "Improving Fracture Toughness of Silicon Carbide Ceramics with Nanodiamond Reinforcements," in *American Society for Composites*, Pennsylvania, 2013.
- [183] Sheikh F Ferdous and Ashfaq Adnan "Tailoring Fracture Toughness of Silicon

Carbide Ceramics Film via Nanoscale Multilayering with Diamond," in *American Society for Composites*, San Diego, CA, 2014.

### Biographical Information

Sheikh Fahad Ferdous was born in Barisal and raised in Faridpur. He passed from M N Academy high school his 10<sup>th</sup> grade then he admitted in Dhaka Bigyan College and passed his 12<sup>th</sup> grade. He has completed his BSc in Mechanical Engineering from Bangladesh University of Engineering and Technology (BUET) in 2008. He is then moved to University of Texas at Arlington for pursuing Doctor of Philosophy in 2010. He was awarded with Graduate Doctoral Teaching Fellowship and Enhanced Graduate Teaching Assistantship. He joined the MMPL lab of Dr. Ashfaq Adnan. He focused on his research in toughening mechanism of ceramic based materials.